AXISYMMETRIC OPTICAL MEMBRANE MODELING BASED ON EXPERIMENTAL RESULTS

THESIS

Brian J Lutz, Captain, USAF
AFIT/GAE/ENY/04-M11

DEPARTMENT OF THE AIR FORCE
AIR UNIVERSITY

AIR FORCE INSTITUTE OF TECHNOLOGY

Wright-Patterson Air Force Base, Ohio

APPROVED FOR PUBLIC RELEASE; DISTRIBUTION UNLIMITED

The views expressed in this thesis are those of the author and do not reflect the official policy or position of the United States Air Force, Department of Defense, or the United States Government.

AFIT/GAE/ENY/04-M11

AXISYMMETRIC OPTICAL MEMBRANE MODELING BASED ON EXPERIMENTAL RESULTS

THESIS

Presented to the Faculty

Department of Aeronautics and Astronautics

Graduate School of Engineering and Management

Air Force Institute of Technology

Air University

Air Education and Training Command

In Partial Fulfillment of the Requirements for the

Degree of Master of Science in Aeronautical Engineering

Brian J Lutz, BSE

Captain, USAF

March 2004

AFIT/GAE/ENY/04-M11

AXISYMMETRIC OPTICAL MEMBRANE MODELING BASED ON EXPERIMENTAL RESULTS

Brian J Lutz, BSE
Captain, USAF

Approved:

____//Signed//__________________________ __________
Prof. Anthony N Palazotto (Chairman) date

____//Signed//__________________________ __________
Major Richard Cobb (Member) date

____//Signed//__________________________ __________
Lt Col Robert A Canfield (Member) date

AFIT/GAE/ENY/04-M11

Abstract

The United States Air Force, Department of Defense and commercial industry have recognized the great value of near-earth space development, specifically in satellites for use in communications, ground and space surveillance and more active roles. However, resolution, or the primary optic's diameter, has been a limitation, especially for ground surveillance. Deployable optics has been investigated to allow larger optics in space and membrane optics has received increasing attention recently. The membrane's flexible nature requires some passive and possibly active control to reduce optical distortion caused by manufacturing, deployment, or other effects during use. Piezoelectric surface controllers are one option to actively control the membrane on the order of optical measurements (micron displacement or less). Multiple configurations of transverse displacements are feasible depending on the piezo zone locations and activation.

The current thrust of industry is reducing the effort, time and cost of manufacturing and testing through use of computerized modeling and simulation; therefore, this was investigated for a membrane mirror and piezoelectric combination. Prior experiments using 6-inch diameter membranes have been conducted with an axisymmetric piezoelectric material layer on the non-optical surface. Various voltage differentials were applied to the piezo and the transverse displacement was measured. A finite element code, using perturbation techniques, was written in MATLAB and tested to check the feasibility of using computer models for the micro-displacements occurring with the membrane-piezo lay-up. The computer program considered was developed for axisymmetric conditions; however, in many cases, these conditions tended to dominate. Under these conditions, the finite element code produces results that represent the axisymmetrically reduced experimental data.

Dedication

I honorably dedicate this work to my precious mariposa Megan. She is my princess and light of my life. For the many long nights we have spent talking together and the many that will be in the future.

Acknowledgements

There are always many people to thank during an endeavor like this one. First, I would like to thank my advisor, Dr. Anthony Palazotto, for the instruction he has given me in and out of the classroom and the kindness he has always shown toward me. Lt Col Canfield has always been a friend and spiritual guide. For all the people that have been involved and helped me during the process of this thesis, Maj James Rogers, Dr. David Mollenhauer, and Capt Mike Sobers. Thanks has to go out to Mr. Dan Marker for financial contribution to this project from AFRL/DEBS, but more importantly as a mentor and friend.

I'd like to thank all my friends that have helped keep me sane, especially Chris Blackwell and Ray Holstein, during this crazy expedition of AFIT. They were always there to help with homework, life and to listen to all the nonsense.

Table of Contents

Page

List of Figures

Figure Page

Figure Page

List of Tables

Table Page

AXISYMMETRIC OPTICAL MEMBRANE MODELING BASED ON EXPERIMENTAL RESULTS

I: Introduction and Background

Space Optics And Other Uses

The United States Air Force and Department of Defense, as well as other government and civilian organizations, have recognized the need for larger space telescopes for investigating the far reaches of the universe and discovering parts of the Earth otherwise impossible to see (Marker/Jenkins, 2001). The motivation behind this is to avoid atmospheric disturbances when searching the stars and for the coverage the altitude gives when viewing the Earth. However, the resolution is reduced due to this altitude. As a general rule, the resolution is directly related to the diameter of the primary mirror. (Sobers, 2002) Solid optics has been the chief type used on these systems in the past. Due to limitations in payload space and weight, these optics are not feasible over a few meters in diameter.

The military community and DoD are most interested in an earth observing ability. Past technologies to accomplish this have focused on solid optics. The most familiar and well-known optical quality telescope is the Hubble (possessing a 2.4-m solid primary), used to photograph the stars and distant galaxies. If this were turned toward the ground it would have resolution capabilities of 0.15 m. (AFRL/DEBS TMR, 2002). There are also other satellite platforms, one such named IKONOS, capable of ground resolution of 0.6 m. A 25-m membrane placed at 12000 km could potentially have a ground resolution of

0.3 m, while having a swath width of 840 km verses the Hubble at only about 1.2 m. These calculations are completed using the following equation:

$$\text{Resolution} = 1.22 l R / D \tag{1}$$

where l =0.5 µm, D is the mirror diameter and R is the range of the system.

While serving some of the needs for which they were designed, a higher resolution system is desired. Achieving this requires redesigning the primary mirror to better suit the needs and capabilities of modern space systems. Some ideas for the redesign include a segmented solid or a membrane optic. Both have their own limitations and strengths, and both are being developed at some level in and out of the DoD; however, only one is investigated in this study. (Magee, Carlin)

Segmented solid optics have been investigated as a solution for quite some time as a way to increase the full primary mirror size, but have the same or less payload size. This requires deployment of the optic in some fashion, such as a flower opening or fanning and positioning of the segments to within fractions of a wavelength. They offer the opportunity to increase the optic size using current solid optics technology mated with current control systems to bring the segments into the proper positioning. (Li, 1998) Segmented optics share some of the same shortcomings as solid optics, including, but not limited to the weight of all the segmented pieces, the complications of deployment when on station and the expensive and timely procedure of polishing the mirror pieces. (Magee, 2002)

In recent years, there have been space telescope experiments using polymers; one such was NASA's Inflatable Antenna Experiment (IAE), which is a pressurized lenticular about 14 meters in diameter. It was designed as a radio antenna and its main purpose was verification of the deployment mechanics. (L'Garde, 2004) Figure 1 shows the inflated antenna in the laboratory. This technique has little application in the visible and shorter wavelengths since the front canopy causes diffraction of the light wave before reflecting off the primary, which itself is not of diffraction limited quality; however, the success of IAE has lead to the exploration of polymers as a probable primary mirror.

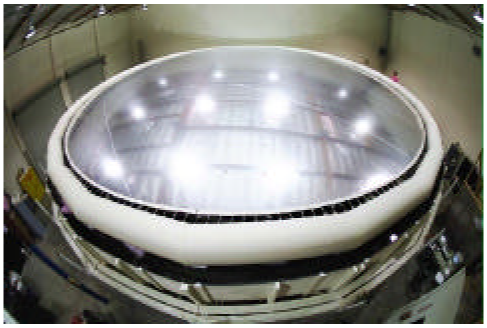

Figure 1. Laboratory IAE

Following on project successes such as the IAE and the continued desire to advance current capabilities, thin polymers have been researched in greater depth to discover their possible uses in optical systems. There have been many speculations on the end product of the membrane mirror. For instance, reconnaissance satellites, relay satellites, and ground-based astronomy. (Rotge, 2002) Recently, there has even been discussion on the use of the membranes in a Relay Mirror Airship used in conjunction with the Airborne Laser (ABL) to increase the coverage and decrease the absolute number of ABL platforms that need to be airborne at any one time. For these reasons and to help make the previous possible, membrane optics are selected to be further studied for large aperture space telescope development.

Membrane Optical Considerations

Membrane optics provide many advantages over traditional solid optics. First, they are usually cheaper and more time efficient to manufacture, since there is only one manufacturing stage, eliminating the polishing process. (Rotge, 1999) They have the opportunity to reduce the payload weight by many magnitudes, since their thickness is essentially nil compared to their diameter, reducing the cost of the launch. Lastly, the membrane has the opportunity to be adapted to many other missions with greater ease than a solid optic. One example is the use of the membrane as an extremely thin optical window, thus preventing the light from slowing or being diffracted in thicker glass windows. Of course, membrane optics share deployment complications with their segmented cousins, as well as their own limitations, such as surface deflections caused by slewing the structure and manufacturing the membrane to near optical tolerances over multi-meter sections without polishing; however, the benefits outweigh the difficulties and many of the limitations have been addressed and some of them are already overcome. (Marker, 2002) The chief reason for investigating membrane optics is overall weight reduction of the total system by using a membrane whose weight in comparison to the support structure is nil; thereby, reducing launch cost and increasing the opportunity to place into a higher orbit.

Before membranes could be considered further, better manufacturing techniques were needed to produce the optical tolerances without polishing. A few techniques were investigated and one method commonly used is a spin casting method that is currently able to manufacture flat membrane mirrors on the order of 1-m diameter with l /20 diffraction over the whole span, meaning that there is a thickness difference of about 30 nm across the membrane for a green light laser (*l* = 633 nm).(SRS website) The material science development of these membranes (CP-1) was completed through USAF contracts at the AFRL Directed Energy Directorate and NASA. This work is ongoing to accomplish this same feat on the multi-meter level. (Rotge, 2000)

The manufacturing of any optic is usually developed around the global shape while polishing the glass or metal will reduce the amount of local hills and valleys. This affects the path of the incident light on the optic. As collimated light encounters a surface, it behaves in two fashions. First, there is a global reflection and refraction that behaves geometrically, i.e. if the light is incident to the surface at a certain angle, it will reflect (bounce off surface) at the same angle and refract (enter the medium) at an angle based on Snell's Law:

$$n_i \sin q_i = n_t \sin q_t \qquad (2)$$

where $n_{i,t}$ is the index of refraction (Hecht)

The reflection is of more concern, since any light that enters the membrane will mostly exit the other side and a thin layer of a specific wavelength reflective coating can prevent much of the refraction. The second reflection characteristic requires looking at the more localized surface, since in optics the light is usually a specific laser wavelength, usually a shorter one, such as green (633 nm) in this case. The best way to explain what happens locally is to examine Figure 2.

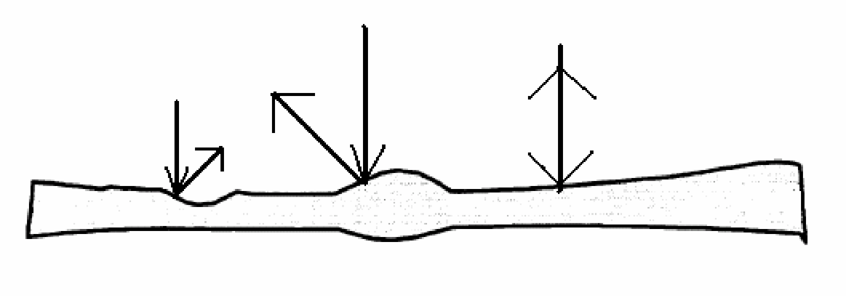

Figure 2. Local Reflection

As it can be seen, the hills or valleys will cause a portion of the light to reflect at a different angle from its incident angle. This can cause quite a bit of loss of photons, thereby reducing the light entering into the rest of an optical system. However, there is a way to prevent or correct for this phenomenon. One current method is real-time holography, a method that has been proven for many wavelengths of diffraction off a membrane (Gruneisen, 1999). The basic explanation of this method is to use two beams of light, one simulating a point source at infinity and another beam that is "separated" into a few sets of beams. The point source and part of the second beam are collimated and reflected off the aberrated membrane. The point source beam, post reflection, is interfered with a piece of the original second beam and combined with another piece of the original second beam at a Spatial Light Modulator (SLM), where the reflected second beam meets them. The SLM is where the correction is completed and the light is reflected back to a camera. This setup can be seen in Figure 3 and more information is supplied in the literature (Gruneisen, 1999).

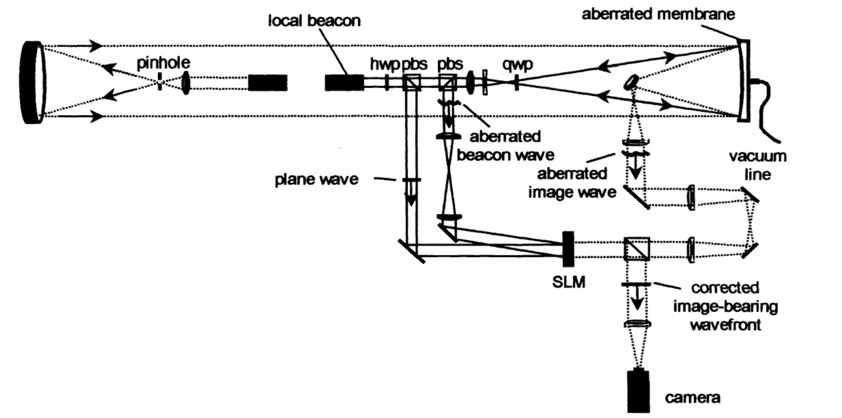

Figure 3. Holographic Setup

The current holography methods have the capability to correct for many wavelengths of diffraction from any mechanism, from physical distortion of the membrane due to deployment to manufacturing deficiencies. There is also the ability to correct for dynamic changes coming about from slewing or other dynamic changes. Although the holography can correct many wavelengths, it was recognized early that this may still not be enough and an actual mechanical correction may be needed as well. While there have been many ideas, including full actuator sets as was planned for use with segmented optics and MicroElectroMechanical Systems (MEMS), another relatively inexpensive and seemingly non-intrusive idea is the use of Polyvinylidene fluoride (PVDF) materials, which may be capable of active control through a voltage differential placed across a very specific surface area on the membrane. Multiple zones can be etched out and therefore be activated separately or in conjunction to reshape the membrane to suit the needs of the mission, the manufacturing deficiencies or for any other reason that the membrane needs to be tweaked.

Currently, most membrane manufacturing techniques have concentrated on developing optical quality flats, thin films with no curvature from the manufacturing process. (Rotge, 1999) Within the earth environment, a vacuum could be applied behind the membrane to pull it into a convex shape, but this idea has two problems, it takes on a spherical shape rather than a parabolic shape usually desired and it is not feasible in the space vacuum. The solution is a mirror that is globally manufactured to the desired net-shape, a mirror that already has the global convex, parabolic shape immediately after manufacturing. This mirror would also require the same optical toleranc es at the small-scale to avoid diffraction of the incoming light. Fortunately, the technology used for flat membrane manufacturing is applicable to net-shape membranes. (Marker, 2002) The main difference is the casting mold shape, namely flat or a specific net-shape. An advantage to this technique is the elimination of an optically toleranced mold, since the air surface is the optical surface.

These net-shape membranes provide a versatile range of uses from space-based primary mirrors to various ground uses. One concept currently in development is to use the membrane as an optical coating on ceramic mirrors, thereby reducing the need to polish the mirror. This in effect reduces time from start of mirror manufacturing to "first light", or when the mirror can first be illuminated in use. As with many other types of solid mirrors, the difficulty and costly procedure of polishing the ceramic mirror, a materially hard substance, to optical tolerances is eliminated. These dual layer mirrors can be used in ground applications and would provide the capability to use the bottom layer (metal or ceramic) as the mold.

Another challenge of the membrane is the lack of rigidity; therefore, a Middle or Geosynchronous Earth Orbit (MEO/GEO) is optimal to avoid atmospheric disturbances, as well as other concerns at a Low Earth Orbit (LEO). From these altitudes, a much larger area of the world could be covered by a single satellite, although larger primaries would have to be manufactured to meet resolution requirements. If local defects are kept to l /20 optical tolerances over 3-m areas of the membrane, a 30-m membrane mirror could potentially be feasible for the visible wavelengths; especially with optical correction methods that are available and being developed.

Membrane optics have many unique qualities over traditional glass, metal or other solid optics. The first one that normally comes to mind is the small thickness-to-diameter ratio. In most traditional optics, the thickness-to-diameter ratio has been figured at about 1:6 to ensure structural and dimensional stability. (Carlin) Weight reduction of solid optics have been completed through use of honeycombing or bonding a face sheet to a back plate; however, there are inherent difficulties with these methods, such as the fragility of the mirror and out of plane bending after honeycombing. For this reason another method is desired.

A membrane optic, on the other hand, can be manufactured through a curing process that can be completed on the order of hours or days rather than weeks or months, to the required optical tolerances at thickness-to-diameter ratios of 1:100000 for a 1-m membrane. This involves an extremely stable manufacturing system to achieve a l /20 Root-Mean-Square (RMS) geometrical figure, the surface roughness difference across a specific portion of the total membrane. This may be best described using a sine wave. A perfect sin(q) wave has a Peak-to-Valley value of 2 l and an RMS value of .707 l .

Imagine a sine wave with some positive error at the first positive peak. This would drive the P-V to increase the total amount of the error and the RMS value to increase by an average value across as defined by the definition of the calculation. Notice, the RMS value describes the average of the local wavefront in comparison to the global wavefront, rather than describing the maximum local defects like the Peak-to-Valley, which is the difference between the tallest peak and the deepest valley.

It would be ideal to have these specifications across the whole membrane at large diameters, but is unlikely to occur, whether for membranes or glass. To envision this, imagine a mirror designed for green light reflection (633 nm); the l /20 requirement would mean an average surface difference nearly 30 nm across the whole front surface. To further emphasize this, this corresponds to a ratio of surface roughness to 10-m diameter mirror of 30 x 10^{-10} m or approximately 1/8000th the diameter of the human hair! Obviously, the larger the mirror the more difficult this task is to complete; however, if this requirement can be accomplished over any 3-m diameter area of the membrane, other correction methods (optical holography and/or active control) may supply enough correction to meet many optical missions.

The focus of many projects has been modeling and simulation to save cost and time from manufacturing and to test new ideas based on a prior idea. This is in the early stages for membrane mirrors to discover how they will respond to specific forces or control mechanisms. There is a crucial difference between finite element modeling of membranes and that of other structures, namely, the order of deflections. Deflections in most structures are usually on order of at least 100s of microns (0.1 mm), if not much more; however, due to the precision of an optical system, a finite element code that can handle nanometer level displacements is required. In earlier completed experimental work, the deflection of a ¼” thick membrane instigated by a PVDF layer was on the order of 2 l or about a micron. (Sobers, 2002) This is usually the high end displacements and fractions of one wave deflection may be necessary within the code. Current commercial codes don’t possess this capability or all the mechanics of the PVDF layer; therefore, the theory was researched and a finite element code was developed based on this theory. (Rogers, 2001)

The scope of this thesis is a culmination of one graduate thesis and one dissertation. The thesis dealt with experimental results of activating a PVDF layer and how it affected the shape of the membrane. The dissertation involved the development of a perturbation technique finite element code. This study covers the use of this code to check it against the reality of the experimental results. This work will be covered in a general sense in the next two chapters.

II: EXPERIMENTAL DATA

Overview

As stated before, all experimental testing was completed under a separate thesis. The goal was to improve the control capability of an optical surface. Past systems were limited to global shape control or small, expensive microelectricalmechanical (MEM) devices. To improve on these techniques, four mirrors were manufactured using a polymer-based optical surface in conjunction with two types of bonded materials. The first was constructed of a piezo-ceramic bonded to a copper-clad circuit board. The one investigated in this study was a stretched PVDF membrane bonded to an aluminum ring. The polymer is a two part liquid silicone that was cured in the ring on top of the PVDF (see Figure 4).

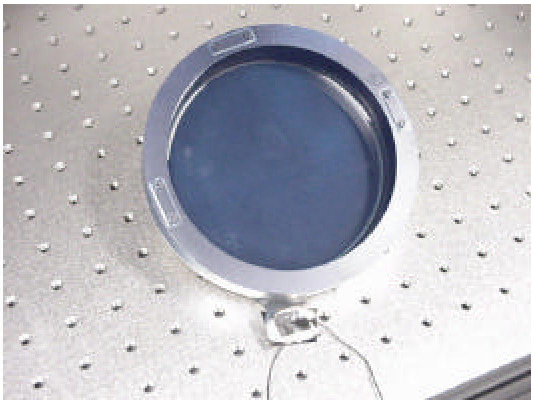

Figure 4. Cured Polymer in Mount

The mirrors were tested using a Shack-Hartmann wavefront sensor to determine surface flatness. The surface flatness measurements were used to test the system and verify it was setup properly. They are used to normalize the deflection plots, since capturing the deflection and not the initial manufacturing wavefront is desired.

Mirror Construction

The membranes were constructed of two materials, namely GE Silicone RTV615 and a piece of PVDF. They were given the designation M1 and M2. Both mirrors used the same manufacturing technique with a slight difference in the PVDF. The stretching system consisted of an aluminum ring and rubber O-ring, aluminum faceplate and four bar-clamps.

The membrane manufacturing started with the PVDF being placed between the o-ring and faceplate. The bar-clamps were placed over the outside edge of the faceplate and tightened until the PVDF was taut. Epoxy was applied to the aluminum mounting-ring on the middle surface between the two grooves and then place on the stretched PVDF. To further ensure an even and stretched membrane, weights were place on top of the mounting ring. The PVDF was later cut out from the stretching system after the epoxy cured.

The initial purpose of M1 was to test the mounting techniques; however, the etching procedures were later developed and a control pattern was etched on the back surface after mounting. This process was reversed in M2. The etched pattern was completed before the PVDF was mounted. Figure 5 shows the actual M2 PVDF layer and Figure 6 shows a layout of the activation zones. Notice the leads to each of the zones. Zone 7 is of most interest due to its perfectly axisymmetric location.

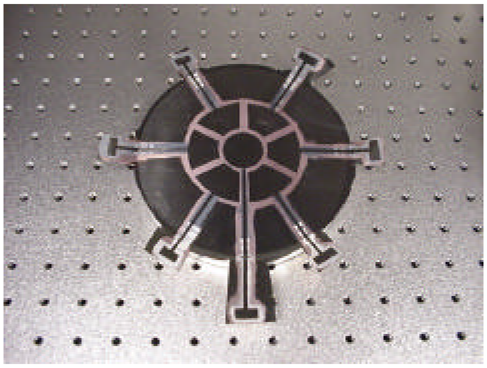

Figure 5. Etched PVDF film

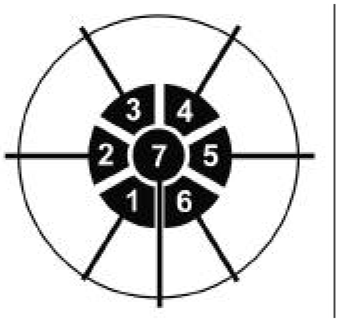

Figure 6. M2 Activation Zones

To learn more about the etching procedure, refer to *Smart Structures for Control of Optical Surfaces* Appendix A (Sobers, 2002).

In both cases after the mounting procedure was complete, the mirror was spray-painted, silicone rubber primer applied and a layer of GE Silicones RTV615 was poured into the mounting ring on the opposite side of the electrodes. A second layer of RTV was poured due to curvature that developed during curing. The combination of the two polymer layers was measured to be approximately 6 mm M1 and 4 mm for M2. The PVDF for M2 was slightly thicker at 52-µm verses 32-µm for M1.

Test Methodology

The surface flatness measurements were completed using a 20 mW helium-neon laser with a wavelength of 633 nm and a WaveScope® Shack-Hartmann wavefront sensor built by Adaptive Optics Associates. The data outputted was used to calculate a surface plot, synthetic interferometric fringe pattern and the first 35 coefficients of the Zernike polynomial set. The surface data and Zernike polynomials were exported to be plotted in MATLAB® to enhance the display.

Using various optical path setups and neutral density filter ranges, the surface flatness was measured for each mirror. The detail of this method can be found in Chapter 3 (Sobers, 2002). After the surface flatness was measured and beam expansion rates were determined, the actual testing of the membrane mirror was completed. The Shack-Hartmann was used to measure the test and reference surfaces separately. This was accomplished in this manner since the reference surface has a much greater reflection than the test specimen. It also removes the majority of test equipment bias and presents an opportunity to compare different specimens. Various figures of the setups could be seen in Figure 7-Figure 8.

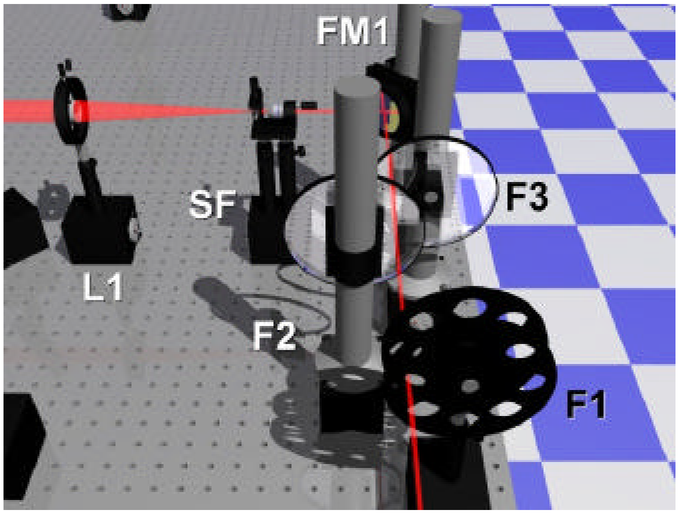

Figure 7. Experimental Filter Setup

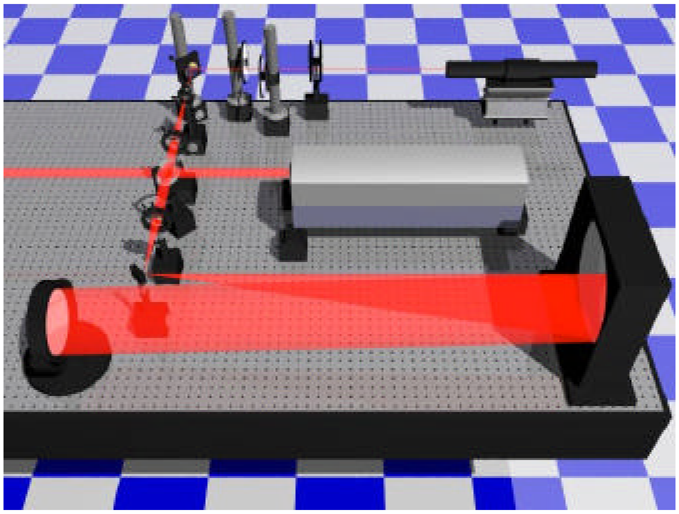

Figure 8. Beam Expansion

Along with different setups, a few different types of equipment were used. The Monolithic Lenslet Modules MLM lenslets size used determines the fidelity of the data. During the initial testing used to refine the techniques, the lenslet size was 480µm and later was upgraded to a higher fidelity MLM, with lenslets of 133µm across. The

Wavescope® software allowed various inputs for each test. The initial testing with the 480µm MLM was completed with 5 measurements per test, 5 frames for each measurement collected at 30Hz, while collecting one data point for each lenslet. The finer 133 µm MLM produced a much larger quantity of data; therefore, the tests were reduced to 3 measurements, five frames per measurement at 5 Hz. All the test data were exported from the Wavescope® software to data files. MATLAB® script was written to process this data and output raw displacement data, Zernike plots and surface smoothed plots.

Mirror Deflection Results

The objective behind the above experiment was to show the controllability of the polymer membrane through voltage differential across specific piezoelectric designs. There was definite proof that the 0.25" thick membrane and piezoelectric backing displaced together as seen in the non-actuated and actuated displacement plots in Figure 9.

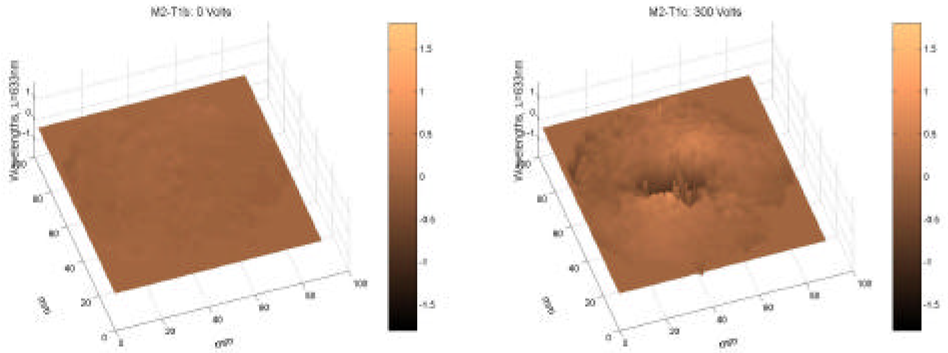

Figure 9. Non-Activated and Activate Membrane Plots

For the most part, the piezoelectric placement was even and symmetric. This may not be the case for a final membrane, as there may be a desire to activate zones of different shapes across the whole membrane. This study was not concerned with that aspect, but only to show that it is possible to displace the membrane.

The results of all these tests supplied plots of raw data of the surface of each membrane. The polymer membranes were relatively optically flat (3.95 *l* PV, 0.63 *l* RMS); however, there was definite high frequency distortion, at submicron resolution, across the whole membrane. This was partly resolved by "zeroing" out the initial 0V deflection plot from each raw data plot for each voltage condition. The "zeroing" process was accomplished by subtracting out the initial wavefront gathered when no activation was applied. This self-referencing technique leads to a great surface flatness improvement. For example, the zero voltage case when self-referenced is nearly an order of magnitude better than the raw data (0.59 *l* PV, 0.07 *l* RMS).

Much of the distortion encountered for each voltage case was reduced using this method, but another approximation used within the optics community, namely Zernike polynomials, supplies another way to look at the data. The Zernike polynomials are a way to express the wavefront deviation of each term with respect to the actual wavefront. In other words, a combination of a series of multipliers (Zernike coefficient) and polar-represented polynomials (Zernike polynomials) tallied to give a representation of displacements.

As stated before, the two PVDF membrane configurations have the important test results. There were numerous tests completed on both membranes at different voltage conditions. M1 was used mostly to determine testing procedures. The first three tests were completed before the second layer of RTV615 was applied. The following figures are deflection plots of M1 and their corresponding Zernike plots.

After applying positive or negative voltages, it was noticed that there was some residual deflection in the region of actuation. This may be a residual charge on the control surface. The WaveScope® was recalibrated to compensate for this residual before more tests were conducted. Much more was realized throughout the testing of M1, but the most important aspect was that these tests proved low-order, global shape control of lightweight membrane mirrors is achievable using piezoelectric control layers, such as PVDF. The order of magnitude of this control is the same as that of the surface features, demonstrating that it might be possible to correct for them.

After the knowledge gained from the testing of M1, M2, which had different control zones (refer back to Figure 6) was tested. As with M1, M2 was evaluated before any voltage was applied to check the surface flatness. The control region 7 (a 3-mm circle in the center) tests are the most important to look at for this study, since they represent an axisymmetric case. Other results can be seen here, but are only to show the ability of activation and displacement of other areas of the membrane.

Control region 7 was first activated with 300, followed by 600V. The magnitude of the depression increased by approximately one wave as the voltage was increased (2.33 λ versus 3.22 λ, respectively). Again, the following plots are the displacement plots along with their respective Zernike plots for each case. Figure 10 is the 300 V case and Figure 11 is the 600 V case.

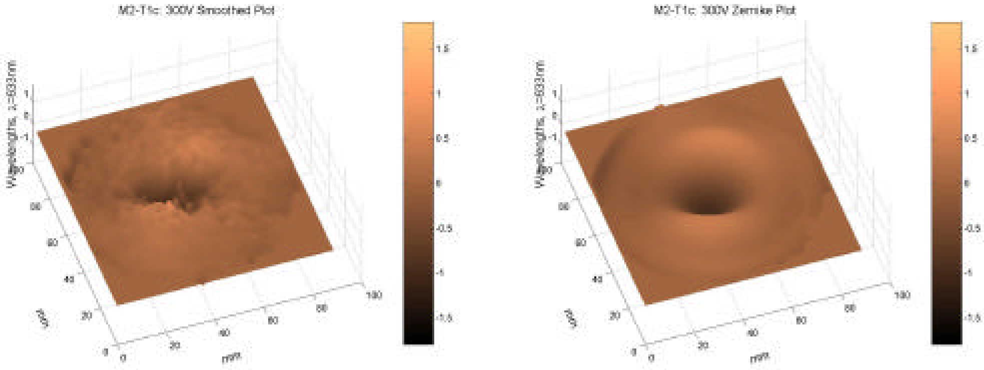

Figure 10. 300V Experimental Plots

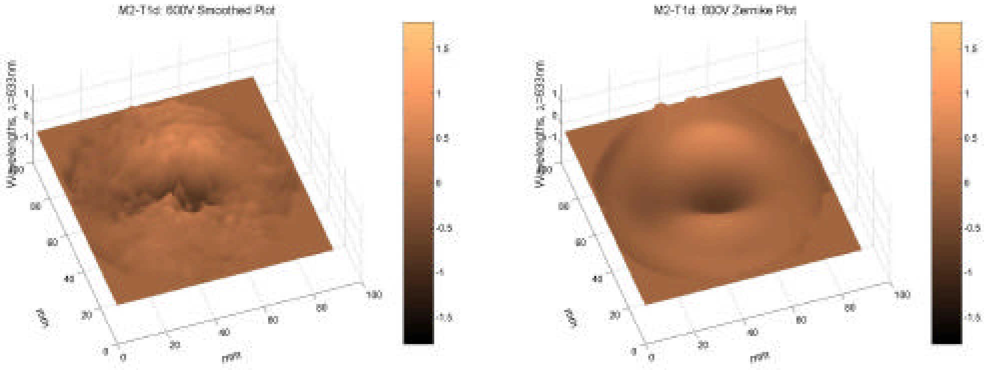

Figure 11. 600V Experimental Plots

After the positive voltage tests, the control leads were grounded to discharge the PVDF layer and retested at 0V. Figure 12 corresponds to the 0V case. Notice just a little distortion in these plots caused by the deflection of the residual positive voltage.

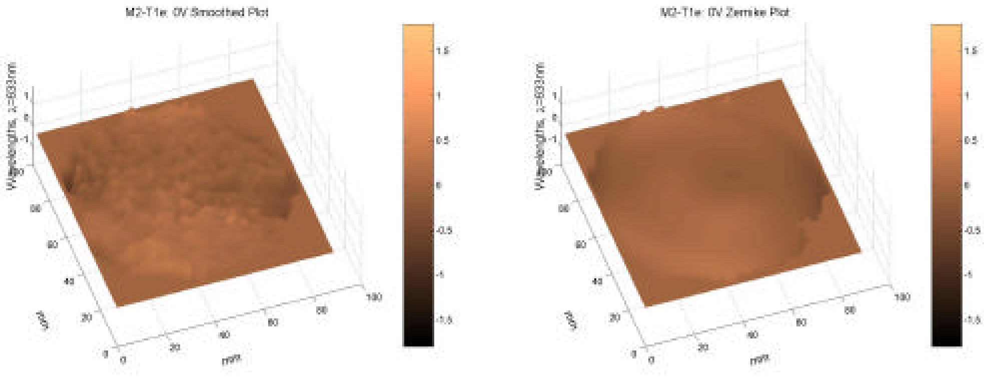

Figure 12. 0V after positive voltage

The tests were re-accomplished at the same magnitude negative voltages. There was again about a one-wave change in the deflection (2.39 *l* PV for -300V and 3.4 *l* PV for -600V). The width of the deformed area was slightly larger than the control region. The deformed area was about 40mm and 50mm for -300v and -600V, respectively. Figure 13 is the -300V case and Figure 14 is -600 in the center region. Notice that the negative voltage produced a positive displacement. The Zernike plots seem to still have a representation of the raw data.

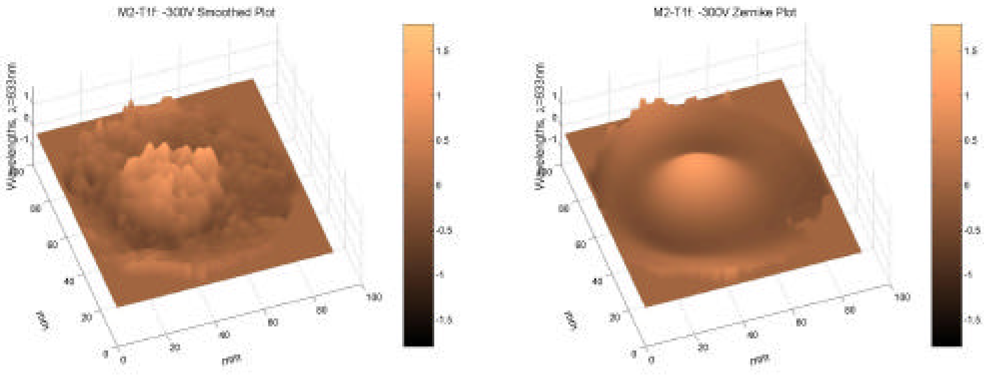

Figure 13. -300V Experimental Plots

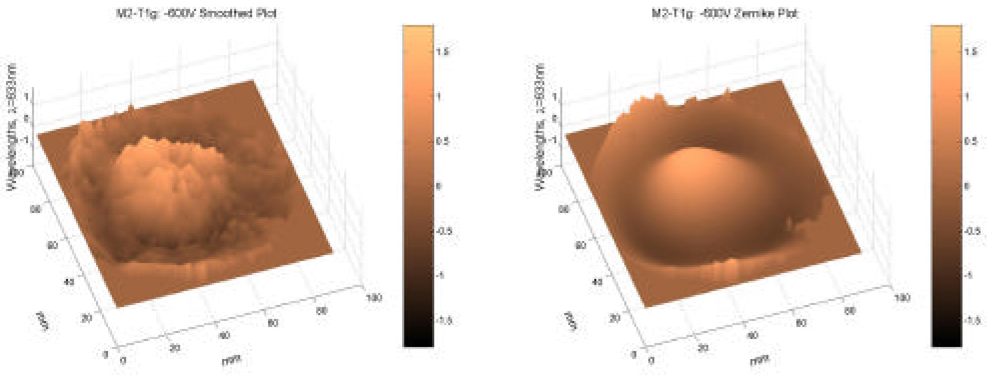

Figure 14. -600V Experimental Plots

Once more the 0V case is included after the negative voltages are applied to check for any effects of the deformation. Figure 15 show that there is a trace of a positive deformation, caused by the negative voltage.

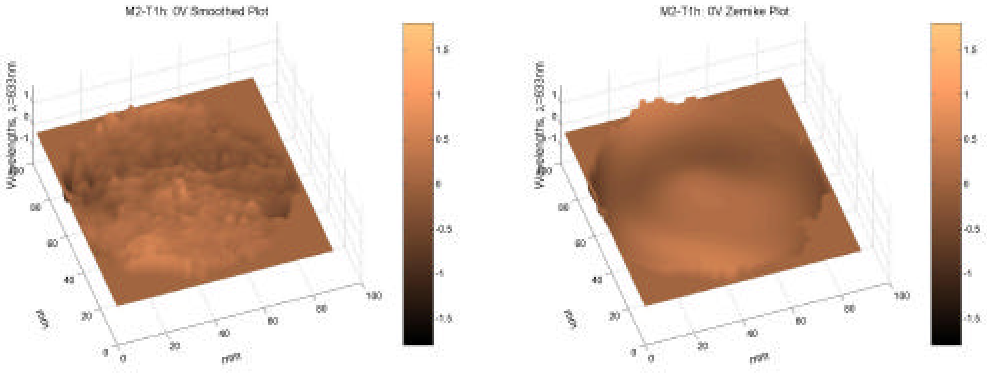

Figure 15. 0V after negative voltage

As stated before, various zones were activated alone and together to verify the controllability of the membrane surface. They are included here only to show the effects of these zones and are not used later in the study. Figure 16 shows zones 3 and 6 activated with 300 volts in each section. Notice how much control over the membrane is possible. Many different zones could be designed that would allow a fair amount of local control without overly affecting the adjacent zones. This concludes the discussion of work completed by Sobers, which demonstrates a very crucial ability of static control over a membrane at the minimum.

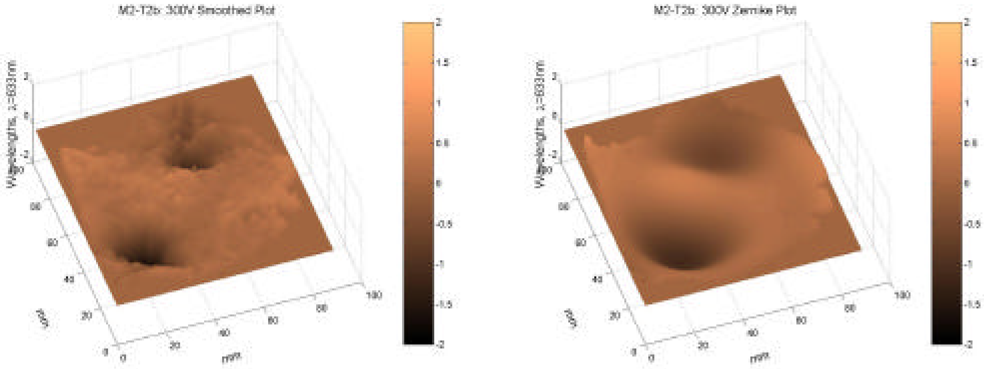

Figure 16. 300V activation in Region 3 and 6

Material Property Test and Results

The material properties of many polymers are unknown due to some complications in the testing procedure and the lack of need in the past; however, the Modulus of Elasticity and Poisson’s Ratio are required components to the finite element solution. A method was therefore designed by the Air Force Research Laboratory and some affiliates using a combination of Moiré Interferometry and tensile testing. The method was originally designed for testing of 3-dimensional woven materials, but was easily adapted to the testing of the RTV615 polymer used in the preceding mirror tests.

In most tensile tests, where a material similar to a metal is being tested, the grips of the tensile testing machine can be directly attached to the specimen in a region that is not to be involved in the test. This can be accomplished if the material will not compress significantly under the grip strength and will not tear as loaded; however, this would happen with a polymer. A carbon fiber two-end mounting tab system was designed that would serve as the "grip zones". They actually were center drilled and a string was inserted to hold the specimen from the top and a "bucket" where the weight would be applied on the bottom.

The preparation of the polymer specimen involved the machining of a few aluminum pieces about 2" long x .25" thick to be used as a mold while the two part liquid polymer RTV 615 was poured and cured. Aluminum was used to ensure the cured polymer could be released from the sidepieces without destroying the specimen, since the polymer would not adhere to this metal. The carbon fiber pieces were also machined to about ½" x ¼". Two aluminum end tabs were machined to about the same dimensions and a transverse hole was drilled in them to be used in conjunction with thread as the mechanism to hold the ends of the specimen. The specimen can be seen in Figure 17. Notice that one of the aluminum end tabs has fallen off. The carbon fiber was chosen for its porous quality into which the polymer could infuse, so the pieces would not separate during the test. After accomplishing the machining, a diffraction grating was selected that would serve as the mechanism to imprint onto the specimen an equivalent tool most closely related to a strain gauge in a normal tensile test. This diffraction grating imprinted polymer, the Al end tabs and carbon pieces are the only parts of the specimen tests. All other parts were removed.

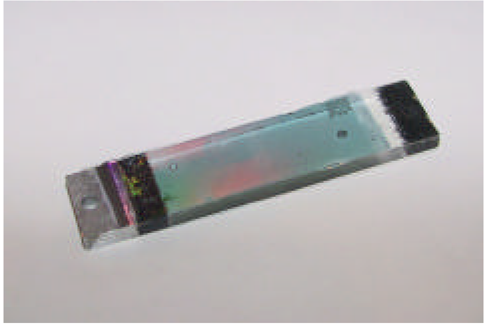

Figure 17. RTV 615 Specimen

The specimen was created in the following fashion: The two aluminum and two carbon fiber pieces were glued onto an area of the diffraction grating such that a channel of about 1.5”x ½” was created, so the RTV would not be able to escape from the channel. The polymer was mixed thoroughly by hand and placed in a centrifuge machine to remove all the air pockets and bubbles. During this time, a bit of polymer bonding agent was applied to the carbon pieces to further enhance the bonding of the polymer and carbon. The polymer was then poured into the channel onto the diffraction grating. It was allowed to cure for about a week, removed with an imprint from the diffraction grating. The aluminum pieces were also removed from the sides of the specimen.

The next step was securing the specimen in the test setup by threading the two holes in the carbon. The specimen was hung by this thread at the top. A small bucket was hung from the other side, toward the ground, of the specimen where the weight would be applied. Different attempts at constraining the loading angle were made to ensure little, or ideally, no bending when weight is added. Different tests were accomplished and the early tests were unsuccessful mostly due to bending in the specimen. New constraints of the loading angle using bars holding the thread to ensure vertical displacement were applied and the test was rerun.

As with most tensile tests, the specimen was loaded in the axial direction with the procedure stated above. Prior to loading, the diffraction grating was brought into view through the Moiré Interferometer, as seen below in Figure 18.

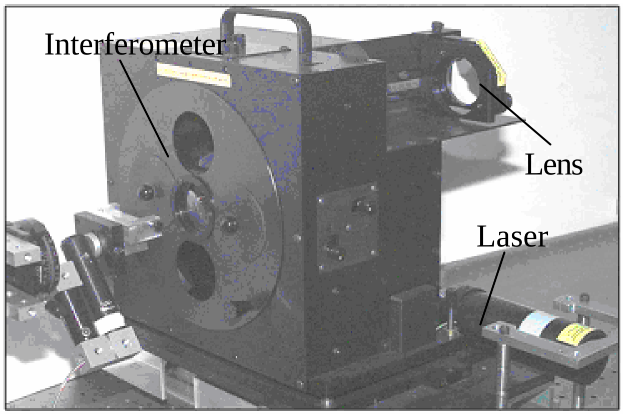

Figure 18. Moiré Interferometer

This is accomplished by exposing the diffraction grating to two collimated, coherent beams of laser light. A schematic is shown here in Figure 19. Before deformation of the specimen is accomplished, one diffraction order from each beam is assured to be perpendicular to the specimen, by adjusting the angle of incidence of the two beams.

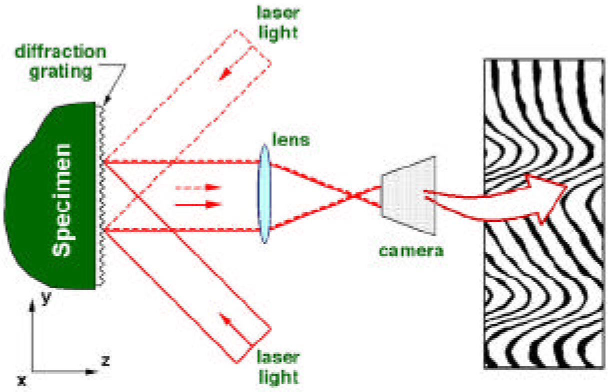

Figure 19. Moiré Schematic

The specimen is deformed causing the diffraction grating frequency to change and warpage appears in the flat wavefronts diffracting from the specimen. An interference fringe pattern, or a contour map of in-plane displacements in direction perpendicular to grating lines, is the result. Another set of incident laser beams are rotated 90 degrees about the z-axis from the above laser light. The beams in the y-z plane are blocked. This is accomplished to measure displacements in two orthogonal directions.

The displacements are obtained through a simple relation as seen in the following equations:

$$U(x,y) = \frac{1}{f} N_x(x,y)$$
$$V(x,y) = \frac{1}{f} N_y(x,y) \qquad (3)$$

(Mollenhauer)

where f is twice the diffraction grating and N_x and N_y are the "fringe orders", a numerical value assignment to each fringe. Due to the small deflections, the strains may be determined through standard small deformation-strain relationships of the derivatives of the above displacement equations. It is possible to perform the analysis either manually or using advanced digital phase-shifting techniques. For this analysis, about 80% of the width in the center of the specimen was used for the calculations. The strains were calculated using a standard numerical differentiation scheme. The detailed information corresponding to the tests can be seen in Table 1. The two tests were averaged to obtain 147 psi (approximately 1 Mpa) and 0.497 for the Elastic Modulus and Poisson's ratio, respectfully. These numbers are the starting point for the finite element modeling analysis. The development of the finite element code is covered in the next chapter and the results covered in the second half of Chapter 4.

Table 1 Tensile Test Details

Test #	Loading	Axial Strain	Transverse Strain	Shear Strain	Poisson's Ratio	Modulus
1	10.528	1686	-789	-112	0.468	143
2A	7.018	1025	-540	-57	0.527	157
2B	14.037	2206	-1156	-106	0.527	146
Average 2	10.5275	1615.5	-848	-81.5	0.527	151.5
Average	10.5278	1650.75	-818.5	-96.75	0.4975	147.25

III: Theoretical Development and FEM Code

Introduction

Now that the ability to have some active and specific control over transverse membrane deflection has been shown, a way to model this behavior would prove useful to discover the many possibilities of control over the membrane without having to accomplish physical tests, especially when the membranes are very large. The commercial market of finite element modeling was investigated to attempt to accomplish the solution of a piezo-silicone membrane mirror. Unfortunately, none of the investigated software packages met all the requirements for this analysis; Some of these requirements included, but not limited to, micron level displacements, a piezoelectric element that suited the purposes of the experiment, and modeling the polymer to behave in the manner of a membrane. Therefore, after extensive theoretical development in beam and membrane finite element modeling, a new mathematical methodology based on fundamental perturbation techniques was born, and given the name *Method of Integral Multiple Scales (MIMS).* (Rogers, 2001)

This technique has selectable precision when applied to a Langrangian represented class of dynamic systems. As a proving ground, MIMS was first applied to a simple linear beam and was shown to produce boundary layer results. The method was applied fully to a finite element approach and the accuracy was shown to be three orders of magnitude greater than standard finite element formulation. This FE methodology was finally applied to nonlinear beam and axisymmetric circular membrane to compare to analytical solutions. (Rogers) At the time the dissertation was completed, the objective was to setup the solutions so they matched the analytical solutions, but was not necessarily representative of the experimental solution.

Beam String

A beam-string is represented by an inner and outer region to describe the deflection. The outer region or the center (i.e. away from the boundary condition) of the beam-string is represented by string equations, while the inner or edge region, is represented by beam equations. An energy-based derivation method is used produced the necessary equations used in this analysis. The details of the total derivation are not included here, but an outline of the method is shown to familiarize the reader with the notation and to setup an example. The literature has the complete derivation in Chapter 3 of Rogers. (Rogers, 2001) A strain-energy representation, the potential energy of an elastic beam is defined by:

$$\boldsymbol{V} = \int_V \frac{1}{2}\{e\}^T\{s\} - \{e\}^T\{s_0\} + \{e_0\}^T\{s\}dV$$

$$+\frac{1}{2}K_0 w_{,x}^2(0,t) + \frac{1}{2}K_L w_{,x}^2(L,t) \qquad (4)$$

where $\boldsymbol{e}$ and s are the strain and stress terms, $w_{,x}$ terms are the slope of the displacements at the boundaries and the K terms are the spring stiffness at the membrane boundary.

The beam's kinetic energy can be expressed as:

$$\boldsymbol{T} = \int_V \frac{1}{2} r(u_{,t}^2 + w_{,t}^2)dV \qquad (5)$$

where r is the density and the u and w terms are the time derivative of the displacements.

Making the assumption of small deflection with respect to overall dimensions, the system's non-conservative forces from a pressure force (P) and displacements (u and w) can be approximated by:

$$W = -\int_x P(w + u_{,x}w - w_{,x}u)dx \tag{6}$$

Analysis of a laminate requires further analysis, seeing as each layer may have independent material properties. The laminate could be reduced to a one-dimensional integro-differential equation when the through-the-thickness strain is assumed to be constant at any cross section. Using Hamilton's Principle,

$$\int_{t_1}^{t_2} (dT - dV + dW)dt = 0 \tag{7}$$

where d is used to represent variation. The following dimensionless variables are defined as:

$$\begin{array}{lllll} \hat{x} = \dfrac{x}{L} & \hat{z} = \dfrac{z}{L} & \hat{u} = \dfrac{u}{L} & \hat{w} = \dfrac{w}{L} & \hat{r} = \dfrac{EI}{L^2 EA}h \\ \hat{P} = \dfrac{PL}{EA}h & \hat{N}_0 = \dfrac{1}{h} & \hat{N}_z = \dfrac{N_z}{LEA}h & \hat{E}A_z = \dfrac{EA_z}{LEA}h & \hat{E}A_{ez} = \dfrac{EA_{ez}}{LEA}h \\ \hat{K}_1 = \dfrac{K_L}{LEA}h & \hat{K}_0 = \dfrac{K_0}{LEA}h & \hat{E}A_e = \dfrac{EA_e}{EA}h & \hat{t}^2 = \dfrac{c_2^2}{L^2}t^2 & \end{array} \tag{8}$$

The variation is carried out and the above dimensionless variables introduced to produce the following equations of motion:

$$u_{,tt} - hu_{,xx} = -2uu_{,t} + \frac{1}{2}(h - 1 + EA_e)\frac{\partial}{\partial x}(w_{,x}^2 - 2u_{,x}w_{,x}^2)$$
$$- 2Pw_{,x}^2 - EA_z\frac{\partial}{\partial x}[w_{,xx}(1 - \frac{1}{2}w_{,x}^2 + u_{,x}w_{,x}^2] \tag{9}$$

$$w_{,tt} - (1 - EA_e)w_{,xx} + r^2 w_{,xxxx} = -2mw_{,t} + (h - 1 + EA_e)\frac{\partial}{\partial x}(ew_{,x})$$
$$+ P(1 - 2u_{,x}) - EA_z\frac{\partial}{\partial x}[u_{,xx}(1 - \frac{1}{2}w_{,x}^2 + u_{,x}w_{,x}^2] \tag{10}$$

$$e = u_{,x} - u_{,x}^2 + \frac{1}{2}w_{,x} \tag{11}$$

These equations must satisfy the following non-dimensional boundary conditions:

$$u_i(0) = u_{i,x}(0) = 0 \qquad w_j(0) = 0 \qquad N_0^2 w_{2,xx}(0) = -K_0 w_{2,x}(0)$$
$$N_0^2 w_{3,xx}(0) = -K_0 w_{3,x}(0) - EA_{ez3} \qquad N_0^2 w_{4,xx}(0) = -K_0 w_{4,x}(0) + EA_{z2}u_{3,x} \tag{12}$$

where i = 3, 4, 5 and j = 2, 3, 4.

At this point, a perturbation solution is sought on a radius of gyration, r, and using the following non-dimensional expansions:

$$t = wt \qquad T_n = e^n t \qquad w = w_0 + ew_1 + e^2 w_2 + ...$$
$$w(x, t, e) = e^2 w_2(x, t) + e^3 w_3(x, t) + ...$$
$$u(x, t; e) = e^3 u_3(x, t) + e^4 u_4(x, t) + ... \tag{13}$$
$$D = D_0 + eD_1 + e^2 D_2 + ... \qquad e = r \qquad D_i = \frac{\partial}{\partial T_i}$$

The string equation is produced by substituting the expansion into the differential equation and collecting powers of e. The coefficient of the lowest power of e produced the following equation:

$$\frac{\partial^2 w_2}{\partial t_0^2} - \left(\frac{1 - EAe}{w_0^2} \right) \frac{\partial^2 w_2}{\partial x^2} = -2 \frac{m}{w_0} \frac{\partial w_2}{\partial t} + \frac{\tilde{P}_2}{w_0^2} \tag{14}$$

After solving this equation for w$_2$, it is noted that only two boundary conditions are satisfied. This is not enough to solve the unperturbed equation. To satisfy the complete set of boundary conditions, it is necessary to examine the original equations in the neighborhood of the boundary. This is accomplished by rescaling x near the boundary. For example, $x = \mathrm{x}/ e$ is how this rescaling is accomplished at x = 0 and $x = (\mathrm{L - x})/e$ at x= 1. Notice that x is zero at x=0, while, if x is any other value, x approaches infinity as e approaches zero. Using Equations 9-11, and following the above procedure, the resultant is:

$$(1 - EA_e) \frac{\partial^2 w_2}{\partial x^2} + \frac{\partial^4 w_2}{\partial x^4} = -2me^2 \frac{\partial w}{\partial t_0} + (1 - EA_e) \frac{1}{e} \frac{\partial}{\partial x} ((u_x - u_x^2 + \frac{1}{2} w_x) \frac{e^2}{e} \frac{\partial w_2}{\partial x}) \tag{15}$$

To complete the solution, the behavior near the boundary must be matched with the membrane solution, using Matched Asymptotics (Rogers, 2003). This identifies the thickness of the boundary layers. The result of this matching leads to the deflection results:

$$\begin{aligned} & u^c(x) = 0 \\ & w^c(x) = e^2 \frac{P_2}{2} (x - x^2) - e^3 [\Gamma_0 (1 - x - e^{-x/e}) + \Gamma_1 (x - e^{-\frac{1-x}{e}})] \end{aligned} \tag{16}$$

where

$$\begin{aligned} & \Gamma_0 = \frac{K_0}{K_0 - N_0^2} [\frac{P_2}{2} + \frac{EA_{ez3}}{K_0}] \\ & \Gamma_1 = \frac{K_1}{K_1 - N_0^2} [\frac{P_2}{2} + \frac{EA_{ez3}}{K_1}] \end{aligned} \tag{17}$$

The K terms are the spring constants defined (with 'hats') in Equation 8 and characterize the torsional spring boundary conditions at the ends of the membrane. N_0 is the tension also defined in Equation 8. EAe_{z3} represents the non-dimensional moment imposed by the piezoelectric layers. Now that the static solution is fully developed for a beam-string, an example solution to observe the effects of some of the variables (material properties or system properties) is completed here before continuing onto the membrane problem.

This is a mini-parametric study of a beam string problem, changing a few of the variables to see the effects. These numbers will be similar to the numbers that will be used in the parametric study of the membrane solution. The code for this problem was written by Rogers in MathCAD. The importance of the results lies in the magnitude of the deflection; therefore, the plots will be quickly talked about for each case. The model is represented by a two layer system (1 membrane, 1 piezo layer); however, this is just a demonstration of the effects of material properties.

The first variable to be varied is the tension term, defined by N_0 in the equations. A few tension values tested are 1, 5, 10, 100, and 1000 N. The voltage condition used is -300 V on the piezoelectric layers, no pressure term, thicknesses of 0.0001 m for both layers, 2.8 GPa and 1.8 GPa for the membrane and PVDF moduli, respectfully. These cases can be seen below in Figure 20-Figure 24, in the order defined above. Both axes are scaled on all the following figures. The abscissa is scaled by the length of the beam (x=x/L) and the ordinate contains the radius of gyration and an actual displacement.

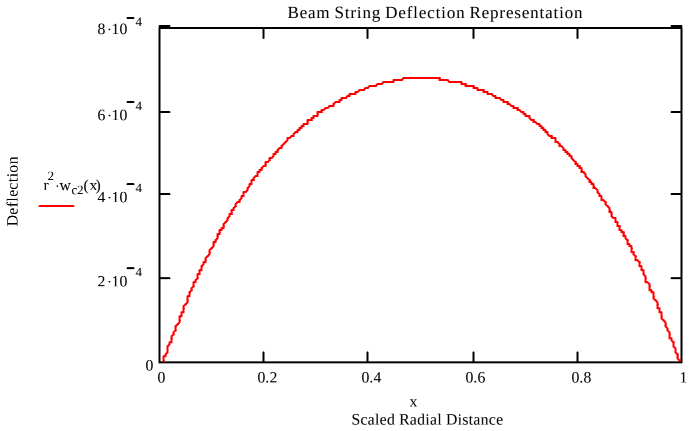

Figure 20. Beam String Deflection for N_0=1

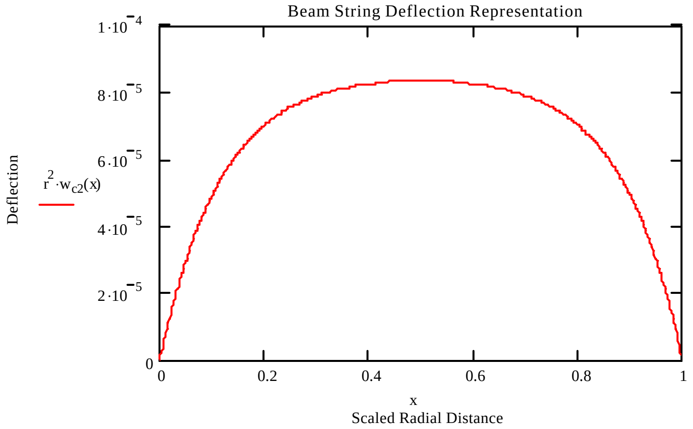

Figure 21. Beam String Deflection (N_0=5)

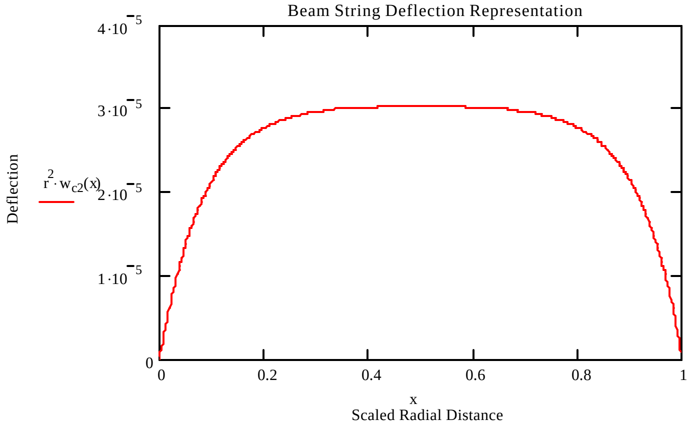

Figure 22. Beam String Deflection (N_0=10)

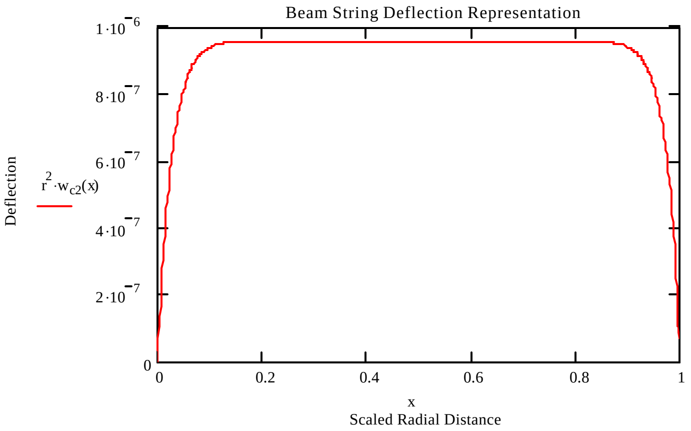

Figure 23. Beam String Deflection (N_0=100)

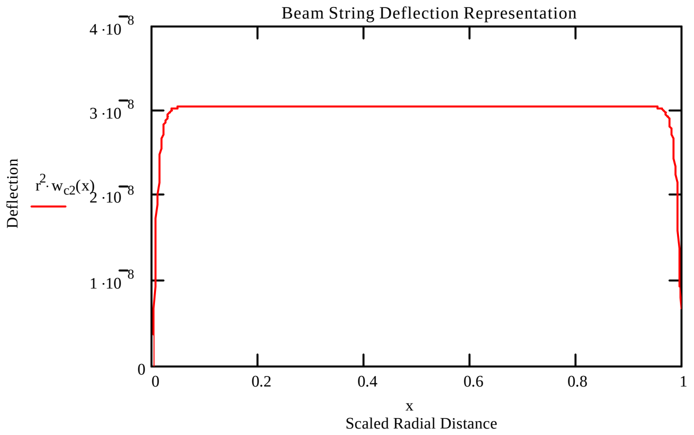

Figure 24. Beam String Deflection (N_0=1000)

Notice how the increase in the tension term decreases the deflection magnitude. This is an obvious effect of the tension applied at the two boundaries. The other effect is that the beam-string initially behaves as a string, where the piezo layer is deflecting the structure in a parabolic shape, with the boundaries only holding to the fixed condition. As the tension is increased, the structure starts to become stiffer and therefore has a very small deflection that occurs across the whole boundary, with a greater slope at the boundary.

The next parameter that is investigated in this study is the thickness. The tension value used was 25 N for this case. It does not have any specific correlation, but was chosen just to have reasonable results for a few of the thickness conditions. The moduli were kept constant as defined above for the tension study. The different thicknesses tested were as follows, along with their percentage related to the "original" thickness: 0.00001 m(1/10th), 0.0002 m(2x), 0.001 m(10x), 0.005 m(50x), and 0.00635 m(.25"). This study was based solely on tria l and error and therefore these thicknesses were chosen as a basis for what might hold in some real cases. Figure 25-Figure 29 show these results.

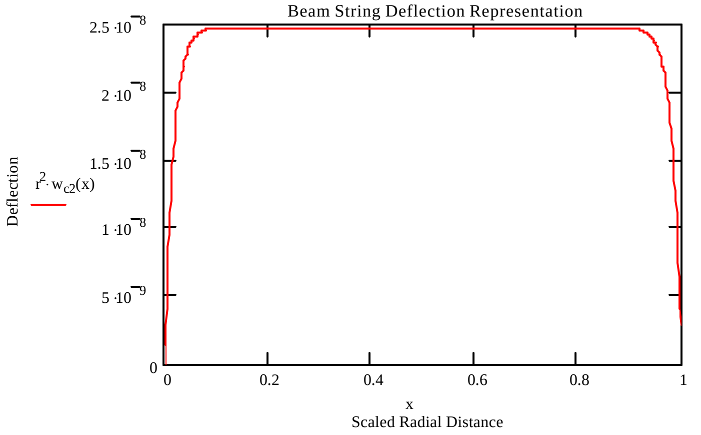

Figure 25. Beam String Deflection (t=1e-5 m)

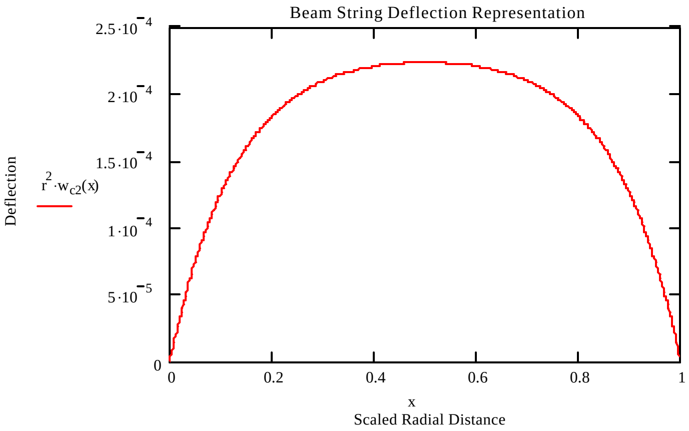

Figure 26. Beam String Deflection (t=2e-4 m)

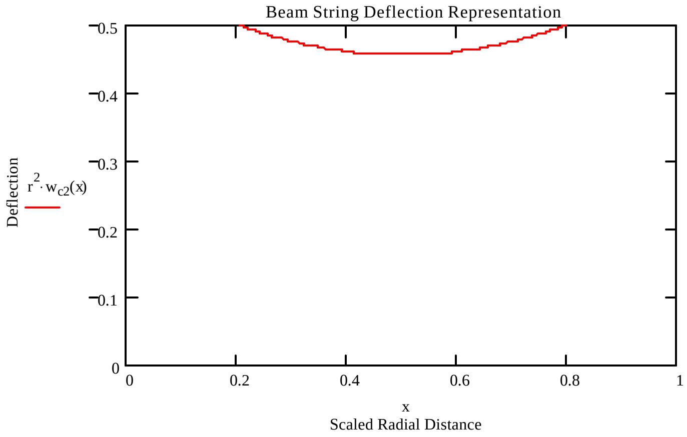

Figure 27. Beam String Deflection (t=0.001 m)

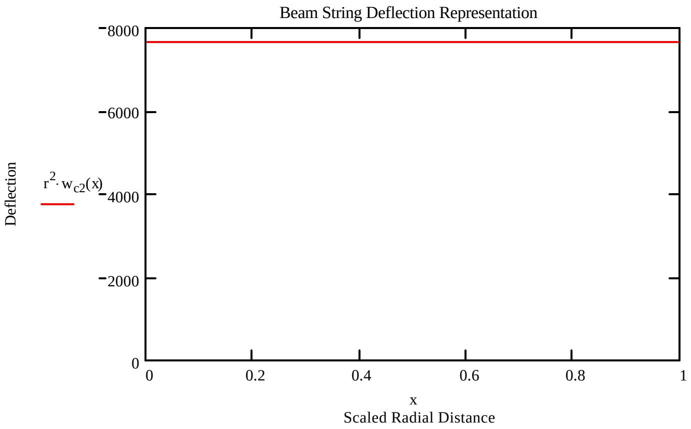

Figure 28. Beam String Deflection (t=0.005 m)

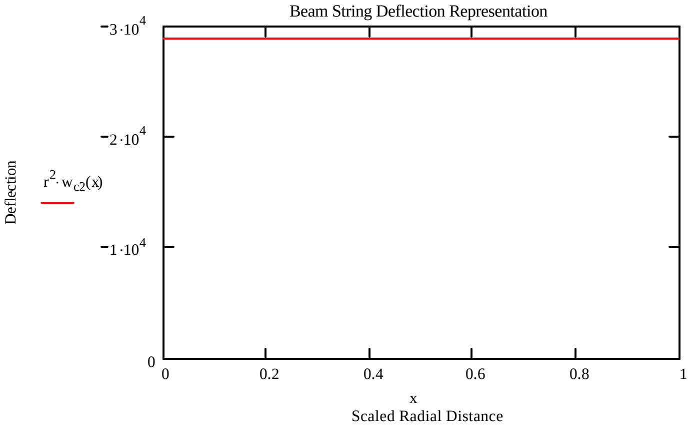

Figure 29. Beam String Deflection (t=0.00635 m)

Notice the quick changes as the thickness increases. This study shows how important it is to know the thickness and how it effects the small epsilon term. The larger thickness causes the epsilon terms to grow to the point that the solution can no longer be considered valid. The first plot for the small thickness possesses very small displacement and the tension seems to have dominance. It behaves as a membrane with the small thickness and a beam as the thickness is increased by an order of magnitude. As the thickness is further increased, the solution starts to blow up. The one with the same order of thickness has a reasonable string-like solution. As soon as the thickness becomes too large, the result stops resembling a beam string and has no real meaning. The reason behind the negative displacement in the thicker membrane is caused by the solution blowing up. The thicker layer seems to cause the solution to produce results of large deflection and the layer pulls the whole system flat. This shows the sensitivity to thickness changes in the non-piezo layer which violated the small perturbation term defined by the radius of gyration. The thickness seems to have to be on an order of 10^{-4} for the other conditions to have a practical result. Once the thickness was increased enough, the solution doesn't maintain an actual result. Now that the system properties have been evaluated, the next step is to test the effects of a material property.

The main material property that should have an effect on the deflection is the modulus of the polymer layer. A range of magnitudes were tested, namely 10^6, 10^7, 10^8, and 10^9 Pa. The piezo layers were maintained at 1.8 GPa. They can be seen below in Figure 30-Figure 33.

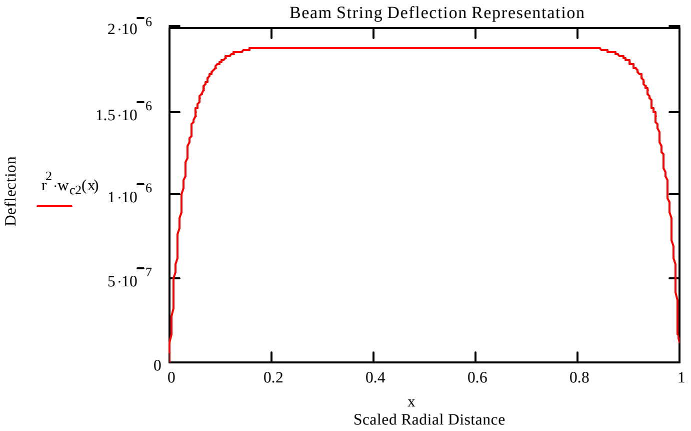

Figure 30. Beam String deflection (E=10^6)

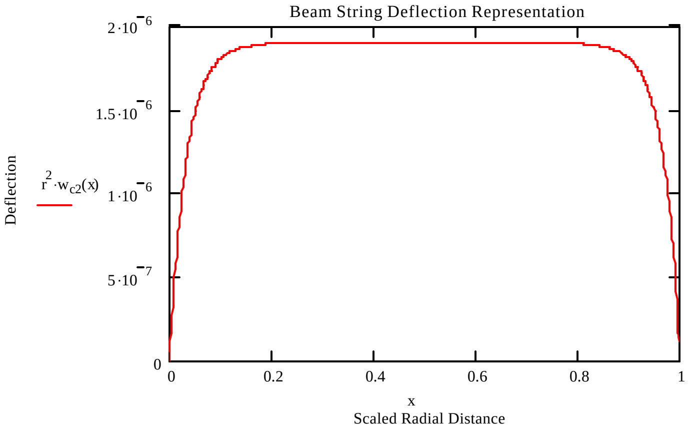

Figure 31. Beam String deflection (E=10^7)

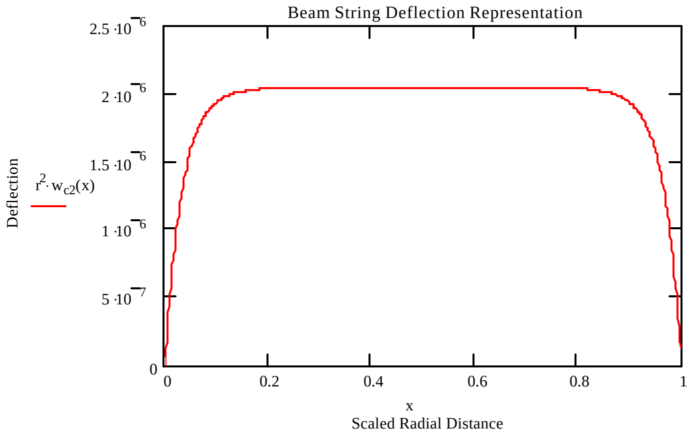

Figure 32. Beam String deflection (E=10^8)

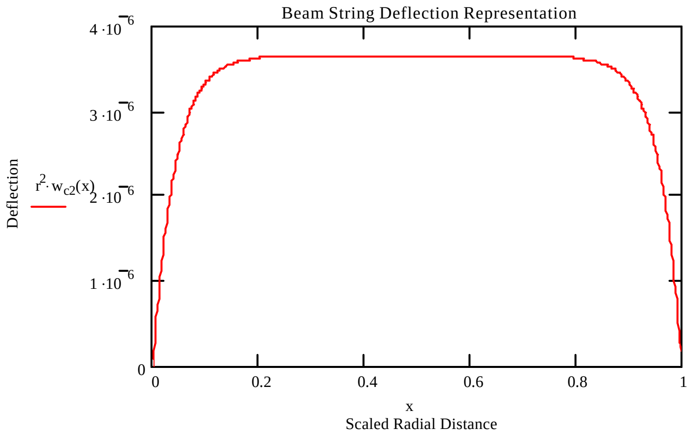

Figure 33. Beam String deflection (E=10^9)

Somewhat surprising is the lack of sensitivity as the modulus is increased. This may just be due to the piezo layer dominating the solution. More investigation will be placed on changing the piezo properties in the membrane solution; however, since the modulus did not affect the deflection solution by much, a larger range of moduli will be studied to see what would happen with different materials.

While all of the above material properties show changes in the deflection order and shape, some of them actually affect the solution in a different manner. Recall, e is a small non-dimensional term that plays a crucial role in the perturbation techniques. This term actually appears in the shape functions used. A large e changes the shape functions; thereby, causing the solution to become unrealistic. The finite element solution is only valid for the small epsilon. This is evident as the thickness was increased and the plots started to have results that are not actually representative of a beam-string solution.

This is a short introduction on the beam problem and proves useful in looking at the next step, the axisymmetric membrane. The whole derivation can be investigated in the literature, although the important points are shown here (Rogers, 2001). Table 2 shows all the different tests in the above parametric study

Table 2 Parametric Study

Test name	Membrane Modulus (GPa)	PVDF Modulus (GPa)	Membrane Thickness (m)	PVDF Thickness (m)--Both layers	Tension	Voltage
Tension	2.8	1.8	0.0001	0.0001	1	-300
	2.8	1.8	0.0001	0.0001	5	-300
	2.8	1.8	0.0001	0.0001	10	-300
	2.8	1.8	0.0001	0.0001	100	-300
	2.8	1.8	0.0001	0.0001	1000	-300
Thickness	2.8	1.8	0.00001	0.0001	25	-300
	2.8	1.8	0.0002	0.0001	25	-300
	2.8	1.8	0.001	0.0001	25	-300
	2.8	1.8	0.005	0.0001	25	-300
	2.8	1.8	0.0635	0.0001	25	-300
Modulus	0.001	1.8	0.0001	0.0001	25	-300
	0.01	1.8	0.0001	0.0001	25	-300
	0.1	1.8	0.0001	0.0001	25	-300
	1	1.8	0.0001	0.0001	25	-300

Plate Membrane Equivalent

Now that the beam-string problem has been developed and a parametric study completed, the next step is to show the development of the model of a thin membrane-like system. This can be accomplished using a plate-membrane, where low bending stiffness results in localized effects. Again, a Langrangian system is used for this development. The equivalent equations related to the beam-string problem will be defined here. (Rogers, 2001)

The potential energy is developed in a cylindrical coordinate system of r-q-z and is seen defined here:

$$\boldsymbol{V} = \int_V \frac{1}{2}\{e\}^T\{s\} - \{e\}^T\{s_0\} + \{e_0\}^T\{s\}dV \tag{18}$$

$$+\frac{1}{2}K_0(q)w_{,r}^2(R,t)$$

The K term represents a torsional edge spring, which was incorporated into the equations for need if there is a flexible boundary. The potential energy can be rewritten in terms of the strain relations for the laminate. The kinetic energy can be represented by:

$$\boldsymbol{T} = \int_V \frac{1}{2}\, r(u_{,t}^2 + v_{,t}^2 + w_{,t}^2)dV \tag{19}$$

Assuming constant through-the-thickness strain, the system can be collapsed into a one dimensional integro-differential system. The resulting equations of motion become:

$$\begin{gathered} rhu_{,tt} - EH\frac{1}{r}\{[r(e_r + ue_q)]_{,r} + \frac{1}{2}(1-u)e_{rq,q} - e_q - ue_r\} - \frac{1}{r}[N_r - N_q] = \\ EH_z\frac{1}{r}\{\frac{1}{r^2}w_{,qq} + \frac{1}{r}w_{,r} - [rw_{,rr} + u\frac{1}{r}w_{,qq}]_{,r} - (1-u)[\frac{1}{r}w_{,rq} - \frac{1}{r^2}w_{,q}]_{,q}\} \end{gathered} \tag{20}$$

$$\begin{aligned}&rhv_{,tt}-EH\frac{1}{r}\{[(e_q+ue_r)]_{,q}+\frac{1}{2}(1-u)[e_{rq}+(re_{rq})_{,r}\}=\\&EH_z\frac{1}{r}\{[\frac{1}{r^2}w_{,qq}+\frac{1}{r}w_{,r}+uw_{,rr}]_{,q}+(1-u)[\frac{1}{r}w_{,rq}-\frac{1}{r^2}w_{,q}+(\frac{1}{r}w_{,rq}-\frac{1}{r^2}w_{,q})_{,r}]\}\end{aligned}\tag{21}$$

$$\begin{aligned}&rhw_{,tt}-N_r\frac{1}{r}(rw_{,r})_{,r}-N_q\frac{1}{r^2}w_{,qq}-2N_{rq}\frac{1}{r}w_{,rq}+D\nabla^4w=\\&EH\frac{1}{r}\{[rw_{,r}(e_r+ue_q)]_{,r}+[\frac{1}{r}w_{,q}(e_q+ue_r)]_{,q}+\frac{1}{2}(1-u)[(w_{,q}e_{rq})_{,r}+(w_{,r}e_{rq})_{,q}]\}\\&EZ\frac{1}{r}\{[(e_q+ue_r)+rw_{,r}[w_{,rr}+u(\frac{1}{r}w_{,r}+\frac{1}{r^2}w_{,qq})]+(1-u)\frac{1}{r}w_{,q}(w_{,rq}-\frac{1}{r}w_{,q})]_{,r}\\&+[(1-u)\frac{1}{r}e_{rq}+\frac{1}{r}w_{,q}[\frac{1}{r}w_{,r}+\frac{1}{r^2}w_{,qq}+uw_{,rr}]-(1-u)\frac{1}{r}w_{,r}(w_{,rq}-\frac{1}{r}w_{,q})]_{,q}\\&-[r(e_r+ue_q)]_{,rr}+[\frac{1}{r}(e_q+ue_r)]_{,qq}+(1-u)e_{rq,rq}\}\end{aligned}\tag{22}$$

The following boundary conditions are applied to obtain a solution:

$$\begin{aligned}&u(R,q)=0\qquad u_{,r}(R,q)=u_{,q}(R,q)=0\qquad u(r,q)=0\\&v(R,q)=0\qquad v_{,r}(R,q)=v_{,q}(R,q)=0\qquad v(r,q)=v(r,q+2p)\\&v_{,q}(r,q)=v_{,q}(r,q+2p)\\&w(0,q)=a;a<\infty\qquad w_{,r}(0,q)=-w_{,r}(0,q+p)\\&D[rw_{,rr}(R,q)+u(\frac{1}{r}w_{,qq}(R,q)+w_{,r}(R,q))]=\\&N_{rz}-EZ_e(R,q)+K(q)w_{,r}(R,q)\\&+EZr[(u_{,r}(R,q)+\frac{1}{2}w_{,r}^2(R,q))-u(\frac{1}{r}u(R,q)+\frac{1}{r}v_{,q}(R,q)+\frac{1}{2}\frac{1}{r^2}w_{,q}^2(R,q)]\end{aligned}\tag{23}$$

These systems of equations are put in non-dimensional form before applying the expansions just like the beam-string:

$$t=wt\qquad T_n=e^ut\qquad w=w_0+ew_1+e^2w_2+...$$

$$u(r,q,t;e) = e^3 u_3(r,q,t) + e^4 u_4(r,q,t) + \ldots$$

$$v(r,q,t;e) = e^3 v_3(r,q,t) + e^4 v_4(r,q,t) + \ldots \qquad (24)$$

$$w(r,q,t;e) = e^2 w_2(r,q,t) + e^3 w_3(r,q,t) + \ldots$$

$$D = D_0 + eD_1 + e^2 D_2 + \ldots \qquad e = r^*$$

$$h = \frac{1}{e} h_1 \qquad D_i = \frac{\partial}{\partial T_i}$$

From this point, axisymmetric conditions can be applied, thus removing all θ dependence. It is also assumed $EH_{eq} = EH_{er} = EH_e$, meaning bidirectional piezoelectric materials are being used, which is also true for the PVDF. The system is represented by membrane equations in the center of the system, while near the edges they are beam equations (boundary layer). Once all this procedure is completed, the time dependency can be removed to yield a closed form static solution, much as above in the beam-string problem:

$$\begin{aligned} w^c(r) &= e^2 \frac{P_2}{4}(1-r^2) + e^3\left\{\frac{K}{K-1}\left[\frac{P_2}{2}+\frac{EZ_{e3}}{K}\right]\left(e^{-x}-1\right)\right\} \\ &+ e^4\left\{\frac{P_2}{4}h^2(1+u)EH_{e2}(1-r^2)\right\} \\ &+ e^4\left\{\frac{K}{K-1}\left[\frac{2K-3+2u}{K-1}\left(\frac{P_2}{2}+\frac{EZ_{e3}}{K}\right)-\frac{EZ_{e3}}{K^2}\right]\left(e^{-x}-1\right)\right\} \end{aligned} \qquad (25)$$

The e term for this case needs to remain very small (<.01 for most cases). The static displacement for a thin membrane plate is now fully developed. The finite element approach was also developed by Rogers (2001); however, it will not be discussed here, but the shape functions are scaled in a similar fashion to the previous parameters as a function of e. The Langrangian expansion is also grouped into an e-order. Applying Euler's equations to the selected Langrangian element produces the system of finite element equations that are directed to the desired solution. Rogers and Agnes (2003) have performed a complete stiffness matrices development applying C^1 shape functions. The e function is quickly noticed to be a dominating player in the finite element solution and thereby kept very small for accurate results.

More specifics about the program, as well as parts of the code are included in the Appendices. As stated before, the above theoretical development is a synopsis of the work completed under another study and only serves as a guide for how development of the equations for a membrane was created and the steps needed to program a new finite element code that can handle the small displacements involved with a mirror system as defined.

IV: Results and Discussion

Introduction

Now that the development of the analytical solution to the axisymmetric membrane plate has been shown and the finite element method defined by Rogers discussed, it is time to run solutions for the membrane. The beam-string example run in the previous chapter illustrates the need to perform a parametric study based on some of the material and system properties throughout different ranges. This parametric study is unrelated to the experimental study from Chapter 2; however, the study that follows this compares the finite element solution with the experimental results. It is designed to demonstrate how each material or system property affects the solution independently. The input properties (material and system) may affect the solution drastically and therefore a parametric study was designed to investigate these effects.

Another study completed is the comparison of the reduced experimental results from Sobers and the finite element solution based on realistic material properties. This study is to look at the capabilities of the finite element program in comparison to actual real world results. This can serve as an avenue to find the strengths and limitations of the program to see what can be completed in the future to improve applicability. Before proceeding into the results of these studies, a short explanation of how they are laid out follows.

Zernike Coefficients

As stated numerous times throughout this thesis, the deflection of the membrane is very small. In the optical community, it is common to describe the wavefront shape, the deviation from the planar and perpendicular, in terms of Zernike polynomials, a polar coordinate oriented system. Through the use of a multiplier and a polynomial with radial and angular description of each location on a wavefront, the wavefront deformations can be represented. These polynomials are unique and possess desirable properties because of their orthogonality. This provides the opportunity to sum the terms in the following fashion for the wavefront (W):

$$W(r,q)=\sum_{r}^{L}A_r U_r(r,q) \tag{26}$$

where A_r is the Zernike coefficient and U_r represents the Zernike polynomials.

ρ represents the distance from the center of the membrane, while θ is the angle from the positive y-axis moving in the clockwise direction. Many texts have defined the Zernike polynomials in different orders. Table 3 below is a portion of the 35 Zernike numbers used in the experimental thesis described in Chapter 2. The Zernike polynomials used in the finite element code in Chapter 3 were ordered in a slightly different way. This was not a concern since it is the combination of all Zernike polynomials that defines the wavefront; therefore, when the same polynomials are included in the final formulation the result is the same.

Table 3: Zernike Polynomials

Zernike number	Zernike Polynomial	Meaning
1	$r \cos q$	Tilt
2	$r \sin q$	Y axis tilt
3	$2r^2$-1	Defocusing
4	$r^2\cos 2q$	Astigmatism with axis at +/- 45 deg
5	$r^2\sin 2q$	Astigmatism with axis at +/- 0 or 90 deg
6	$(3r^2-2)\ r\cos q$	Primary coma along y axis
7	$(3r^2-2)\ r\sin q$	Primary coma along x axis

8	$6r^4-6r^2+1$	Primary spherical aberration
9	$r^3\cos(3q)$	Triangular astigmatism, base on y axis
10	$r^3\sin(3q)$	Triangular astigmatism, base on x axis
11	$(4r^2-3)\ r^2\cos2q$	Secondary Astigmatism x
12	$(4r\ r^2-3)\ r^2\sin2q$	Secondary Astigmatism y
13	$(10r^4-12r^2+3)\ r\ r\cos q$	Secondary coma x
14	$(10r^4-12r^2+3)\ r\sin q$	Secondary coma y
15	$20r^6-30r^4+12r^2-1$	Secondary Spherical

Reduced Experimental

As explained in Chapter 2, the WaveScope® exports raw data vectors and calculates the Zernike coefficient for each polynomial based on an approximation program. The data was exported to MATLAB®, which was used to create the figures. Figure 34 is a sample of the Zernike plots, both in 3-D plot and in a contour plot for a 300 volt differential in the center 3mm of the membrane.

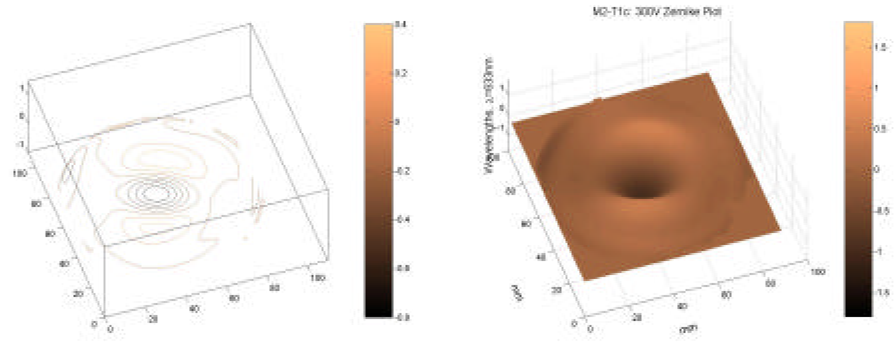

Figure 34. 300V Zernike Plots

The wavefront produced from the raw data can be seen here in Figure 35. Notice the similarities in the general shape the raw data and Zernike plots.

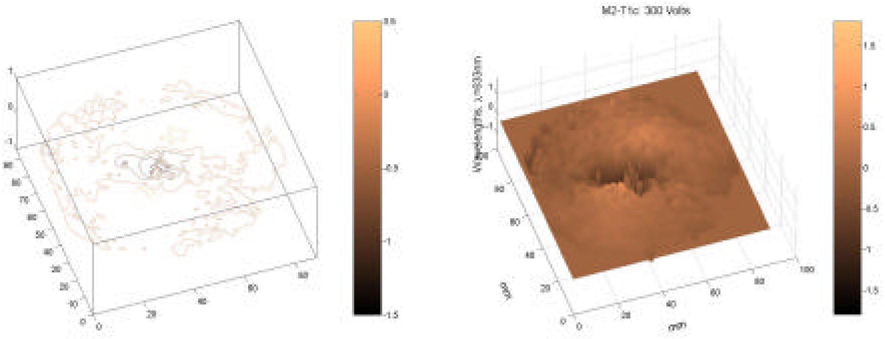

Figure 35. 300V Raw Data

As seen in the surface plots of the Zernike and raw data above, it is seen that the polynomial fit for 35 Zernike numbers doesn't cover all the small peaks and valleys that is seen in the raw data; however, the general shape (center valley shape and size) is captured, which is enough to describe the wavefront for most applications. The Zernike plot could therefore be considered an accurate representation of the mirror wavefront. The majority, 30 of 35 to be exact, of the Zernike polynomials are not symmetric terms, as a result of the angle dependence. It was determined early on in the experimental problem to define the piezoelectric actuation zones in a symmetric layout with other zones that could be activated with asymmetric results. This was seen in the 7 actuation zones defined in Chapter 2 for M2. The center zone 7 was activated for most voltage conditions and axisymmetric solutions were therefore produced.

Unfortunately, the solution still had some asymmetric effects; however, the terms corresponding to these 30 terms as a whole happen to be a smaller order than the 5 symmetric terms. This can be seen first in Figure 34 above, as most of the concentration on the contour plot is in the center section, the zone activated. There is some deflection in other areas, but as can be seen in the reduced Zernike contour plot in Figure 36, the reduced data is representative of the full Zernike data set. Obviously, the two contour plots are not exactly the same, implying that there is some non-axisymmetric solution in the above case. This was known previously, as is evident in the Zernike coefficients of the 30 non-axisymmetric terms; however, the effects of the 30 terms need to be investigated to see how large they are in relation to the other 5 terms.

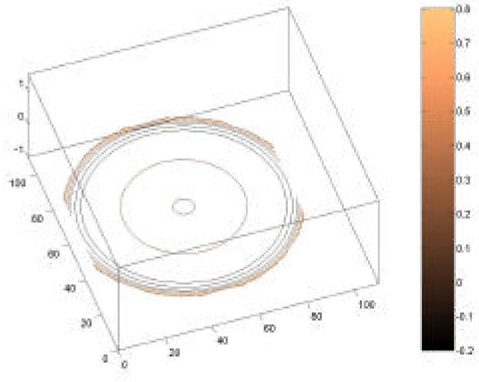

Figure 36. Symmetric Contour Zernike Plot

This investigation was completed using the finite element code to plot out a few cases of the asymmetric solution. This plot is shown here in Figure 37. On all the following plots the center of the membrane is on the right hand side. This applies from now until the end of the paper. The plot corresponding to the symmetric solution is included to show the difference in order. Recall the ordinate is defined in wavelengths of light (value multiplied by 633 nm). These solutions provide an insight and create some questions into where the difference in the wavefront comes about.

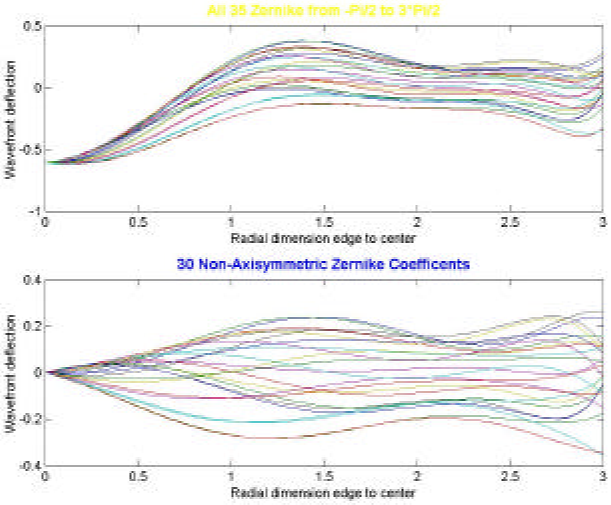

Figure 37. Non-Axisymmetric deflections

Figure 37 represents the experimental non-reduced solution for all 35 Zernike numbers and the 30 non-symmetric polynomials for a number of radial lines at different angles from the y axis. Both of these are included to show how much of an effect the non-symmetric polynomials add (bottom plot) in comparison to the whole deflection (top plot). The bottom plot has approximately half the order of the top one. The value of the 30 asymmetric Zernike polynomials is a fraction, albeit a large fraction, of the symmetric solution, so it shows that eliminating these terms is quite a leap of faith. An asymmetric solution comparison would prove to be more useful, but the capabilities of the finite element code only allow axisymmetric solutions; therefore, the experimental results have to be reduced to this level of axisymmetric to be checked against the finite element solution.

Figure 38 is the 5 symmetric Zernike polynomials plotted out to see the order of the center deflection in comparison to the non-symmetric.

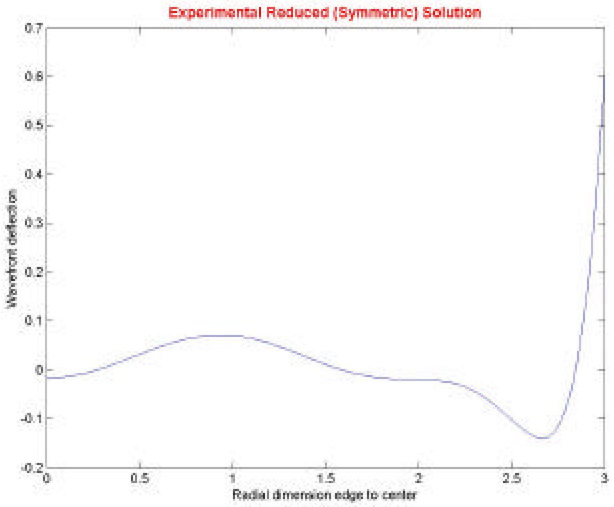

Figure 38. 5 Symmetric Deflections

It is noticed that the effect of these terms is not completely insignificant, causing large fractions of a wavelength in wavefront difference. Since this information comes from an experiment, there could be a multitude of factors that lead to this wavefront shape. One idea for this effect may lie in the initial wavefront caused by manufacturing. The casting process was not performed under the most ideal conditions, i.e. not in clean room conditions or the process of removing the air bubbles with a dental pick. This effect may be shown in a 0 V case, as shown in Figure 39. The scale for this zero voltage case is very small (10^{-3} l), so the solution is nearly zero everywhere, but it is noticed that it isn't exactly zero at the edge. Remember that these plots for the experimental correspond more to the wavefront and not just the deflection, so this part of the membrane was actually a hill compared to a flat wavefront.

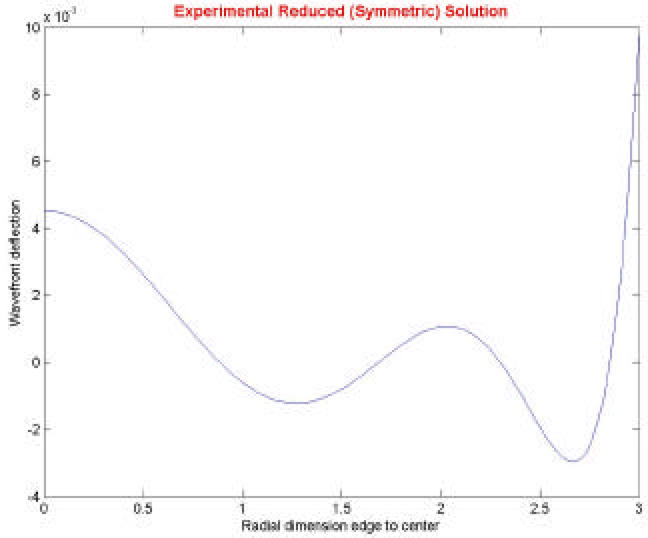

Figure 39. 0V Reduced Experimental Deflection

Sobers had taken action to avoid this effect by "subtracting" out the 0 V information from each of the plots. Unfortunately, it was shown by Sobers that there are residual effects from applying voltages, so there cannot be any guarantee that all the effects of the material is eliminated in the solution.

Another possibility resides in the layout of the piezoelectric zones. Sobers mentioned M1 may have had a "leak" from one activation zone to another. M2 didn't seem to have this effect; however, the leads to the center zone and other zones may affect the solution to create non-axisymmetric deflections. The other component of this idea is that the membrane is a continuous surface and the axial effects of the bi-directional piezoelectric layer may actually cause some deflection that changes other areas of the membrane in a non-axisymmetric way. The last part of this effect is the process of etching the piezoelectric layer, meaning they may not have been perfectly etched; therefore, causing some leak over or shape change in the membrane.

While these above ideas may not be the only reasons or may not be the actual reason, they demonstrate that when dealing with very small deflections, many factors may lead to errors in the solution. It may be possible and necessary to ignore some of these errors. The motivation behind carrying out this exercise was to show that the axisymmetric polynomials provided a representative solution to the full solution. With this being the case and the reduced solution produced, the next step of employing the finite element code could be prepared to process different conditions that could be then compared to the experimental; however, as stated before, the material properties are crucial to the solution.

Parametric Study

The finite element code has been shown to be very sensitive to the e term and can therefore have solutions that are no longer representative of the analytic solution or the experimental. This parametric study will investigate how the solution responds to various changes in the input properties, namely the boundary tension (N), thickness (t), Modulus of Elasticity (E) and element size, determined by the number of elements used. The membrane is assumed to have a constant radius throughout all of these studies of 3”, which is representative of the experimental membrane.

The first variable tested is the tension at the boundary. This term is a non-dimensional force term represented by pulling on the membrane on the outside boundary and in reality is caused by the stretching of the membrane described in Chapter 2. This is an unknown, unmeasured value. There may be ways to obtain this value through a vibration test or other method, but for sake of this study this was not completed. During this test, the first membrane simulation to be tested is the case for a Kapton-PVDF layup, which is not the membrane that was experimentally tested, but serves as a benchmark to test various properties. The Kapton has material properties of 406 ksi, 0.006" and 0.3 for modulus, thickness and Poisson's ratio, respectfully. The PVDF is modeled with 261 ksi, 0.003" and 0.3 for the same properties. Nine elements across the radius were used, giving an element size of approximately 1/3". A 300 V differential is supplied to an approximate 3 cm center "circle" in the PVDF layer.

Interestingly, the tension has a major effect on the total solution. A small tension of 0.1 produced a center deflection of 7000 l or roughly 5 mm, which would be a visible deflection and not reality. Figure 40 shows this deflection plot for this condition of N. Observe the negative deflection represented by this N value. This is one of the quirks of the tension that will be discussed shortly.

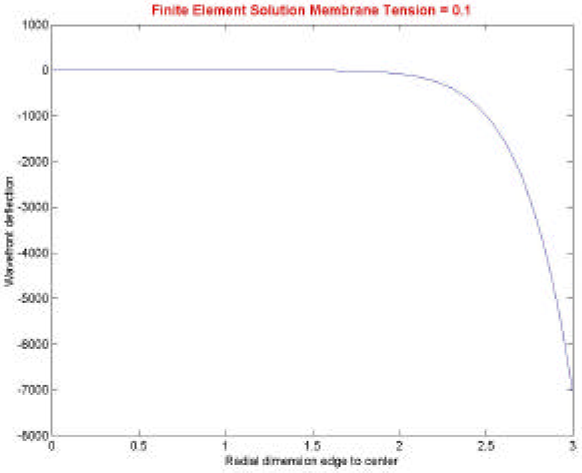

Figure 40. Membrane Deflection (N=0.1)

Intuitively, on the other end of the scale (a very large N), the solution should and does show very small deflections. This is demonstrated for an N equal to 10^9. For all intents and purposes, the deflection produced by this N is nearly 0 (order is 10^{-6} l). For this large tension, the deflection is now positive, as seen in Figure 41.

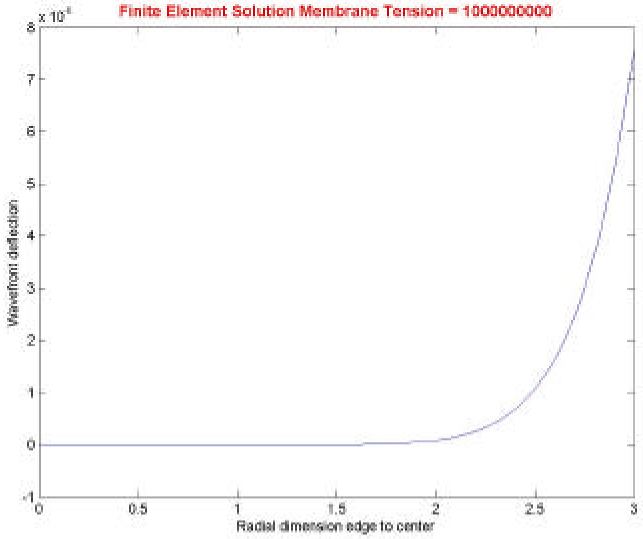

Figure 41. Membrane Deflection (N=10^9)

The change in deflection sign may be explained in the fact that the tension is in a few of the non-dimensional terms, therefore mathematically, there could be a point where the tension can change the non-dimensional terms enough to cause the deflection to flip. Therefore, the next part of this study is investigating this phenomenon. A few values were chosen to have both a negative and positive deflection. Just a few representative cases are displayed here. The following Figure 42 represents tensions of 2500 on the top and 10,000 on the bottom.

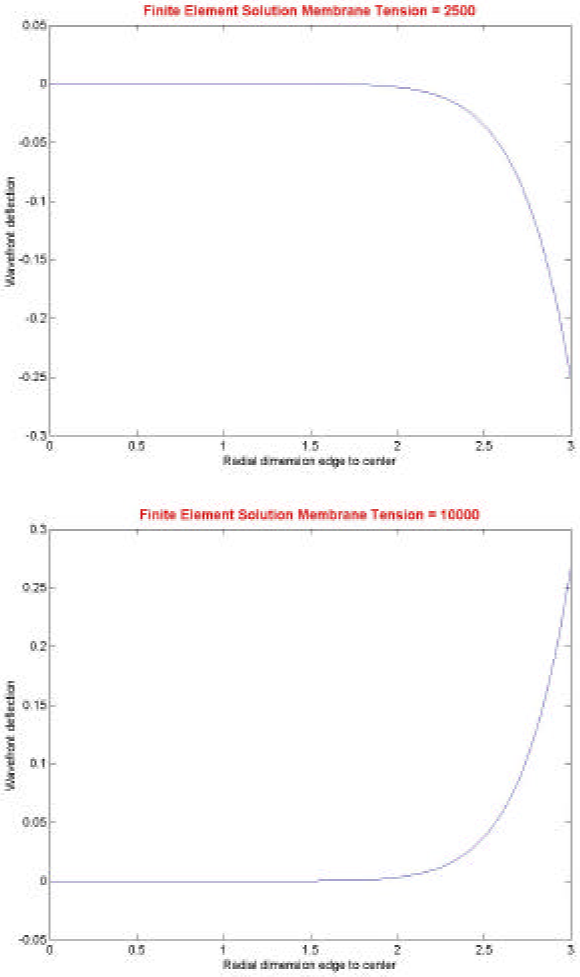

Figure 42. Membrane Deflection (N=2500, 10,000)

These are shown mainly because they have the same magnitude of deflection, but are opposite in sign. Therefore, there is definitely a snap through point in between these two values.

Before investigating the actual point of this happening, a few more values were run to see if another "singularity" existed to produce another result of snap through. Although not every case was investigated, enough runs were completed to show that once above the initial snap through point, up to the 10^9 case, the deflection never again became negative. This may be seen in Figure 43 for the tension equal to 25,000 and the deflection starts to become small as it approaches very small values for much larger N values. This phenomenon is purely a mathematical one that comes about from the non-dimensionalzing of the input variables. There is not likely to be a physical representation.

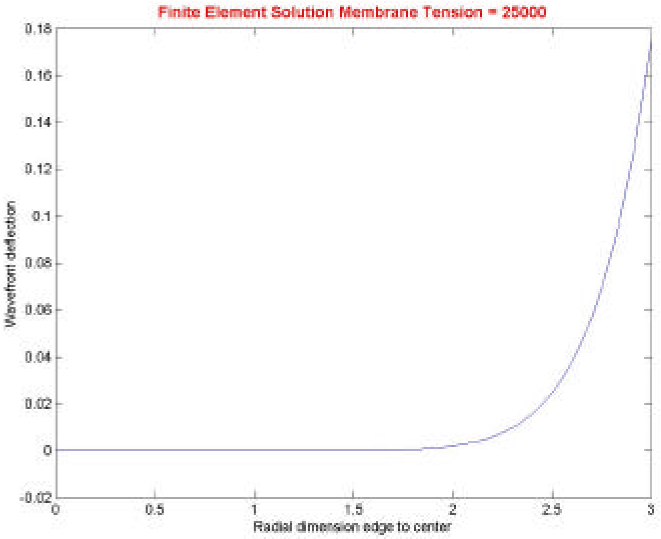

Figure 43. Membrane Deflection (N=25000)

The snap through point is of some interest, since it represents some sort of singularity in the code that might warrant further investigation, if the code is ever modified or enhanced. A manual convergence study was completed. A middle point between 2500 and 10,000 was chosen, the program run a few times until it was noticed that the deflections were becoming very small. One more case was run at N equal to 3242.5. Figure 44 shows this deflection plot.

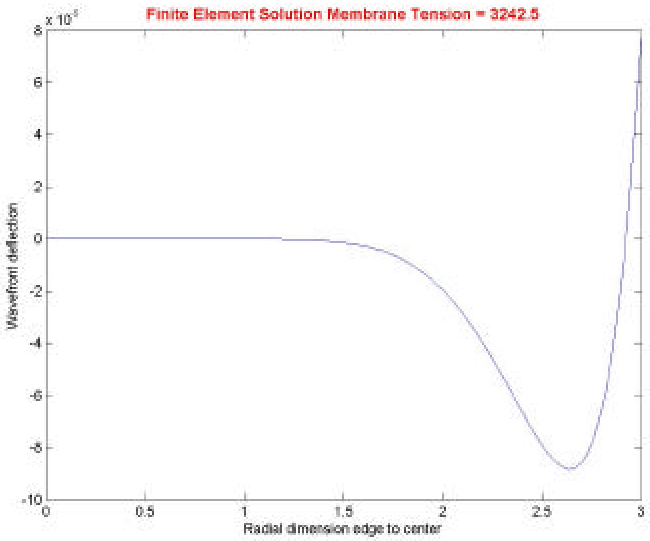

Figure 44. Membrane Deflection (N=3242.5)

The piezoelectric element in the program's code and the non-dimensioning of the terms result in the flip effect and this dip at this value. The tension at the edge should reduce the deflection as it is increased, but it doesn't seem like it should cause an opposite deflection. The deflection scale on this plot is on the order of 10^{-5} λ ; therefore, this is essentially no deflection. The dip negative before the upward deflection is probably just an anomaly that is inherent in the code. An intermediary study at this point may prove to yield some information on the tension in regard to some of the other material properties.

Would a change in the thickness of the PVDF layer or the modulus of either layer change the point where this deflection flip happens? The thickness of the PVDF layer was reduced to $3x10^{-5}$ in and this created changed the point of flip. This order of the thickness is more realistic, as will be seen in the actual comparison to experimental results later in this chapter. Increasing the PVDF modulus to the order of 10^{9} has a similar effect of eliminating the anomaly. This goes to show that the non-dimenional terms are easily modified to change the flip value of tension. Since the modulus and thickness have some control over the solution, they warrant further study. Both plots can be seen in Figure 45.

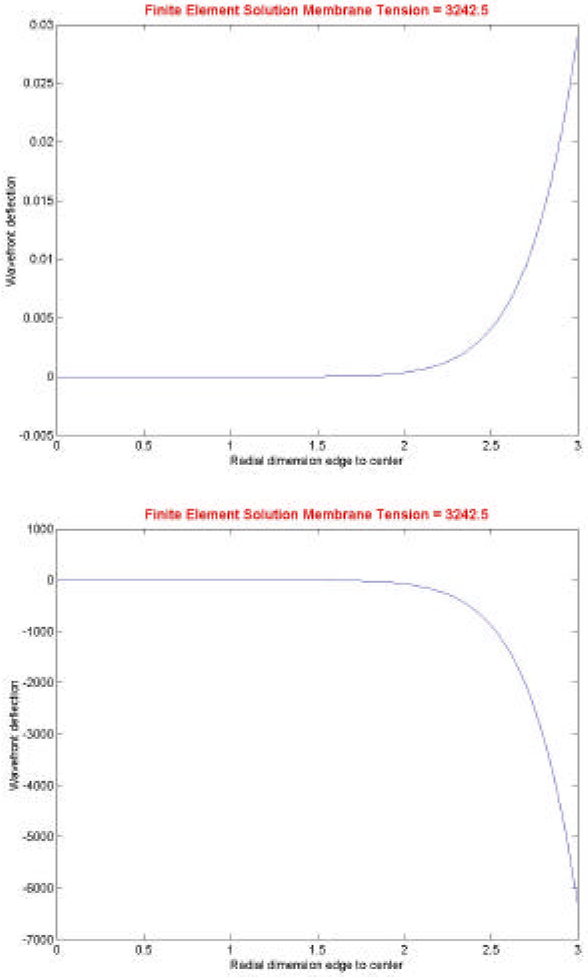

Figure 45. Anomaly Plots ($t=3x10^{-5}$ and $E_{PVDF}=10^{9}$)

This unknown quantity of tension has quite a bit of control over the final solution. With that said, there are ranges of N values that would make more sense than others. Obviously, the small value near zero and the very large value produce poor results and do not have physical significance, i.e. nearly no tension for N equal to 0.1 and a tension where the epoxy would fail for the 10^9 case. The middle case is also not an acceptable tension; therefore, tension could almost be considered a subjective variable that could be modified slightly to produce reasonable results. For most ranges of tension, the general shape of the deflected membrane was the same; consequently, N may be treated as if it were a linear scale factor in many cases. Not having a secure value for N is not an ideal situation, of course, but there may be a way to obtain a reasonable value for it as the results are compared to the experimental later in this chapter. Experiments may be designed to test and discover this number in the future.

The tension does play a major part in controlling how much deflection occurs in the membrane, but it is not one of the variables that controls the critical factor of e mentioned before. This is directly influenced by the thickness of the membrane layer. This study investigates the changes in that thickness within a relatively tight range. All properties are kept the same as the tension study above and a few tensions were investigated for each thickness. The thickness tested were +/-10, 30 and 50% from the original value of 0.006" or 0.0066, 0.0078, and 0.009", respectfully.

The solution in this range of thicknesses was very sensitive. The best example of this was for a tension that was small (N = 100). Figure 46 below is this case for 0.0066" and 0.009". As it is seen, the smaller thickness produced approximately 35 l of deflection and the thicker membrane has over 5000 times that displacement. This has to be caused by the perturbation epsilon value growing too large for the integral. The effects of all the terms together lead to the integral solution to blowing up.

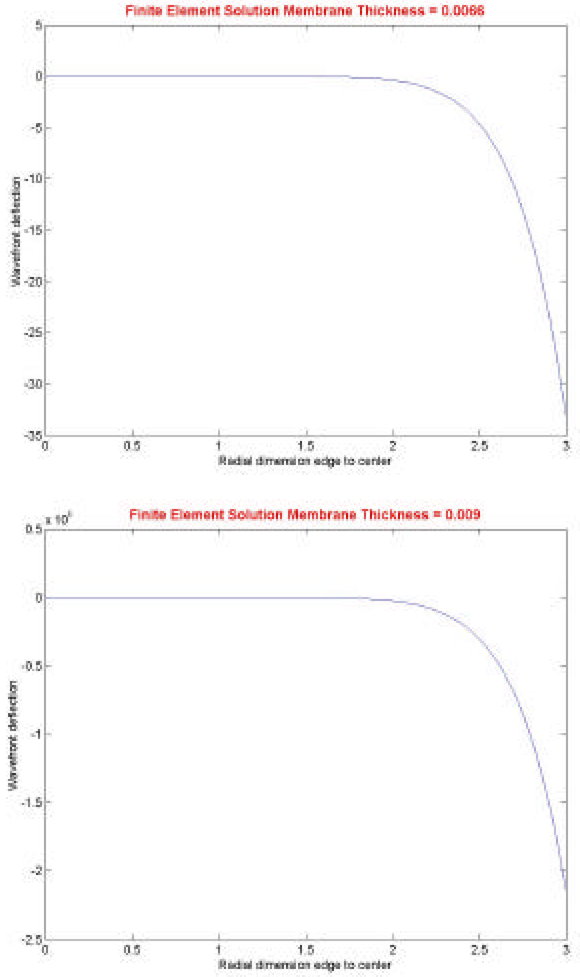

Figure 46. Membrane Deflection (t=0.0066 and 0.009)

For other values of tension, the result wasn't quite that much difference, but there still was still on the order of 4-5x for N=1000 and 5000. Besides the scale in this thickness range, there isn't much else to change; therefore, the other plots at different tensions values are not included in the paper. While these thicknesses are not representative of the experimental membrane, they are within one order of magnitude of the thickness of other membranes that are being applied to optics project in other areas in the USAF (Marker, 2002).

Since the e term is directly related to the thickness, it makes sense the solution remains sensitive to the changes in thickness, since the perturbation technique using MIMS diverges with increasing e. This is the extent of the study dealing with the thickness until later when it will be compared to the experimental results.

Up to this point, only system properties have been investigated. They are quantities that could be changed through methods other than changing the actual material. What effect does the material have on the solution? There are basically two material properties that can be modified for the static solution, namely Young's Modulus and Poisson's ratio. The next part of this study investigates different moduli, representing changing the material being tested. During this test, the material may not be related to an actual material, but is designed as method to see the effects on the solution.

The tests involved here basically used a range of E values from 100 to 10^6 psi for the membrane. The modulus of the PVDF layer was given three different values for each value of membrane moduli. All other material and system properties were kept the same as the original tension tests and the tension was given a value of 1000. The first test was using a PVDF layer with 261 ksi for its modulus. This test produced results that behaved similar to the change in tension. At one point, the solution flips from negative to positive deflection and there happens to be a solution where there is a dip, similar to the case for tension. The solution flips near an E value of 240 ksi, with the dip noticed at 239 ksi. Figure 47 shows both these plots. Compare the 240 ksi case with Figure 48 below.

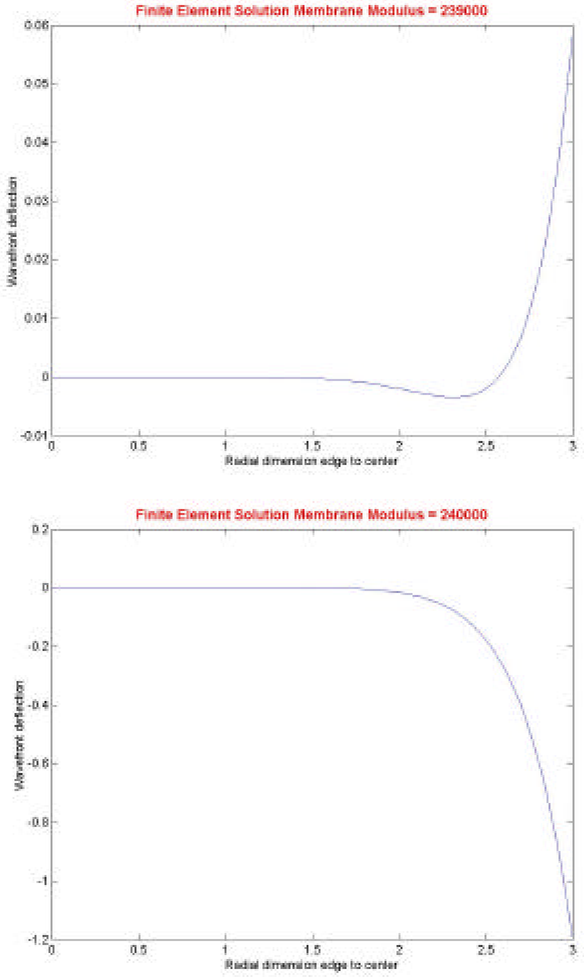

Figure 47. Membrane Deflection (E_{mem} = 239 and 240 ksi)

The change in E seems to determine when one layer dominates over the other one. Getting far enough from the “flip” value, it is noticed the E value changes are not affecting the final solution drastically. This can be seen in the Figure 48, which has E=100 psi on the left and E=10 ksi on the right. Observe that the two orders of magnitude difference in the modulus only lead to a deflection change of a small fraction of a wavelength.

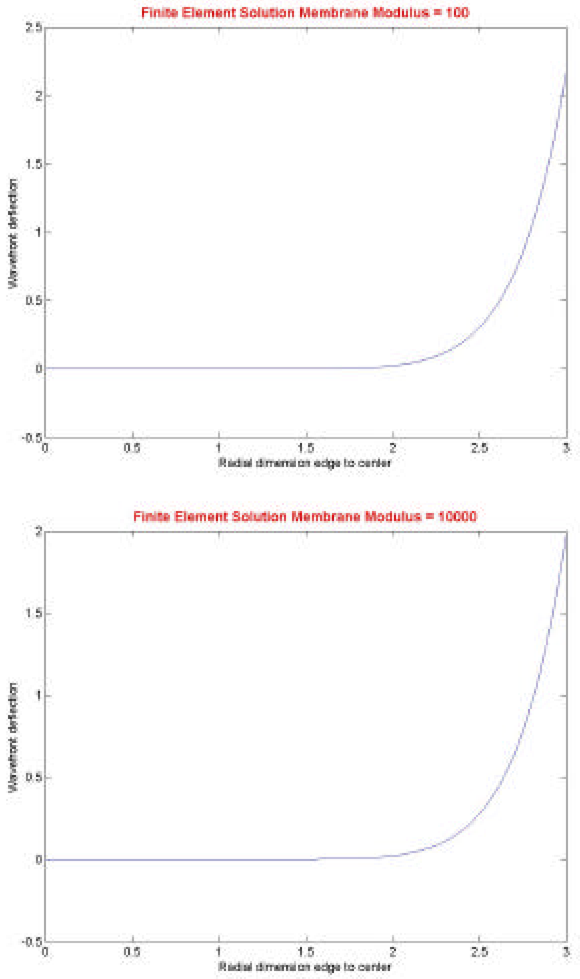

Figure 48. Membrane Deflection (E_{mem} = 100 psi and 10 ksi)

This phenomenon becomes more prominent when the PVDF modulus was increased to 2.8 Msi and 2.8 Gsi. Until the modulus of the membrane layer was increased to similar orders, the solutions remained nearly the same for all membrane moduli, as seen in Figure 49, plots for E = 100, 10000 and 100000 from left to right for 2.8 Msi.

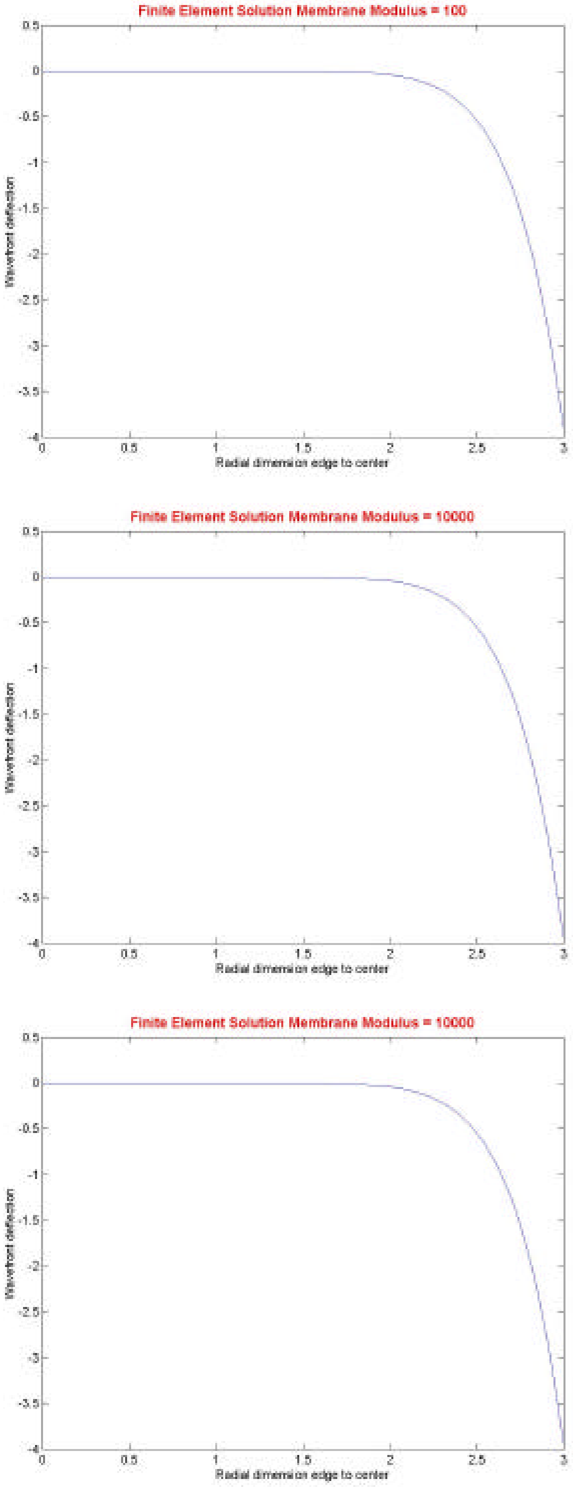

Figure 49. Membrane Deflections (Emem = 100, 10000 and 100000 psi)

Once the membrane modulus was increased to a greater order of magnitude as the PVDF for the 2.8 Msi case, the solution began to show different deflections, but they only increased slightly (a couple of wavelengths).

One last part of this test is to show the effects of the PVDF layer having a large value of E=2.8 Gsi. The three plots below in Figure 50 are for the membrane modulus of 1000, 10^6 and 10^9. The opposite effect as that of the other PVDF moduli happened. When the membrane modulus was increased to the same order of magnitude as the PVDF layer, the deflection actually decreased. The scale on the two lower order moduli is 10^4, while it is 10^3 for the PVDF and membrane moduli at 10^9. This shows how much the PVDF layer can control the whole system without the influence of the membrane layer having that much effect.

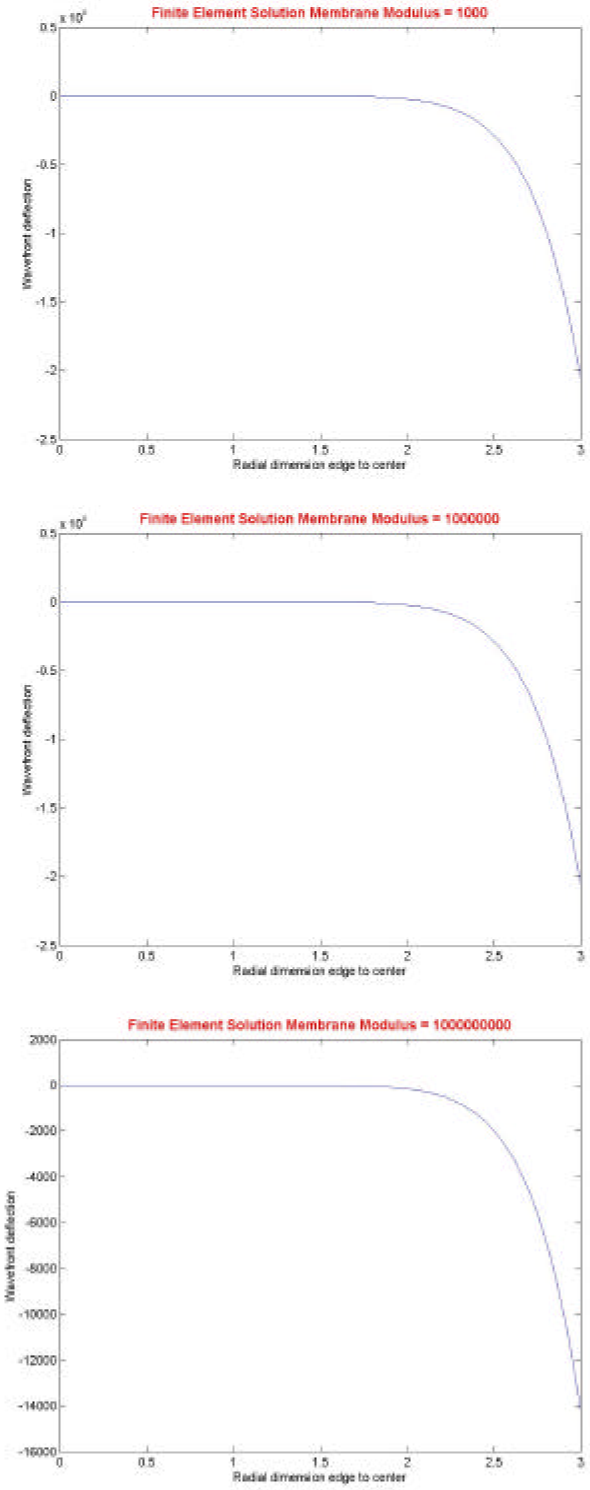

Figure 50. Membrane Deflections (E_{mem} = 1000, 100000 and 10^9 psi)

The last test performed is the element size. This is another variable that affects the e factor. The size is controlled by number of elements across the membrane centerline, i.e. the more elements, the smaller the element size and therefore, the larger the e. The program is setup in such a way that only certain element numbers can be setup with certain configurations. For the configuration that has been used in all the tests up to this point, approximately 3 cm center region, an odd amount of element numbers is required. It is also to be noted that while the element number is chosen to have a certain value, once the Zernike coefficients were found, the solution plots created are always based on 0.1" increments to make the solution more continuous as is the case in the experimental. This should be an easy adjustment if it is desired to look at a straight line solution between nodes.

This test performed results for five sets of element numbers, namely 3, 9, 15, 21, and 35 elements. The number of elements across the whole diameter would actually be double across a diameter, but since this was an axisymmetric solution, the solution covers across one radius. While many other tests could be completed in this arena, these five show enough of the solution to give understanding into how the element number controls the solution by completing a whole cycle of deflection plots, as will be described below.

The first test had the lowest amount of elements possible for this configuration, three. During the process of understanding and learning operation of the program it quickly became obvious that three elements were going to be a problem. A representative test using the following properties, E_{mem}=100 psi, E_{PVDF}=261 ksi, t_{mem}=0.006", t_{PVDF}=0.003", N=1000, 300 V in center, n =0.3 for both, leads produced a solution as seen in Figure 51.

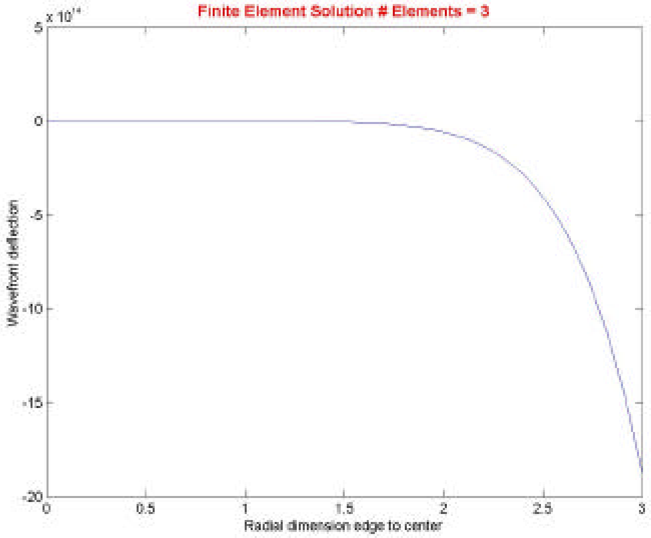

Figure 51. Membrane Deflection (3 Elements)

Notice the very large deflection with this amount of elements. The e for this case would be very small, so there must be something else causing the error. One suggestion for this may be the lack of rigidity in the element caused by being too large. There are configurations that the three elements may provide reasonable results, but at this time they are not explored.

For the time being, the nine element case is going to be skipped for sake of seeing what happens as the number of elements is increased. The 15 element case is therefore next. The same material properties as above are used and the results seem reasonable for the low modulus of the membrane, see Figure 52. It shows about 6 l (approximately 4 µm) of deflection at the center. This is more than is desired, but the solution doesn't seem far off. This is the beginning of the divergence on the high number of elements.

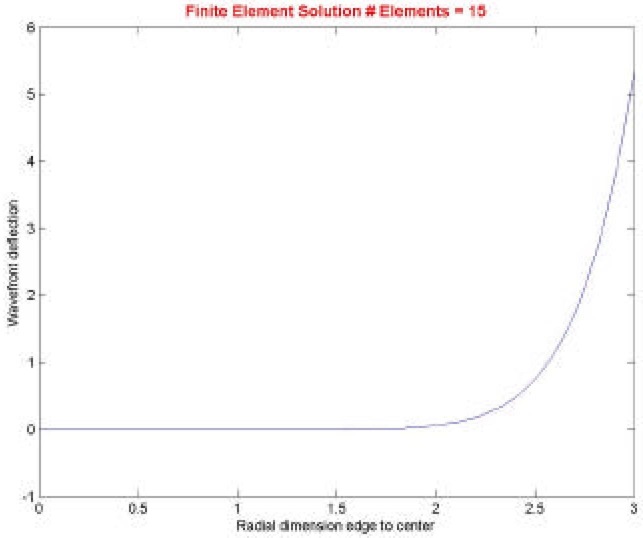

Figure 52. Membrane Deflection (15 Elements)

Next, 21 elements are tested and the deflection is five times greater than the 15 element solution, see Figure 53. The solution illustrate deflections that wouldn't be expected for the relatively low voltage conditions. One more test is required to verify this.

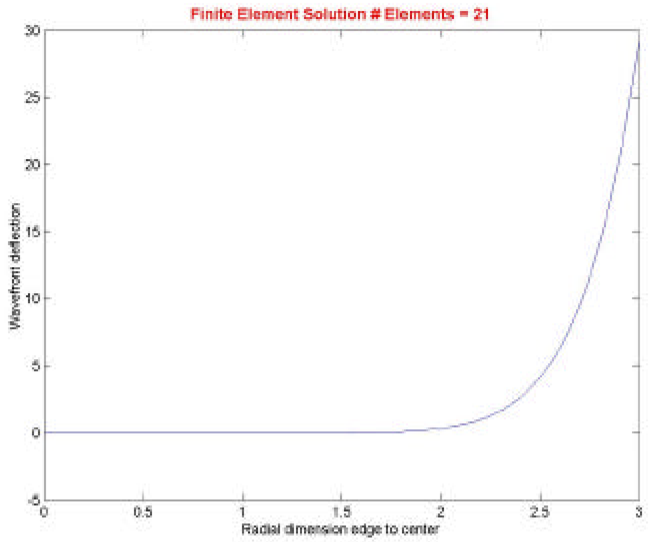

Figure 53. Membrane Deflection (21 Elements)

The number of elements was increased by a little more than 50 percent to 35 elements. Figure 54 illustrates the solution 'blowing up' again for the high number of elements having nearly $10^5 l$ of displacement or on the order of ¼", which is clearly impossible for the conditions given. This is caused by the elements causing a large epsilon. Since this epsilon term is fed into a few of the non-dimensional terms, which are used in the nonlinear finite element code, the effects of it increasing in the integral leads to the total solution becoming invalid. Further study of this effect is desired and required. The reasoning behind the element rigidness is the e term. As the element size becomes so small, e becomes very large. The perturbation solution is thereby not satisfied by the order e^2 assumed. This is a local effected e that becomes large and not the global one; however, it must still be satisfied for the solution to remain reasonable. Epsilon is directly defined by the thickness and length of each element. The adjustment of this term is done through changing the values of these two parameters. One other feature in this study is the “flip” happening from negative to positive to negative deflections. The two negative solutions are discounted as poor solutions and therefore, not considered viable solutions.

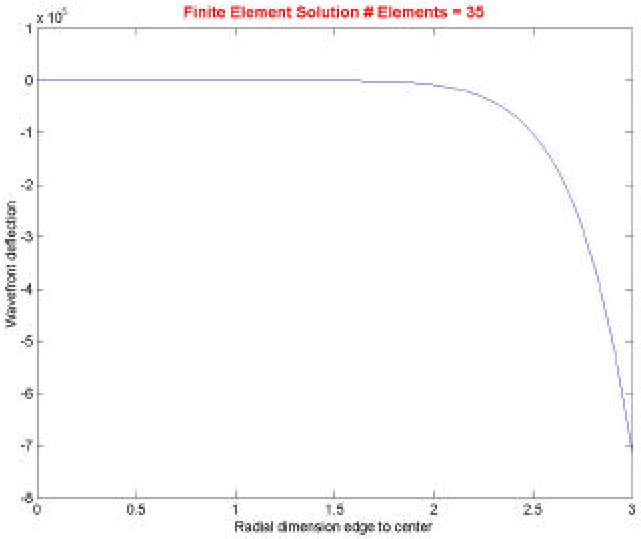

Figure 54. Membrane Deflection (35 Elements)

Retreating back to the 9-element case, it is seen that this supplies the best solution for this configuration. The deflection plot can be seen in Figure 55. Notice that there are just a few wavelengths of deflection. This is much more comparable to what is expected, on the order of a micron of deflection.

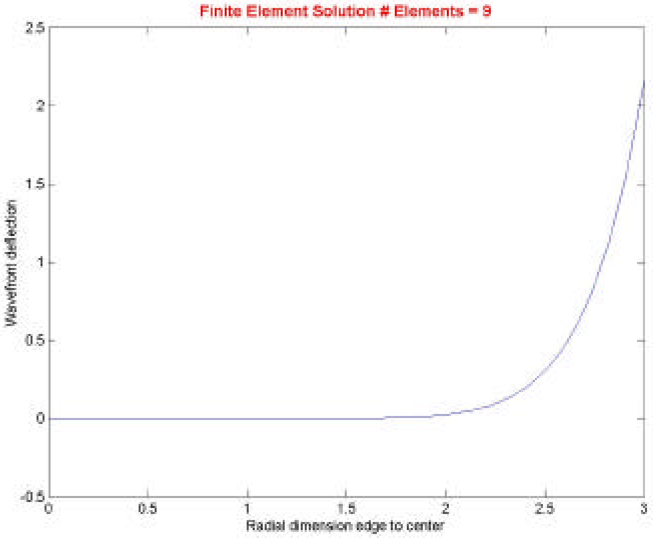

Figure 55. Membrane Deflection (9 Elements)

The above study dealing with the element size shows how important it is to have elements that are just "rigid" enough to provide solutions that make sense and are reasonable. In some of the cases, MATLAB provided warning message regarding the size vector not being a row vector with integer elements. This happened at 35 elements and could have caused the large deflection solution. This is usually caused by infinite values in the vectors and is just another verification to avoid the small element size.

The element size study completes the parametric study. The study demonstrated how there is probably an anomaly in the code when it comes to very specific values of the tension and modulus. Around these values the deflection reverses signs. Modulus and tension values may provide poor solutions if not properly applied. Once away from the anomalous values, the solution seemed to behave and actually showed what would be expected as the tension or modulus was increased or decreased. The thickness on the other hand played a crucial role in terms of the magnitude of displacement, granted, it was varied on the same scale of the modulus and tension. The thicker membrane was not a valid model, which also happened with the element size (or element number). The increase in both thickness and number of elements caused the solution to grow very rapidly. There are obviously values for all the variables that would provide excellent solutions and the above study showed the sensitivity to changes in some of them.

The total study shows the influence of the different variables in the final solution. This study was by no means exhaustive, but it covered most of the important components required before moving into the comparison between the finite solution and experimental data.

Experimental Test Runs Available

Before proceeding directly into comparison of the two solutions, a short explanation concerning the experimental data that would prove useful to look at is included here. There was quite a bit of data collected by Sobers during the experimental stage. As described in Chapter 2, there were two “membrane” test articles and two “stiff” articles. The finite element code’s capabilities automatically eliminated the two stiff test articles. M1 was designed mostly to learn more about the manufacturing intricacies. It could be used as a test article to compare with the finite element code, but due to some of the concerns Sobers had with leak over of the piezo layer and other issues, it was determined that it might be best just to stick with M2. M2 had better characteristics in the layout of the piezo zones and provided more data in the axisymmetric cases; therefore, this was to be the sole test article.

Sobers had performed basically four tests, not including the 0V cases, that can be easily compared (perfectly axisymmetric). Each test corresponded to a different voltage condition in 300 V increments from -600 V to 600 V. In each case, after the positive or negative voltages were complete, a new baseline measurement was completed at 0V. This information will be included in the plots below; however, the difference in the 0V finite element solution and the experimental will always be equal to the experimental. This is due to the fact that the finite element solution will always provide no deflection for a 0 V input on the piezo layer, since it basically represents an ideal case. The plots provided here have been produced using Zernike coefficients and polynomials as explained before. The boundary is actually represented at x=0 and the center at x=3. The y-axis represents deflection or, more appropriate, the wavefront deviation from flat. This is mentioned since there are times when the experimental boundary is not located at the zero mark on the y-axis.

The order that appears here will be the same order Sobers used in the testing procedure, or 0V, 300V, 600V, 0V, -300V, 600V, 0V. The contour and fully 3-D plots from the experiment for both the full Zernike plots and the reduced data will be included to have a quick reference. The finite element code will be run with material properties that are most realistic and not the ones that produce the closest solution. The properties used for this solution is 150 psi, 0.497, and 0.25" for the membrane modulus, Poisson's ratio and thickness, respectfully and 261 ksi, 0.35 and .002"for the same PVDF properties. Therefore, there will be plots of the finite element code that potentially could be orders of magnitude different than the experimental. If this is the case, another plot of the experimental will be included, so the shape can be seen more clearly. Other solutions may be included representing solutions that are nearly the experimental. In these cases, the material properties will be given that provides the closest solution.

Experimental and Finite Element Comparison

As stated before, the first case to be compared (or just to set up a baseline) is the 0V case. The 0V experimental plots of the full Zernike and reduced Zernike, along with the raw data are included in Figure 56-Figure 57. This is the first 0V case before any activation was applied to any section of the membrane.

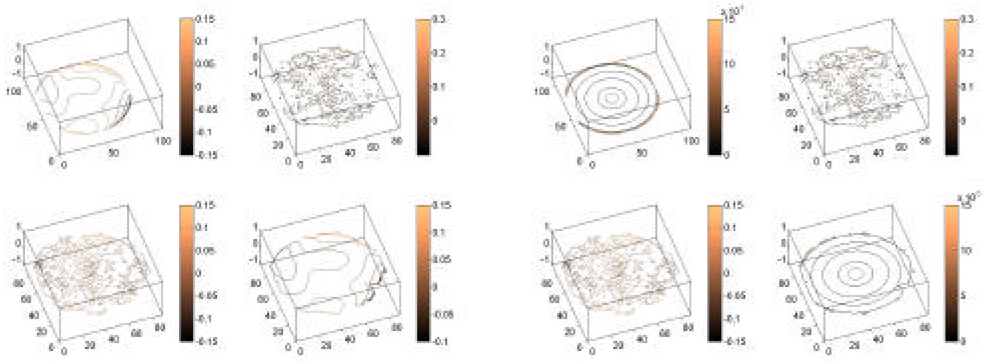

Figure 56. Experimental Contour Plots (Non-axisymmetric and Symmetric)

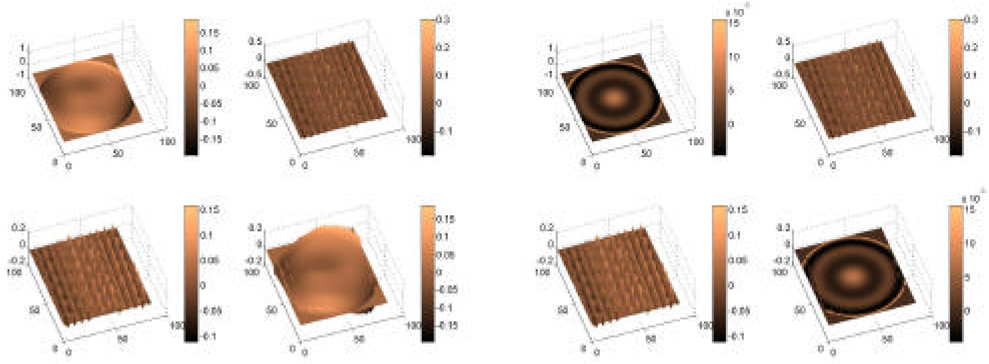

Figure 57. Experimental Surface Plots (Non-axisymmetric and Symmetric)

The above plots are supplied to show the 3-dimensional and contour shapes, as well as both the symmetric and non-symmetric cases. It is seen that there is some difference in wavefront even after there was a self-referencing of the data. This could be shown to be "flat" if the scale on the z-axis were changed; however, it's important to show that there is some wavefront error on some level even if it is very small.

The following plots are self-explanatory. Figure 58 is both the finite element solution defined by flat line at zero deflection and the experimental as the curved line. Since there is no voltage (0V) input, the finite element solution would have no deflection as represented by this plot. The experimental plot is actually caused by the difference in the wavefront as the light reflected, and therefore can have a non-flat shape for no voltage. The plot directly below in the same figure is the difference between the two plots. Obviously, the difference in this case is equivalent to the experimental solution.

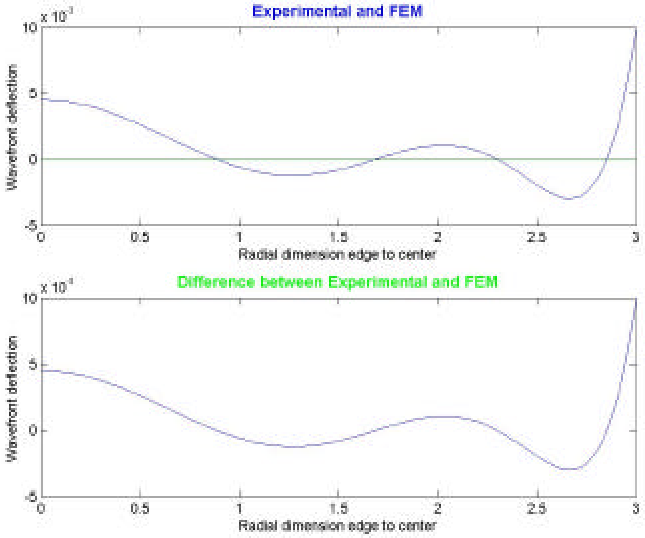

Figure 58. Reduced Experimental and Finite Solution with Difference

Figure 59 represents the total solutions of the 35 Zernike coefficients for the angles defined before along with the 31 Zernike coefficients, these two plots reduced to a single line and the modified versions where the deflections corresponding to the centerlines on the negative x-axis are multiplied by -1, defined before. These plots are based solely on the experimental solution and are included as a reference to show the effects or lack there of the non-axisymmetric components. The scales here are on the order of 0.2 l .

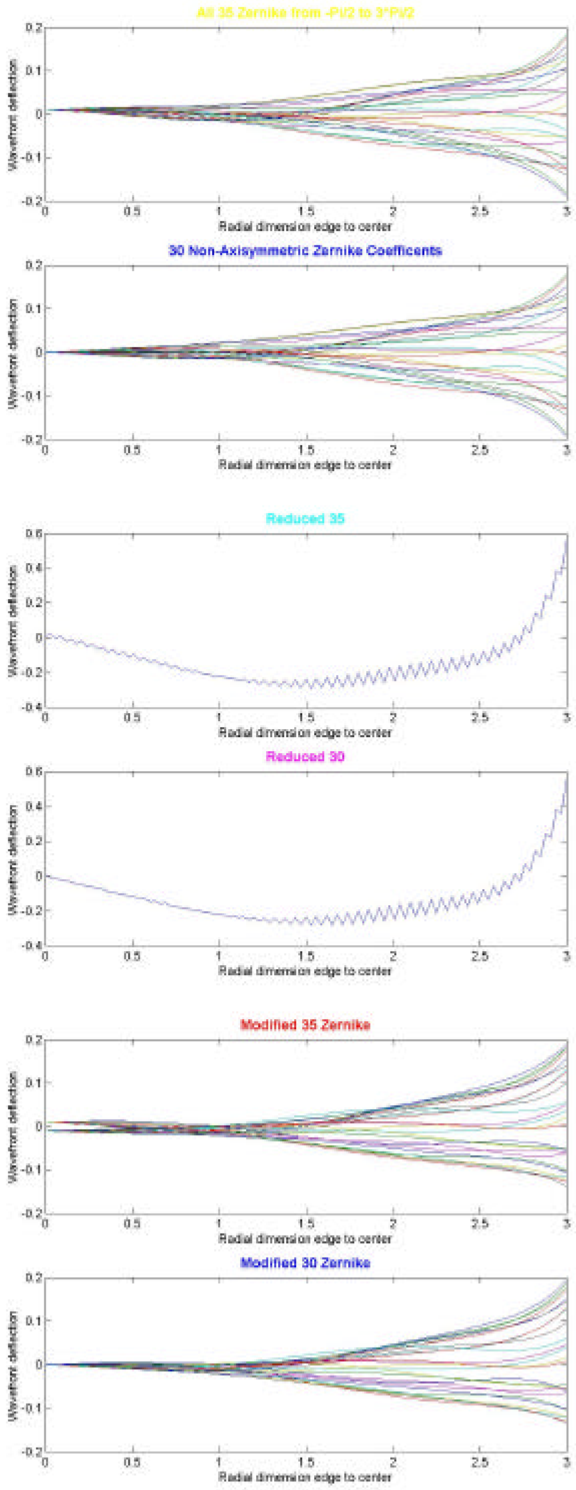
All 35 Zernike from -Pi/2 to 3*Pi/2

30 Non-Axisymmetric Zernike Coefficents

Reduced 35

Reduced 30

Modified 35 Zernike

Modified 30 Zernike

Figure 59. Non-Axisymmetric Solutions

The zero volt case is provided not to try to verify the results in this case, but so the residual effects can be seen after the voltage has been applied. It also presents information about the initial wavefront before testing. The next two tests will show the program's capabilities in regards to a voltage input.

The first voltage condition to be evaluated is a positive 300 V. For now, since the material properties are set by realistic values defined above, the only variable that could change is the tension term. The first test is completed with a tension of 1000. The finite element solution produced is extremely large and not representative of the actual or experimental solution. Figure 60shows the two solutions together.

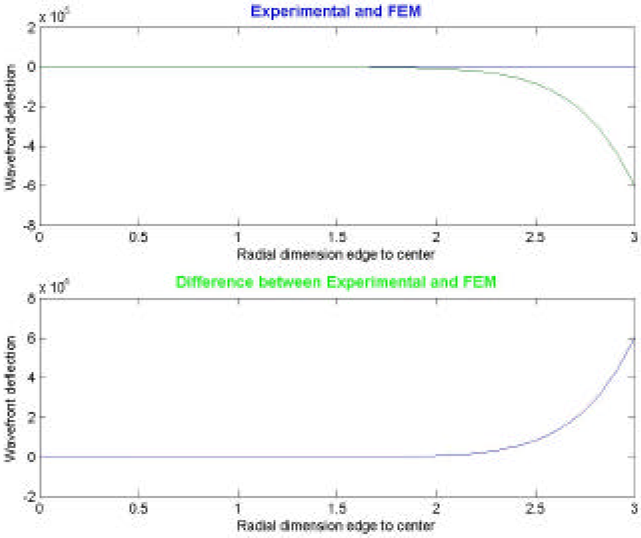

Figure 60. 300V Both Solutions and difference

Notice that the finite solution dominates the plots. Since this is the case, the plots are separated out to see them next to one another, as seen in Figure 61.

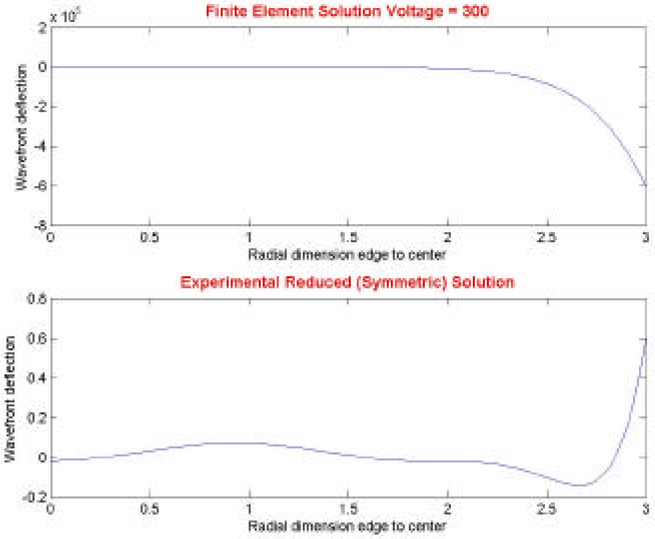

Figure 61. FEM and Experimental on Separate Plots

The next step is to see if there is a possibility that a reasonable tension can be found that would produce a solution representative of the experimental. If this is possible, this tension can be checked against all the other voltage conditions. Unfortunately, the tension alone could not bring the solution to the same order without cranking it up to an unreasonable value. When the value was increased to $8x10^7$, the deflection at the center was almost dead on, approximately 0.1 wavelengths difference, see Figure 62.

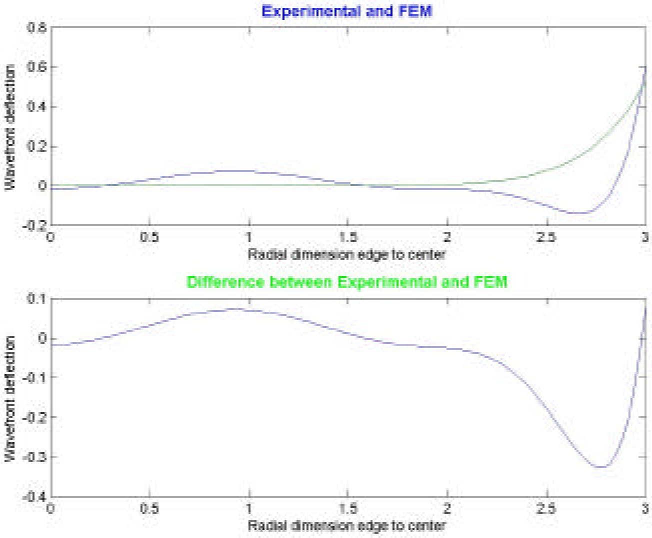

Figure 62. Both Solutions (T=8x10^7)

Following the order Sobers used in testing the membrane, 600 V was tested next. The large tension value from above was used in this case. The solution wasn't as close, but it was still within one wavelength of difference and the deflection was in the same direction. This can be seen in Figure 63.

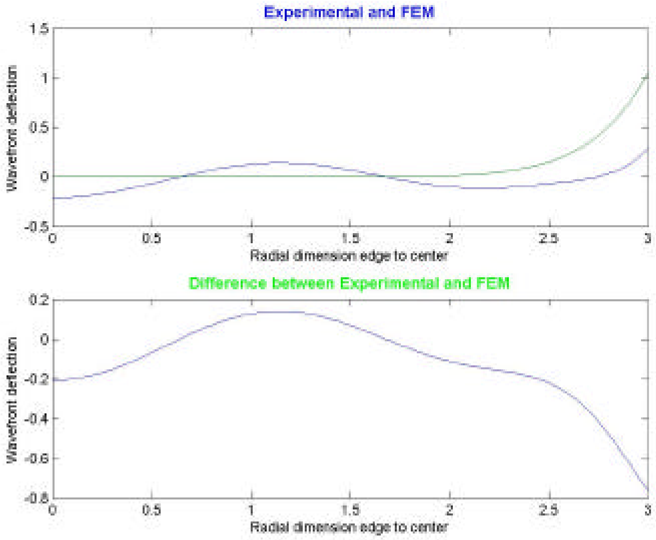

Figure 63. 600V Membrane Deflection

Tweaking the tension, a closer approximation can be found. It was eventually discovered that 1x10^8 was the value that did this. However, this was done through the use of knowing the experimental solution and the solution was still about 1/2 *l* difference. There will be tests that there is no experimental solution to compare and the tension value cannot be adjusted until the solution matches; therefore, for the next two tests, the tension value is going to be reduced back to the 8x10^7 value.

The next two and last tests for the comparison with M2 are the -300 and -600 V cases. The tension case used actually produced results expressive of the experimental. There is approximately 0.2 *l* difference between the two solutions for -300V and nearly ½ *l* for the -600 V case. Both of these plots are in Figure 64.

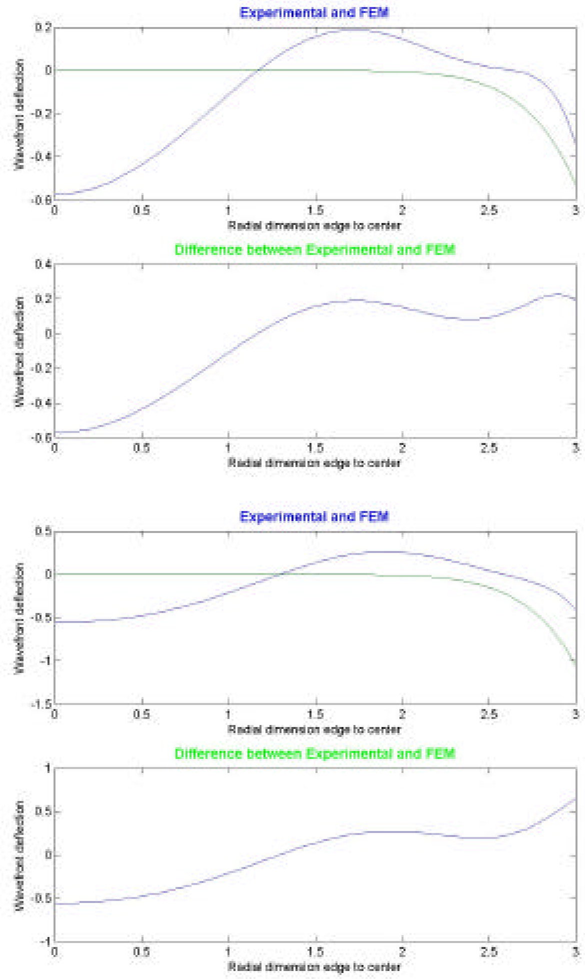

Figure 64. Membrane Deflection (-300 and -600V)

The above tests demonstrate the capabilities of the finite element program both as a separate entity and when in comparison with an actual experimental solution. There are many other tests and conditions that would be interesting to investigate. Some of these will be mentioned in Chapter 5.

On the whole, the finite element code is representative of the experimental solution for a reduced Zernike set. It was possible to obtain solutions that were similar to the experimental solution; however, it required tweaking of a variable, in this case, the boundary tension until a representative value was obtained to match the first voltage condition. This tension value produced solutions for all voltage conditions that represented the experimental results. As the parametric study showed, the many variables available can have drastic effects on the final solution, even to the point of reversing the direction of the deflection. For this reason, it is important to have the best values for the material properties, whether this means actual real-world properties or properties of a nature that produces close solutions. In either case, if there is not an experiment to compare with, coming back to these tests to check for the variable values would prove useful and necessary, so as to avoid creating solutions that wouldn't represent a real experiment.

V: Conclusions and Recommendations

Finite element modeling of polymer membrane-PVDF structures is becoming more necessary with the technology advancements coming down the pike. This study showed the beginnings of this capability in symmetric solutions using perturbation techniques. In many cases, a symmetric solution may be enough for what is required of the mission, implying that the activation zones are needed to change the global shape in a symmetric pattern. If this is the case, this program is invaluable; however, there may be reason to have non-axisymmetric activation zones placed in different regions of the mirror. If this was required and modeling of the system was required before hand to see the wavefront shapes possible, the symmetric equations would not provide the necessary conditions and would therefore need to be modified. This may be accomplished through extending formulation to two dimensions and consequently the shape functions would be better suited to the solution. If this new program was developed, it would be interesting to recheck the experimental solutions without reducing them to the symmetric case.

When the program was first developed and the experimental tests were being completed, it was known that they were related projects and it was determined to have axisymmetric experiments completed. Now that more work has been completed with the program, more experimental tests with different PVDF configurations and voltage conditions would supply more information regarding the capability of the program and give more to compare against. It would also show experimentally what may be possible in shape control on the optical level.

If this were completed, different configurations in the finite element solution could be investigated, rather than just the center circle. There are many different symmetric configurations of concentric circles around the membrane that could produce solutions. If this study is completed, it would be beneficial to rewrite part of the program to have the ability to have different voltage conditions in each of the activation zones. As it stands now, each zone that is given activation (see Appendix B) receives the voltage defined at the beginning. In a real life situation, there may be a few voltage sources that supply different activation zones and therefore would prove useful to be able to have this in the program as well.

The parametric study usually looked at changing one variable at a time to investigate the singular effects of a variable. It may be interesting to investigate various changes together; so as to optimize the material properties to match the experimental results. The results of the comparison showed decent results, but it was not looked at how to match the solution exactly. It may be beneficial to write a short script to converge on the closest zero difference solution possible by varying the modulus, tension, or any of the other material properties together. The solution to this study would be the material and system properties that gave the best solution for each voltage condition. They could be compared to see if the properties were in the same ballpark for each voltage. This should be accomplished by optimizing over all voltage experimental results simultaneously.

As shown, the solution can be very sensitive to increasing e. For this reason, a large tension was required for the actual tests when the membrane was ¼” thick. The viscosity and curing process of the RTV 615 is the reason for the membrane being that thick. Usually, the membranes are more on the order of tens of microns. These polymer membranes (one such is SRS Technologies, Inc. CP-1) available are usually of better surface quality than the RTV 615 and therefore some of the non-axisymmetric wavefront deviations may be reduced or eliminated if they were used. CP-1 or other material may prove useful to test in the same manner of RTV 615. If nothing else, it would provide more data that could be compared. It could also see if CP-1 is a more viable option for wavefront shape control or if it would prove to be as responsive to the PVDF changes as the RTV615. The material used here is just as important as the ability to control and model it.

The study completed above demonstrated the basic capabilities of the finite element code. There are obviously many shortcomings in the solutions. The first test completed was to discover the tension effects on the membrane. The only solutions similar to the experimental results were when the tension was increased to infeasible values. When this value was used under other voltage conditions, the solutions seemed to remain representative of the experimentally. Although the number used to obtain this solution is unreasonable, it may be useful to continue to use this value whenever an RTV membrane is tested. A different membrane material may require a different tension value and even a different RTV membrane may have a different value. A method to find a value experimental could prove useful. A vibration test may be one way this could be accomplished. For comparison to the experimental, this was the only variable varied, since the material properties were set by the values of Chapter 2 Material Testing.

The parametric study showed how changes in different properties sometimes lead to extremely large changes and other times hardly affected the solution. The changes in the modulus fell into the latter category. There was an area of moduli that had large changes; however, once away from these values, the deflection plots are nearly the same order. As with many of the properties, there was a value that had a flip from positive to negative displacement. The rationale behind this is unknown and must correspond to some function in the code or the dominating effect of one layer of the piezo-polymer layup.

As stated before, most of the material properties have this displacement flip. Although written above for the specific comparison, the tension was checked out in the parametric study first. As it was increased to a very large value, it was shown to produce very small displacement plots ($\sim 10^{-6} l$). It also had a flip at a relatively small value, namely 3242.5. On either side of this value, the displacement increased. Values less than the 3200 value the displacement kept increasing as N approached zero. The other side increased for a while, then started to decrease in displacement after that point, until the displacement was nearly zero. Away from the anomaly tension value, the membrane behaves as it should, i.e. low tension will allow greater displacement and higher boundary tension will produce very small displacement. The anomaly is changed from the 3242.5 value if the modulus is increased or the thickness decreased.

The thickness of the membrane also demonstrated quite a bit of change for very small changes. The one case demonstrated that increasing the thickness from 0.0066" to 0.009" lead to a 5000 times increase in displacement. This sensitivity in thickness is most likely explainable in terms of e. As thickness is increased, the e term is also increasing. Once it becomes larger than a certain size, it will cause the solution to blow up. This is supposedly what happened in this case. This sensitivity to e needs to be further investigated to possibly find a way to reduce its effects. The e sensitivity was also noticed in the other component of element size, the number of elements used.

Up to this point, 9 elements were used for all the tests. However, it is important to see what happens using more and less elements. The sensitivity to e was quickly seen when the number of elements was increased; thereby, the element length to thickness was decreased. As more elements were investigated, the displacement kept increasing to areas that were completely impossible (10^5 l). Nine elements always produced what seems like a reasonable solution. Decreasing the number of elements also caused a problem in the code. When three elements were used, the displacement was 10^{14} l. There is some speculation why this happened. The PVDF layer may be dominating, but it is more likely dealing with the element size being so large that the effects of the activation zone is not able to produce a solution. Another possibility may reside in the non-dimensionalizing of the terms and how change one dimensioned term changes a few non-dimensioned terms. These terms are solved through a nonlinear integral and could cause many of the problems with the code not functioning properely for a few of the cases. There are many other tests in this study that could be complete; however, the program's capabilities were shown in it and the effects of different properties investigated.

Overall this study was enlightening to see the modeling abilities in comparison to experiments and as a stand alone program in the parametric study. Since this is still a relatively new field of study there is much to be completed in the future and the above discussion provides a starting point, but doesn't cover all that will be desired in further studies.

Bibliography

Burge, J.H., Cuerden, B. Angel, J.R.P. “Active mirror technology for large space telescopes”, *Proceedings of SPIE Vol 4013*. 640-648. 2000.

Carlin, Patrick S. “Lightweight Mirror Systems for Spacecraft – An Overview of Materials & Manufacturing Needs”, Air Force Research Laboratory, Kirtland AFB NM.

Carreras, R.A, et. al. “Deployable Near-Net Shape Membrane Optics,” *Proceedings of SPIE Conference on High-Resolution Wavefront Control: Methods, Devices, and Applications.* 232-238. Colorado: SPIE Vol 3760: July 1999.

Carreras, R.A., Marker, D.K., Lutz, B.J. “Fuzzy Logic Control for an Optical Membrane Mirror,” Air Force Research Laboratory, Kirtland AFB NM. 2001.

Cesnik, C.E.S, Plaacios, R., “Modeling Piezocomposite Actuators Embedded in Slender Structures”, Proceedings, 44th AIAA/ASME/ASCE/AHS Structures, Structural Dynamics, and Materials Conference, April 2003.

Dimakov, S.A., Bogdanov, M.P., et. al., “Electrically controlled pre-shaped membrane mirror for systems with wavefront correction,” *Proceedings of SPIE Advanced Wavefront Control: Methods, Devices, and Applications.* 147-156. Washington, 2003.

Edgcombe, C.J., “Perturbations of Axisymmetric Systems Described by 2-D Solution Methods,” London*: Institute of Electrical Engineers,* 1995.

Gruneisen, M.T., Martinez, T., et. al., “Holographic Compensation of Severe Dynamic Aberrations in Membrane-Mirror Based Telescope Systems”, *Proceedings of SPIE Conference on High-Resolution Wavefront Control: Methods, Devices, and Applications.* 142-152. Colorado: SPIE Vol 3760: July 1999.

Gruneisen, M.T., Dymale, R.C., et. al., “Near-diffraction-limited compensated imaging and laser wavefront control with programmable diffractive optics”, *Proceedings of SPIE High Resolution Wavefront Control: Methods, Devices, and Applications.* 147-157.: SPIE Vol 4825: 2002

Hecht, Eugene, *Optics*. New York: Addison Wesley Longman, Inc., 2002

Jenkins, C.H., Ash, J.T., Marker, D.K., "Local Defect Study of Membrane Antennas and Reflectors," Compliant Structures Laboratory, Mechanical Engineering Department, South Dakota School of Mines and Technology, SPIE, 2001.

Jenkins, C.H.M., Editor, *Gossamer Spacecraft: Membrane and Inflatable Structures Technology for Space Applications*, Chapter 4, p 111-201, AIAA Progress in Astronautics and Aeronautics, Vol. 191.

L'Garde, Inc., Inflatable Antennae Experiment, February 2004, http://www.lgarde.com/programs/iae.html.

Li, K., et. al., "Control Techniques for a Large Segmented Reflector", Proceedings, 37th IEEE Conference on Decision & Control, December 1998.

Magee, Steven, "Active control systems for large segmented optical mirrors", Engineering Science and Education Journal, August 2002.

Marker, D.K., et. al., "Net-shape polymer mirrors," *Proceedings of SPIE High Resolution Wavefront Control: Methods, Devices, and Applications*. 212-215.: SPIE Vol 4493: 2002.

Mollenhauer, David, et. al. "Moire Interferometry Measurements on a Co-bonded Pi-Preform Composite Tee Joint," Air Force Research Laboratory, Wright-Patterson AFB OH.

Peters, K.W., Bishop J.A., Wilkes, J.M., "An Analysis of Membrane Mirrors For Use in Large Aperture Imaging Systems," Air Force Research Laboratory Space Vehicles, Kirtland AFB NM.

Rogers, James W. *Modeling Axisymmetric Optical Precision Piezoelectric Membranes.* PhD Dissertation, AFIT/DS/ENY/01-02. Department of Aeronautics and Astronautics, Air Force Institute of Technology (AU), Wright-Patterson AFB OH, October 2001

Rogers, J.W. and Agnes, G., "Asymptotic Finite Element Introducing the Method of Integral Multiple Scales," AIAA Journal Vol 41, No 9, Sept 2003.

Rotge, J.R., et. al., "Membrane telescopes: useful in ground-based astronomy?," *Proceedings of SPIE High Resolution Wavefront Control: Methods, Devices, and Applications.* 207-211.: SPIE Vol 4493: 2002.

Rotge, J.R., Dass, S.C., "Progress toward large-aperture membrane mirrors," *Proceedings of SPIE Imaging Technology and Telescopes*, 74-82, 2000.

Rotge, J.R., et. al., “Large optically flat membrane mirrors”, *Proceedings of SPIE Conference on High-Resolution Wavefront Control: Methods, Devices, and Applications.* 232-238. Colorado: SPIE Vol 3760: July 1999.

Sobers, David M. *Smart Structures for Control of Optical Surfaces*. MS Thesis, AFIT/GA/ENY/02-2. Department of Aeronautics and Astronautics, Air Force Institute of Technology (AU), Wright-Patterson AFB OH, March 2002

Wagner, John W. *Optical Metrology of Adaptive Membrane Mirrors*. MS Thesis, AFIT/GA/ENY/00M-05. Department of Aeronautics and Astronautics, Air Force Institute of Technology (AU), Wright-Patterson AFB OH, March 2000.

Yu, W., Hodges, D.H., “The Timoshenko-like Theory of the Variational Asymptotic Beam Sectional Analysis”, Proceedings, 44th AIAA/ASME/ASCE/AHS Structures, Structural Dynamics, and Materials Conference, April 2003.

Appendix A: Finite Element Code

The following appendix is the different parts of the code along with comments about their operation or purpose. All of this code along with other code is supplied on the program CD.

This is a sample of the experimental data that produces the Zernike plots. There is a complimentary raw data file; however, it is just a long column of numbers, so it is not supplied here. Any combination of Zernike coefficients could be typed into a file similar to this and when this file is run in MATLAB®, will create 4 plots of raw data, smoothed raw data, and two Zernike plots.

```
% M2_T1c_300v
% Mon Dec 10 21:51:53 2001
% Zygo Zernike Coefficients
% Obscuration Ratio = 0.0000
% Index Coefs(microns) Equation
% function [z] = three00center
z=[
  1   0.000000  % rcos(t) (X Tilt)
  2   0.000000  % rsin(t) (Y Tilt)
  3   0.000000  % 2r^2-1 (Focus)
  4   0.000000  % r^2cos(2t) (0 Astigmatism)
  5   0.000000  % r^2sin(2t) (45 Astigmatism)
  6   0.000000  % (3r^2-2)rcos(t) (X Coma)
  7   0.000000  % (3r^2-2)rsin(t) (Y Coma)
  8   0.152906  % 6r^4-6r^2+1 (Spherical)
  9   0.000000  % r^3cos(3t)
 10   0.000000  % r^3sin(3t)
 11   0.000000  % (4r^2-3)r^2cos(2t)
 12   0.000000  % (4r^2-3)r^2sin(2t)
 13   0.000000  % (10r^4-12r^2+3)rcos(t)
 14   0.000000  % (10r^4-12r^2+3)rsin(t)
 15   0.188982  % 20r^6-30r^4+12r^2-1
 16   0.000000  % r^4cos(4t)
 17   0.000000  % r^4sin(4t)
 18   0.000000  % (5r^2-4)r^3cos(3t)
 19   0.000000  % (5r^2-4)r^3sin(3t)
 20   0.000000  % (15r^4-20r^2+6)r^2cos(2t)
 21   0.000000  % (15r^4-20r^2+6)r^2sin(2t)
 22   0.000000  % (35r^6-60r^4+30r^2-4)rcos(t)
 23   0.000000  % (35r^6-60r^4+30r^2-4)rsin(t)
 24   0.142927  % 70r^8-140r^6+90r^4-20r^2+1
 25   0.000000  % r^5cos(5t)
 26   0.000000  % r^5sin(5t)
 27   0.000000  % (6r^2-5)r^4cos(4t)
 28   0.000000  % (6r^2-5)r^4sin(4t)
 29   0.000000  % (21r^4-30r^2+10)r^3cos(3t)
 30   0.000000  % (21r^4-30r^2+10)r^3sin(3t)
 31   0.000000  % (56r^6-105r^4+60r^2-10)r^2cos(2t)
 32   0.000000  % (56r^6-105r^4+60r^2-10)r^2sin(2t)
 33   0.000000  % (126r^8-280r^6+210r^4-60r^2+5)rcos(t)
 34   0.000000  % (126r^8-280r^6+210r^4-60r^2+5)rsin(t)
 35   0.123484  % 252r^10-630r^8+560r^6-210r^4+30r^2-1
];

data=textread('M2_T1c_300v.dat', '%f');
% factor(length(T1g))  % [ 3 3 31 37]
rows=111;
cols=93;
zsize=94;
smoothlevel=1;
pupil=0;
shift=[0 0];
MLM=0.133;
ratio=7.6327;
trim=1;

makeplots % Command that calls script file to plot surface plots
```

This file takes the information from the raw data and Zernike file above and creates the plots. It is slightly modified from its original form to put all the plots on the same figure. If surface plots are desired, ***contour*** should be replaced with ***surf***.

```
% makeplots.m subroutine
% Copyright 2002 - Michael Sobers - All rights reserved.
% Modified by Brian Lutz 2004
z=z(:,2);

for j = 1:cols
  data_surf(1:rows,j)=data((j-1)*rows+1:j*rows);
end

if trim==1
  temp=zeros(rows+2,cols+2);
  temp(2:rows+1,2:cols+1)=data_surf;
  data_surf=temp;
  while (sum(data_surf(2,:))==0&sum(diff(data_surf(2,:)))==0)
    data_surf(2:size(data_surf,1)-1,:)=data_surf(3:size(data_surf,1),:);
  end
  r=2;
  while (sum(data_surf(r,:))~=0|sum(diff(data_surf(r,:)))~=0)
     r=r+1;
  end
  data_surf=data_surf(1:r,:);
  while (sum(data_surf(:,2))==0&sum(diff(data_surf(:,2)))==0)
    data_surf(:,2:size(data_surf,2)-1)=data_surf(:,3:size(data_surf,2));
  end
  c=2;
  while (sum(data_surf(:,c))~=0|sum(diff(data_surf(:,c)))~=0)
     c=c+1;
  end
  data_surf=data_surf(:,1:c);
  rows=size(data_surf,1);
  cols=size(data_surf,2);
end

data_surf=data_surf./(0.633);

shift=round(shift/(MLM*ratio));
zsurface = myzern(z,[rows cols], pupil, shift);

array=zsurface;
array=array./(0.633);

if mkpts == 1
   figure
   subplot(2,2,1), contour([0:size(array,2)-1]*MLM*ratio,[0:size(array,1)-1]*MLM*ratio,array);
   view([-19,68])
   axis([0 110 0 110 -1 1.5])
   colormap(copper)
   colorbar
   shading interp
```

```
    xlabel=('Surface Location - mm');
    ylabel=('Surface Location - mm');
    zlabel=('Surface Height - Wavelengths (633nm)');
end

%for j = 1:cols
% data_surf_flip(:,j)=data_surf(:,cols+1-j);
%end

%for r = 1:rows
%    data_surf_rotated(:,r) = data_surf_flip(rows+1-r,:)';
%end

if mkpts == 1
   subplot(2,2,2), contour([0:cols-1]*MLM*ratio,[0:rows-1]*MLM*ratio,data_surf);
   view([-19,68])
    %axis([0 110 0 110 -1 1.5])
   colormap(copper)
   colorbar
   shading interp
end

smooth_data = interpolate2(data_surf,smoothlevel);
if mkpts == 1
   subplot(2,2,3),contour([0:cols-1]*MLM*ratio,[0:rows-1]*MLM*ratio,smooth_data);
   view([-19,68])
    %axis([0 110 0 110 -1 1.5])
   colormap(copper)
   colorbar
   shading interp
end

mask=zeros(rows, cols);

for r=1:rows
  for c=1:cols
     if smooth_data(r,c)~=0
        mask(r,c)=1;
     end
  end
end

% figure(3)
H=axis;

if mkpts == 1
   subplot(2,2,4),contour([0:size(array,2)-1]*MLM*ratio,[0:size(array,1)-1]*MLM*ratio,array.*mask);
   view([-19,68])
   axis(H);
    %axis([0 110 0 110 -2 2])
   colormap(copper)
   colorbar
   shading interp
end
```

This is the first of the finite element code files. It contains the material properties and it prepares them by placing them in matrix form before the information is exported to another file that runs the calculations.

```
function [v,x,d,eps]=testr2(numel,p,t,v,order,verb,dyn,mode,alpha,beta,config);

innerR=0.0001;
outerR=3.0001;
% youngsperlayer=diag([406000 261000 261000]);
% thickperlayer=diag([0.006 0.003 0.003]);
% poissonperlayer=diag([0.3 0.3 0.3]);
% densityperlayer=diag([0.1 0.12 0.12]);
% d31perlayer=diag([0 4 4]*10^(-8));
% thick=thickperlayer*ones(3,numel);
% dens=densityperlayer*ones(3,numel);
% d31=d31perlayer*ones(3,numel);
% youngs=youngsperlayer*ones(3,numel);
% poisson=poissonperlayer*ones(3,numel);
youngsperlayer=diag([100 261000]);
thickperlayer=diag([.006 .003]);
poissonperlayer=diag([.3 .3]);
densityperlayer=diag([.1 .12]);
d31perlayer=diag([0 4]*10^(-8));
nodes=innerR+[0:1:numel]*(outerR-innerR)/numel;
thick=thickperlayer*ones(2,numel);
dens=densityperlayer*ones(2,numel);
d31=d31perlayer*ones(2,numel);
youngs=youngsperlayer*ones(2,numel);
poisson=poissonperlayer*ones(2,numel);
tens=t/sum(sum(thickperlayer));

if mod(numel,2) == 0
   if config == 1
      volts=v*[ones(2,numel-1) zeros(2,1)];   %Configuration 1
   elseif config == 0
      volts=v*[ones(2,numel)];  %Configuration 0
   end
elseif mod(numel,2) > 0
   if config == 4
      volts=v*[zeros(2,numel/3) ones(2,numel/3) zeros(2,numel/3)]; %Configuration 4
   elseif config == 3
      volts=v*[-ones(2,numel/3) ones(2,numel/3) zeros(2,numel/3)]; %Configuration 3
   elseif config == 2
      volts=v*[ones(2,numel/3) ones(2,numel/3) zeros(2,numel/3)]; %Configuration 2
   elseif config == 5
      volts=v*[ones(2,numel/3) zeros(2,numel/3) zeros(2,numel/3) zeros(2,numel/3) zeros(2,numel/3)]; %
3.048 cm circle in center
   end
end

[v,x,d,eps]=memfemr2(order,p,tens,nodes,thick,dens,youngs,poisson, d31, volts,verb,dyn,mode,3,alpha,
beta);
```

The following file is where the calculations are performed. No modifications involved with the simple problem should be made to this file. There are a few files run by this file and are located in the Private folder. This file and the corresponding files contained within are where the theoretical development was programmed.

```
function [vr,xr, dr,eps]=memfemr2(order, p, tens, nodes, thick, dens, youngs, poisson, d31, volts, verbose,
dyn, mode, mx, alpha, beta)
% bs3fem - Finite Element simulation of plate-membrane
% written by : Capt James Rogers, AFIT, USAF
%
%   order   = order of perturbation levels terms to include (0 to 3)
%   p       = pressure differential per unit length applied to beam
%   tens    = pretension applied to beam
%   nodes   = distance from left end of each element interface
%   thick   = thickness of layers
%   dens    = layer material density (mass/L^3)
%   youngs  = layer Young's Modulus (F/L^2)
%   poisson = layer Poisson's Ratio
%   d31     = layer piezo coefficients
%   volts   = layer voltage potential
%   verbose = 0: No Plots Produced
%             1: All Plots Created
%   dyn     = 0: Static Only
%             1: Dynamic \/ \/ \/ \/
%   mode    = 0 : Clamped Natural Modes Returned
%             >0: assumed center mode
%   mx      = maximum modes returned
%
%   vr      = Eigenvectors (Dynamic)
%             Analytic/Total Static FEM/Only 1st Level FEM Solutions (Static)
%   dr      = Eigenvalues (Dynamic)
%           = Corresponding Axial Locations (Static)
%

num=length(nodes)-1;
len = nodes(length(nodes));
if max(size(thick)) == num
  numlayers =  min(size(thick));
else
  numlayers =  max(size(thick));
end
for i=1:num
  hi=0;
  hbu=0;
  hbl=0;
  for j=1:numlayers
    hbu=hbu+thick(j,i)*(2*hi+thick(j,i));
    hbl=hbl+2*thick(j,i);
    hi=hi+thick(j,i);
  end
  hbar=hbu/hbl;
   %Dimensional Values
   els(i).p   = p;
```

```
    els(i).r1   = nodes(i);
    els(i).r2   = nodes(i+1);
    els(i).r    = (nodes(i+1)+nodes(i))/2;
    els(i).len  = (nodes(i+1)-nodes(i));
    els(i).rhoa = 0;
    els(i).t    = 0;
    els(i).eh11   = 0;
    els(i).eh12   = 0;
    els(i).ehe  = 0;
    els(i).ehz11  = 0;
    els(i).ehz12  = 0;
    els(i).ehze = 0;
    els(i).d11   = 0;
    els(i).d12   = 0;
    els(i).nz   = 0;
    els(i).n   = 0;
    hi=0;
    for j=1:numlayers
       z1              = thick(j,i)*(2*hi+thick(j,i)-2*hbar)/2;
       z2              = (thick(j,i)*(thick(j,i)^2+3*hi*thick(j,i)+3*hi*2)-
3*hbar*thick(j,i)*(2*hi+thick(j,i))+3*hbar^2*thick(j,i))/3;
               els(i).rhoa      = els(i).rhoa+dens(j,i)*thick(j,i);
       els(i).eh11      = els(i).eh11  + youngs(j,i)*thick(j,i)/(1-poisson(j,i)^2);
       els(i).eh12      = els(i).eh12  + youngs(j,i)*poisson(j,i)*thick(j,i)/(1-poisson(j,i)^2);
       els(i).ehe       = els(i).ehe + youngs(j,i)*d31(j,i)*volts(j,i)/(1-poisson(j,i));
       els(i).ehz11     = els(i).ehz11 + youngs(j,i)*z1/(1-poisson(j,i)^2);
       els(i).ehz12     = els(i).ehz12 + youngs(j,i)*poisson(j,i)*z1/(1-poisson(j,i)^2);
               els(i).ehze      = els(i).ehze + youngs(j,i)*z1*d31(j,i)*volts(j,i)/thick(j,i)/(1-poisson(j,i));
               els(i).d11       = els(i).d11 + youngs(j,i)*z2/(1-poisson(j,i)^2);
               els(i).d12       = els(i).d12 + youngs(j,i)*poisson(j,i)*z2/(1-poisson(j,i)^2);
               els(i).nz        = els(i).nz + tens*z1;
               els(i).n         = els(i).n + tens*thick(j,i);
               els(i).t         = els(i).t+thick(j,i);
       hi              = hi+thick(j,i);
    end
    %Scaled Values
    els(i).eta2     = els(i).eh11/els(i).n;
    els(i).eta      = sqrt(els(i).eta2);
    els(i).eps      = sqrt(els(i).d11/els(i).eh11)/els(i).len;
    els(i).d12s     = els(i).d12/els(i).eh11/els(i).eps^2*num^2;
    els(i).ps       = p*els(i).len/els(i).eh11/els(i).eps^2*num^2;
    els(i).ehes     = els(i).ehe*els(i).len^2/els(i).eh11/els(i).eps^2;
    els(i).ehz11s   = els(i).ehz11/els(i).eh11/els(i).len;
    els(i).ehz12s   = els(i).ehz12/els(i).eh11/els(i).len;
    els(i).ehzes    = els(i).ehze*els(i).len^2/els(i).eh11/els(i).eps^3;
    els(i).nzs      = els(i).nz/els(i).eh11/els(i).len;
    els(i).nubar    = els(i).eh12/els(i).eh11;
    eps(i)          = els(i).eps;
end

disp=3; %nodes per element
dpn=2;  %displacements per node

kg0=zeros(dpn*((disp-1)*num+1),dpn*((disp-1)*num+1));
```

```
mg0=zeros(dpn*((disp-1)*num+1),dpn*((disp-1)*num+1));
pg0=zeros(dpn*((disp-1)*num+1),1);
w01=zeros(dpn*((disp-1)*num+1),1);

if order > 0
   kg1=zeros(dpn*((disp-1)*num+1),dpn*((disp-1)*num+1));
   mg1=zeros(dpn*((disp-1)*num+1),dpn*((disp-1)*num+1));
   pg1=zeros(dpn*((disp-1)*num+1),1);
   w11=zeros(dpn*((disp-1)*num+1),1);
   if order > 1
      kg2=zeros(dpn*((disp-1)*num+1),dpn*((disp-1)*num+1));
      mg2=zeros(dpn*((disp-1)*num+1),dpn*((disp-1)*num+1));
      pg2=zeros(dpn*((disp-1)*num+1),1);
      w21=zeros(dpn*((disp-1)*num+1),1);
      if order > 2
         kg3=zeros(dpn*((disp-1)*num+1),dpn*((disp-1)*num+1));
         mg3=zeros(dpn*((disp-1)*num+1),dpn*((disp-1)*num+1));
         pg3=zeros(dpn*((disp-1)*num+1),1);
         w31=zeros(dpn*((disp-1)*num+1),1);
      end
   end
end

chunk=1;
ds=zeros(chunk*num+1,order+1);
x=zeros(chunk*num+1,1);
ws=zeros(chunk*num+1,order+1);
w=zeros(chunk*num+1,1);

for i=1:num
  nodeids=[(disp-1)*i-(disp-2) (disp-1)*i+(disp-2) (disp-1)*i];
  k0   = K0fr(els(i).eps,els(i).r,els(i).len) ...
         + K0gr(els(i).eps,els(i).r,els(i).len)/els(i).eta2;
  m0   = M0r(els(i).eps,els(i).r,els(i).len);
  p0   = els(i).ps*P0r(els(i).eps,els(i).r,els(i).len);
  kg0  = BuildStiffness(kg0,k0/els(i).len,nodeids);
  mg0  = BuildMass(mg0,m0/els(i).len,nodeids);
  pg0  = BuildForce(pg0,els(i).eps^2*p0,nodeids);
  if order > 0
            m1    = M1r(els(i).eps,els(i).r,els(i).len);
            k1    = K1fr(els(i).eps,els(i).r,els(i).len) ...
            + K1gr(els(i).eps,els(i).r,els(i).len)/els(i).eta2...
            + els(i).d12s*K1dr(els(i).eps,els(i).r,els(i).len);
    f1    = els(i).ehzes*F0r(els(i).eps,els(i).r,els(i).len);
    p1    = els(i).ps*P1r(els(i).eps,els(i).r,els(i).len);
            kg1   = BuildStiffness(kg1,els(i).eps*k1/els(i).len,nodeids);
    mg1   = BuildMass(mg1,els(i).eps*m1/els(i).len,nodeids);
    pg1   = BuildForce(pg1,els(i).eps^3*(f1-p1),nodeids);
    if order > 1
                    m2     = M2r(els(i).eps,els(i).r,els(i).len);
      k2     = K2fr(els(i).eps,els(i).r,els(i).len) ...
             + K2gr(els(i).eps,els(i).r,els(i).len)/els(i).eta2...
             + K2nr(els(i).eps,els(i).r,els(i).len)...
             + els(i).d12s*K2dr(els(i).eps,els(i).r,els(i).len);
      k2e    = els(i).ehes*K0gr(els(i).eps,els(i).r,els(i).len);
                    kg2    = BuildStiffness(kg2,els(i).eps^2*(k2-k2e)/els(i).len,nodeids);
      mg2    = BuildMass(mg2,els(i).eps^2*m2/els(i).len,nodeids);
      f2    = els(i).ehzes*F1r(els(i).eps,els(i).r,els(i).len);
      p2     = els(i).ps*P2r(els(i).eps,els(i).r,els(i).len);
             pg2    = BuildForce(pg2,els(i).eps^4*(f2-p2),nodeids);
      if order > 2
                   m3  = M3r(els(i).eps,els(i).r,els(i).len);
        k3  = K3fr(els(i).eps,els(i).r,els(i).len) ...
             + K3gr(els(i).eps,els(i).r,els(i).len)/els(i).eta2...
             + K3nr(els(i).eps,els(i).r,els(i).len)...
             + els(i).d12s*K3dr(els(i).eps,els(i).r,els(i).len);
        k3e = els(i).ehes*K1gr(els(i).eps,els(i).r,els(i).len);
        kg3 = BuildStiffness(kg3,els(i).eps^3*(k3-k3e)/els(i).len,nodeids);
        mg3 = BuildMass(mg3,els(i).eps^3*m2/els(i).len,nodeids);
               f3  = els(i).ehzes*F2r(els(i).eps,els(i).r,els(i).len);
        p3  = els(i).ps*P3r(els(i).eps,els(i).r,els(i).len);
               pg3 = BuildForce(pg3,els(i).eps^5*(f3-p3),nodeids);
      end
    end
  end
end

%clamped

% sort 0th order matrices for undetermined displacements
mg01=mg0;
temp1=mg01(1,:);
mg01(1,:)=mg01(2,:);
mg01(2,:)=temp1;
temp2=mg01(:,1);
mg01(:,1)=mg01(:,2);
mg01(:,2)=temp2;

kg01=kg0;
temp1=kg01(1,:);
kg01(1,:)=kg01(2,:);
kg01(2,:)=temp1;
temp2=kg01(:,1);
kg01(:,1)=kg01(:,2);
kg01(:,2)=temp2;

pg0(4)=pg0(4)+pg0(2);
pg0(1)=pg0(1)+pg0(2)*els(1).len/2;
pg01=pg0;
temp=pg01(1);
pg01(1)=pg01(2);
pg01(2)=temp;

m0c=mg01(dpn:dpn*(disp-1)*num,dpn:dpn*(disp-1)*num);
k0c=kg01(dpn:dpn*(disp-1)*num,dpn:dpn*(disp-1)*num);
p0c=pg01(dpn:dpn*(disp-1)*num);

if order > 0
```

```
          % sort 1st order matrices for undetermined displacements
          mg11=mg1;
          temp1=mg11(1,:);
          mg11(1,:)=mg11(2,:);
          mg11(2,:)=temp1;
          temp2=mg11(:,1);
          mg11(:,1)=mg11(:,2);
          mg11(:,2)=temp2;

          kg11=kg1;
          temp1=kg11(1,:);
          kg11(1,:)=kg11(2,:);
          kg11(2,:)=temp1;
          temp2=kg11(:,1);
          kg11(:,1)=kg11(:,2);
          kg11(:,2)=temp2;

          pg11=pg1;
          temp=pg11(1);
          pg11(1)=pg11(2);
pg11(2)=temp;

m1c=mg11(dpn:dpn*(disp-1)*num,dpn:dpn*(disp-1)*num);
k1c=kg11(dpn:dpn*(disp-1)*num,dpn:dpn*(disp-1)*num);
p1c=pg11(dpn:dpn*(disp-1)*num);
c1c = alpha*k0c + beta*m0c;
if order > 1
                    % sort 1st order matrices for undetermined displacements
                    mg21=mg2;
                    temp1=mg21(1,:);
                    mg21(1,:)=mg21(2,:);
                    mg21(2,:)=temp1;
                    temp2=mg21(:,1);
                    mg21(:,1)=mg21(:,2);
                    mg21(:,2)=temp2;

                    kg21=kg2;
                    temp1=kg21(1,:);
                    kg21(1,:)=kg21(2,:);
                    kg21(2,:)=temp1;
                    temp2=kg21(:,1);
                    kg21(:,1)=kg21(:,2);
                    kg21(:,2)=temp2;

                    pg21=pg1;
                    temp=pg21(1);
                    pg21(1)=pg21(2);
                    pg21(2)=temp;

  m2c=mg21(dpn:dpn*(disp-1)*num,dpn:dpn*(disp-1)*num);
  k2c=kg21(dpn:dpn*(disp-1)*num,dpn:dpn*(disp-1)*num);
  p2c=pg21(dpn:dpn*(disp-1)*num);
  c2c = alpha*k1c + beta*m1c;
  if order > 2
```

```
                    % sort 1st order matrices for undetermined displacements
                    mg31=mg3;
                    temp1=mg31(1,:);
                    mg31(1,:)=mg31(2,:);
                    mg31(2,:)=temp1;
                    temp2=mg21(:,1);
                    mg31(:,1)=mg31(:,2);
                    mg31(:,2)=temp2;

                    kg31=kg3;
                    temp1=kg31(1,:);
                    kg31(1,:)=kg31(2,:);
                    kg31(2,:)=temp1;
                    temp2=kg21(:,1);
                    kg31(:,1)=kg 31(:,2);
                    kg31(:,2)=temp2;

                    pg31=pg1;
                    temp=pg31(1);
                    pg31(1)=pg31(2);
                    pg31(2)=temp;

      m3c=mg31(dpn:dpn*(disp-1)*num,dpn:dpn*(disp-1)*num);
      k3c=kg31(dpn:dpn*(disp-1)*num,dpn:dpn*(disp-1)*num);
      p3c=pg31(dpn:dpn*(disp-1)*num);
      c3c = alpha*k2c + beta*m2c;
    end
  end
end

%Static solution

w01(dpn:dpn*(disp-1)*num)=k0c\p0c;
if order > 0
  w11(dpn:dpn*(disp-1)*num)=-k0c\(k1c*w01(dpn:dpn*(disp-1)*num)-p1c);
  if order > 1
    w21(dpn:dpn*(disp-1)*num)=-k0c\(k1c*w11(dpn:dpn*(disp-1)*num)+k2c*w01(dpn:dpn*(disp-
1)*num)-p2c);
    if order > 2
      w31(dpn:dpn*(disp-1)*num)=-k0c\(k1c*w21(dpn:dpn*(disp-1)*num)+k2c*w11(dpn:dpn*(disp-
1)*num)+k3c*w01(dpn:dpn*(disp-1)*num) -p3c);
    end
  end
end

% Resort displacements
w0=w01;
temp=w0(1);
w0(1)=w0(2);
w0(2)=temp;
if order > 0
          w1=w11;
          temp=w1(1);
          w1(1)=w1(2);
    w1(2)=temp;
            if order > 1
                        w2=w21;
                        temp=w2(1);
                        w2(1)=w2(2);
                w2(2)=temp;
            if order > 2
                        w3=w31;
                        temp=w3(1);
                        w3(1)=w3(2);
                    w3(2)=temp;
            end
            end
end

start=els(1).r1;
for i=1:num
    nodeids=[(disp-1)*i-(disp-2), (disp-1)*i+(disp-2), (disp-1)*i];
    d0=GetDisplacements(w0,dpn,nodeids);
    if order > 0
        d1=GetDisplacements(w1,dpn,nodeids);
        if order > 1
            d2=GetDisplacements(w2,dpn,nodeids);
            if order > 2
               d3=GetDisplacements(w3,dpn,nodeids);
            end
        end
    end
    for j=0:chunk
%        ds=(diag([els(i).len 1 els(i).len 1 els(i).len 1])/els(i).eta)*d0;
        x((i-1)*chunk+j+1)=start + (j/chunk)*els(i).len;
        ws((i-1)*chunk+j+1,1)=memshape(d0,x((i-1)*chunk+j+1),els(i).eps,els(i).r,els(i).len);
        if order > 0
            ws((i-1)*chunk+j+1,2)=memshape(d0+d1,x((i-1)*chunk+j+1),els(i).eps,els(i).r,els(i).len);
            if order > 1
                ws((i-1)*chunk+j+1,3)=memshape(d0+d1+d2,x((i-1)*chunk+j+1),els(i).eps,els(i).r,els(i).len);
                if order > 2
                    ws((i-1)*chunk+j+1,4)=mems hape(d0+d1+d2+d3,x((i-
1)*chunk+j+1),els(i).eps,els(i).r,els(i).len);
                end
            end
        end
    end
    start=start+els(i).len;
end

if dyn == 0
    if verbose > 0
        figure
        wslamda=ws/(633*10^-9);
        plot(x,wslamda);
        title('Static Shape');
        legend('w0', 'w1', 'w2');
    figure
    wslamda2(:,order+1)=(ws(:,order+1))/(633*10^-9);
    plot(x,wslamda2(:,order+1));
    title('Static Shape');
%      legend('w');

%      legend('FEM Solution');
  end

  xr = x;
  vr = ws;
  dr = 0;
  return
else

  %Dynamic
  v01=zeros(dpn*((disp-1)*num+1),dpn*((disp-1)*num+1));
  d01=zeros(dpn*((disp-1)*num+1),dpn*((disp-1)*num+1));
  if order > 0
    v11=zeros(dpn*((disp-1)*num+1),dpn*((disp-1)*num+1));
    d11=zeros(dpn*((disp-1)*num+1),dpn*((disp-1)*num+1));
    if order > 1
      v2=zeros(dpn*((disp-1)*num+1),dpn*((disp-1)*num+1));
      d2=zeros(dpn*((disp-1)*num+1),dpn*((disp-1)*num+1));
      if order > 2
        v3=zeros(dpn*((disp-1)*num+1),dpn*((disp-1)*num+1));
        d3=zeros(dpn*((disp-1)*num+1),dpn*((disp-1)*num+1));
      end
    end
   end

   if mode == 0
     [v01(dpn:dpn*(disp-1)*num,dpn:dpn*(disp-1)*num),d01(dpn:dpn*(disp-1)*num,dpn:dpn*(disp-1)*num)]=eig(k0c,m0c);
     % Resort displacements
                v0=v01;
                temp1=v0(1,:);
                v0(1,:)=v0(2,:);
                v0(2,:)=temp1;
     [vc0,dc0]=sorteigs(v0,d0,0,mx);
     if order>0
       for i=1:length(dc0)
         omega1(i)=(v0(:,i)'*(kg1-dc0(i)*mg1)*v0(:,i));
         den=v0(:,i)'*mg0*v0(:,i);
         if den == 0
           omega1(i)=0;
         else
           omega1(i)=omega1(i)/2/dc0(i)/den;
         end
       end
       if order>1
         for i=1:length(dc0)
           omega2(i)=(v0(:,i)'*(kg2-dc0(i)*(omega1(i)^2*mg0+2*omega1(i)*mg1+mg2))*v0(:,i));
                 den=v0(:,i)'*mg0*v0(:,i);
```

```
                    if den == 0
              omega2(i)=0;
            else
              omega2(i)=omega2(i)/2/dc0(i)/den;
            end
          end
           if order>2
             for i=1:length(dc0)
               omega3(i)=(v0(:,i)'*(kg3-
dc0(i)*(2*omega1(i)*omega2(i)*mg0+(2*omega2(i)+omega1(i)^2)*mg1+2*omega1(i)*mg2+mg3))*v0(:,i
));
                      den=v0(:,i)'*mg0*v0(:,i);
                    if den == 0
                  omega3(i)=0;
               else
                  omega3(i)=omega3(i)/2/dc0(i)/den;
               end
             end
                      end
                       end
                    end

     if verbose>0
          if length(dc0)>0
          figure;
          [x,w]=plotmemshape(vc0,dpn,els,2);
          title('Clamped V0 Modes');
            figure;
            bar(dc0);
            title('Clamped D0 - Eigenvalues');
            figure;
            bar(sqrt(dc0/dc0(1)));
            title('Clamped First Order Frequencies (Scaled)');
          end

      if order > 0
        figure;
        bar(omega1);
        title('1st Order Frequency Corrections');

        if order > 1
          figure;
          bar(omega2);
          title('2nd Order Frequency Corrections');

          if order > 2
            figure;
            bar(omega3);
            title('2nd Order Frequency Corrections');
          end
        end
      end
    else
     start=els(1).r1;
```

```
                    for j=1:num
              for k=0:chunk
          x((j-1)*chunk+k+1)=start+(k/chunk)*els(j).len;
                    for i=1:length(dc0)
                    ve=GetDisplacements(vc0(:,i), dpn, [(j-1)*2+1 j*2+1 j*2]);
                    w((j-1)*chunk+k+1,i)=memshape(ve,x((j-1)*chunk+k+1),els(j).eps,els(j).r,els(j).len);
                  end
              end
            start=start+els(j).len;
              end
    end
    vr = w;
    xr = x;
    dr = dc0;
  else
                    %Force Response
    [v01,d01]=eig(k0c,m0c);
    [v0c,d0c]=sorteigs(v01,d01,0,mx);

    for k=1:1:1001
     delta(k)=0.00001*(k-501);
                    a20=v0c(:,1)'*p1c/(v0c(:,1)'*(k1c+sqrt(-d0c(1))*c1c-d0c(1)*m1c-
2*delta(k)*sqrt(d0c(1))*m0c)*v0c(:,1));
     if order > 0
        b1(:,k)=p1c-a20*(k1c+sqrt(-d0c(1))*c1c-d0c(1)*m1c-2*delta(k)*sqrt(d0c(1))*m0c)*v0c(:,1);
        av=(k0c-d0c(mode)*m0c)*v0c;
          c(:,k)=pinv(av)*b1(:,k);
        c(1,k)=a20;
     end
  end
     if verbose > 0
          figure;
            plot(delta,c);
          xlabel('\delta');
     end
    vr = c;
    xr = delta;
    dr = d0c;
  end
end
```

Another file that performs some calculations and creates plots for the Zernike coefficients is included here. The file was reduced for use in the final code and renamed runZernsingle.

```
function runZern(num,verb,config)

if verb > 0
   % Calculations for no pressure and changing voltage and constant tension
   volts=[0:50:1000];
    for i=1:length(volts)
      [v,x,temp,eps]=testr2(num,0,1000,volts(i),2,0,0,0,0,0,config);
      a{1}.coef(i,:)=GetAxiZerntest(x',2*v(:,3)');
      a{1}.eps(i,:)=eps
   end

   % Define voltage vector for output
    Voltage = volts';

   % Calculations for .01 pressure and changing voltage and constant tension
    for i=1:length(volts)
      [v,x,temp,eps]=testr2(num,0.01,1000,volts(i),2,0,0,0,0,0,config);
      a{2}.coef(i,:)=GetAxiZerntest(x',2*v(:,3)');
      a{2}.eps(i,:)=eps;
   end

   % Graphing changing voltage for above cases
    if verb > 0
      figure
      subplot(2,1,1)
      plot(volts,a{1}.coef(:,1),'k--',volts,a{1}.coef(:,2),'k-.',volts,a{1}.coef(:,3),'k-');
      a{1}.title='Pressure = 0';
      title('Pressure = 0');
      legend(['Z_1   '; 'Z_5   '; 'Z_{13}']);
      subplot(2,1,2)
      plot(volts,a{2}.coef(:,1),'k--',volts,a{2}.coef(:,2),'k-.',volts,a{2}.coef(:,3),'k-');
      a{2}.title='Pressure = 0.01';
      title('Pressure = 0.01');
      legend(['Z_1   '; 'Z_5   '; 'Z_{13}']);
      xlabel('Voltage Deviations (T=1000)');
   end

   % Calculations for no voltage, low pressure and changing tension
   tens=[1000:1000:7000];
    for i=1:length(tens)
      [v,x,temp,eps]=testr2(num,0.01,tens(i),0,2,0,0,0,0,0,config);
      a{3}.coef(i,:)=GetAxiZerntest(x',2*v(:,3)');
      a{3}.eps(i,:)=eps;
   end

   % Calculations for .1 pressure and 100 voltage and changing tension
    for i=1:length(tens)
      [v,x,temp,eps]=testr2(num,0.1,tens(i),100,2,0,0,0,0,0,config);
      a{4}.coef(i,:)=GetAxiZerntest(x',2*v(:,3)');
    a{4}.eps(i,:)=eps;
  end

  % Graphing changing tensions for above cases
  if verb > 0
    figure
    subplot(2,1,1)
    plot(tens,a{3}.coef(:,1),'k--',tens,a{3}.coef(:,2),'k-.',tens,a{3}.coef(:,3),'k-');
    a{3}.title='d_{31}V = 0';
    title('d_{31}V = 0');
    legend(['Z_1   '; 'Z_5   '; 'Z_{13}']);
    subplot(2,1,2)
    plot(tens,a{4}.coef(:,1),'k--',tens,a{4}.coef(:,2),'k-.',tens,a{4}.coef(:,3),'k-');
    a{4}.title='d_{31}V = 10^{-6}';
    title('d_{31}V = 10^{-6}');
    legend(['Z_1   '; 'Z_5   '; 'Z_{13}']);
    xlabel('Tension Deviations (P=0.01)');
  end


  % Calculations for changing pressure and no voltage and 1000 tension
  pres=[0:0.001:0.01];
  for i=1:length(pres)
    [v,x,temp,eps]=testr2(num,pres(i),1000,0,2,0,0,0,0,0,config);
    a{5}.coef(i,:)=GetAxiZerntest(x',2*v(:,3)');
    a{5}.eps(i,:)=eps;
  end

  % Calculations for changing pressure and 100 voltage and 1000 tension
  for i=1:length(pres)
    [v,x,temp,eps]=testr2(num,pres(i),1000,100,2,0,0,0,0,0,config);
    a{6}.coef(i,:)=GetAxiZerntest(x',2*v(:,3)');
    a{6}.eps(i,:)=eps;
  end

  % Graphing changing pressure for above cases
  if verb > 0
    figure
    subplot(2,1,1)
    plot(pres,a{5}.coef(:,1),'k--',pres,a{5}.coef(:,2),'k-.',pres,a{5}.coef(:,3),'k-');
    a{5}.title='d_{31}V = 0';
    title('d_{31}V = 0');
    legend(['Z_1   '; 'Z_5   '; 'Z_{13}']);
    subplot(2,1,2)
    plot(pres,a{6}.coef(:,1),'k--',pres,a{6}.coef(:,2),'k-.',pres,a{6}.coef(:,3),'k-');
    a{6}.title = 'd_{31}V = 10^{-6}';
    title('d_{31}V = 10^{-6}');
    legend(['Z_1   '; 'Z_5   '; 'Z_{13}']);
    xlabel('Pressure Deviations (T=1000)');
  end
end
```

The rest of the files are ones created to make the program run smoother and complete all the necessary actions by running only one program. That file is included first, followed by other files that are used for calculations to create the 7 Figures.

```
function Program
% Clearing
  clc
  clear;

% Assignment for while loops and other functions
global zfe
verb1 = 'q';
verb2 = 'q';
zerocond = 'q';
rover = [0:.03:3]';
rmin = rover/max(rover);
ang = [-pi/2:pi/12:3*pi/2]';
mkpts = 1;  % Zero to Stop Experimental Plots, 1 to see them
verb = 0;  % Change to 1 (one) if you want to see the plots created by original FEM code

% Questions that need to be answered to get program to run
% num1 = input('How many symmetric elements do you want? ');
% config = input('What configuration do you want to activate(0 or 1 for even elements, 2-5 for odd
elements--5 is 1" circle in center)? ');
% volt = input('What voltage do you want to apply to the membrane(for comparison -600 to 600 in 300V
increments)? ');
% % p = input('What pressure do you want to apply to the membrane? ');
% t = input('What tension is placed on the membrane (use 1000)? ');

% Setting values so questions don't have to be there--Comment if you have questions active
num1 = 9;
config =5;
volt=-600;
p=0;
t=80000000;

% Stuff for graphs
Element = num2str(num1);
V=num2str(volt);
P=num2str(p);
N=num2str(t);

% Different solutions for the zero voltage case
if (volt == 0)
    while (zerocond ~= 'b') & (zerocond ~= 'm') & (zerocond ~= 'a')
        zerocond = input('Which 0 V condition do you want (before, mid, after)? ','s');
        if (zerocond == 'b')
            zerocon = 1;
        elseif (zerocond == 'm')
            zerocon = 2;
        elseif (zerocond == 'a')
            zerocon = 3;
        else
```

```
         'Please answer with proper input'
      end
   end
else
   zerocon = 0;
end



% FEM output
runZern(num1,verb,config)
Zcoeff = runzernsingle(num1,verb,config,volt,p,t);
for i=1:6
   zfe(i) = Zcoeff(1,i);
end

testr2(num1,p,t,volt,2,verb,0,0,0,0,config);
[v,x,d,eps,youngsperlayer,thickperlayer] = testr2(num1,p,t,volt,2,verb,0,0,0,0,config);
Emem = num2str(youngsperlayer(1,1));
tmem = num2str(thickperlayer(1,1));
% Experimental output and deflection vectors
if volt == 0
   if zerocon == 1
      zerocenter
   elseif zerocon == 2
      zerocentermid
   elseif zerocon == 3
      zerocenterafter
   end
   elseif volt == 300
     three00center
   elseif volt == -300
     neg300center
   elseif volt == -600
      neg600center
   elseif volt == 600
      sixhundredcenter
end

% Running outside script for deflection calculations
[wfem,wexp,wexpall,wexpnon] = deflection(zfe,z,rover,rmin,ang,volt,mkpts,t);

wexpallmod = wexpall;
wexpnonmod = wexpnon;

% Deflection plots
wvs = wexp-wfem;
ang1 = -pi/2;
for i = 1:size(rmin)
   wexpallred(i) = 0;
   wexpnonred(i) = 0;
   for j = 1:size(ang)
      if (ang1 >= pi/2)
         for k = 1:size(rmin)
```

```
                for m = 1:size(ang)
                    test = abs(ang(m) - ang1);
                    if (test < pi/24)
                        n = m;
                    end
                end
                wexpallmod(k,n) = -wexpallmod(k,n);
                wexpnonmod(k,n) = -wexpnonmod(k,n);
            end
        end
        ang1 = ang1 + pi/12;
        wexpallred(i) = wexpallred(i) + wexpallmod(i,j);
        wexpnonred(i) = wexpnonred(i) + wexpnonmod(i,j);
    end
end

wexpallred';
wexpnonred';

figure
subplot(2,1,1), plot(rover,wexp,rover,wfem),title('Experimental and
FEM','FontSize',12,'FontWeight','bold','Color','b'),xlabel('Radial dimension edge to center'),...
    ylabel('Wavefront deflection')
subplot(2,1,2), plot(rover,wvs),title('Difference between Experimental and
FEM','FontSize',12,'FontWeight','bold','Color','g'),xlabel('Radial dimension edge to center'),...
    ylabel('Wavefront deflection')
figure
subplot(2,1,1),plot(rover,wfem),title(['Finite Element Solution Voltage = '
V],'FontSize',12,'FontWeight','bold','Color','r'),xlabel('Radial dimension edge to center'),...
    ylabel('Wavefront deflection')
subplot(2,1,2),plot(rover,wexp),title('Experimental Reduced (Symmetric)
Solution','FontSize',12,'FontWeight','bold','Color','r'),xlabel('Radial dimension edge to center'),...
    ylabel('Wavefront deflection')
figure
subplot(2,1,1),plot(rover,wexpall),title('All 35 Zernike from -Pi/2 to
3*Pi/2','FontSize',12,'FontWeight','bold','Color','y'),xlabel('Radial dimension edge to center'),...
    ylabel('Wavefront deflection')
subplot(2,1,2),plot(rover,wexpnon),title('30 Non-Axisymmetric Zernike
Coefficents','FontSize',12,'FontWeight','bold','Color','b'),xlabel('Radial dimension edge to center'),...
    ylabel('Wavefront deflection')
figure
subplot(2,1,1),plot(rover,wexpallred),title('Reduced
35','FontSize',12,'FontWeight','bold','Color','c'),,xlabel('Radial dimension edge to center'),...
    ylabel('Wavefront deflection')
subplot(2,1,2),plot(rover,wexpnonred),title('Reduced
30','FontSize',12,'FontWeight','bold','Color','m'),xlabel('Radial dimension edge to center'),...
    ylabel('Wavefront deflection')
figure
subplot(2,1,1),plot(rover,wexpallmod),title('Modified 35
Zernike','FontSize',12,'FontWeight','bold','Color','r'),xlabel('Radial dimension edge to center'),...
    ylabel('Wavefront deflection')
subplot(2,1,2),plot(rover,wexpnonmod),title('Modified 30
Zernike','FontSize',12,'FontWeight','bold','Color','b'),xlabel('Radial dimension edge to center'),...
    ylabel('Wavefront deflection')
```

This file is a sub file to the above Program file and is used to calculate the deflections based on the Zernike polynomials.

```
function [wfem,wexp,wexpall,wexpnon] = deflection(zfe,z,rover,rmin,ang,volt,mkpts,tension)

rover = [0:.03:3]';
rmin = rover/max(rover);
ang = [-pi/2:pi/12:3*pi/2]';

% Code for deflections along any center line (FEM and experiment -- 5 zernike numbers)
for i = 1:size(rmin)
   wfem(i,:) = zfe(2)*(2*((rover(i,:))^2)-1) + zfe(3)*(6*((rover(i,:))^4)-6*((rover(i,:))^2)+1) +
zfe(4)*(20*((rover(i,:))^6)-30*((rover(i,:))^4)+12*((rover(i,:))^2)-1) + ...
      zfe(5)*(70*((rover(i,:))^8)-140*((rover(i,:))^6)+90*((rover(i,:))^4)-20*((rover(i,:))^2)+1) + ...
      zfe(6)*(252*(rover(i,:))^10-630*(rover(i,:))^8+560*(rover(i,:))^6-
210*(rover(i,:))^4+30*(rover(i,:))^2-1);

   wexp(i,:) = z(3,:)*(2*(rmin(i,:))^2-1) + z(8,:)*(6*(rmin(i,:))^4-6*(rmin(i,:))^2+1) +
z(15,:)*(20*(rmin(i,:))^6-30*(rmin(i,:))^4+12*(rmin(i,:))^2-1) + ...
      z(24,:)*(70*(rmin(i,:))^8-140*(rmin(i,:))^6+90*(rmin(i,:))^4-20*(rmin(i,:))^2+1) + ...
      z(35,:)*(252*(rmin(i,:))^10-630*(rmin(i,:))^8+560*(rmin(i,:))^6-210*(rmin(i,:))^4+30*(rmin(i,:))^2-
1);
end
if (volt < 0)
   wexp = wexp * -1;
end
% Code for Experimental deflection for angles from 0 to Pi (35 zernike numbers)
if volt == 0
   if zerocon == 1
      [z]=M2_T1b_0v(mkpts);
   elseif zerocon == 2
      M2_T1e_0V(mkpts);
   elseif zerocon == 3
      M2_T1h_0V(mkpts);
   end
   elseif volt == 300
      [z]=M2_T1c_300v(mkpts);
   elseif volt == -300
      [z]=M2_T1f_Neg300v(mkpts);
   elseif volt == -600
      [z]=M2_T1g_Neg600v(mkpts);
   elseif volt == 600
      [z]=M2_T1d_600v(mkpts);
end
for i = 1:size(rmin)
   for j = 1:size(ang)
      wexpall(i,j) = z(1,:)*(rmin(i)*cos(ang(j))) + z(2,:)*(rmin(i)*sin(ang(j))) + z(3,:)*(2*rmin(i)^2-1) +
z(4,:)*(rmin(i)^2*2*cos(2*ang(j))) + ...
         z(5,:)*(rmin(i)^2*2*sin(2*ang(j))) + z(6,:)*((3*rmin(i)^2-2)*rmin(i)*cos(ang(j))) +
z(7,:)*((3*rmin(i)^2-2)*rmin(i)*sin(ang(j))) + ...
         z(8,:)*(6*(rmin(i))^4-6*(rmin(i))^2+1) + z(9,:)*(rmin(i)^3*cos(3*ang(j))) +
z(10,:)*(rmin(i)^3*sin(3*ang(j))) + ...
         z(11,:)*((4*rmin(i)^2-3)*rmin(i)^2*cos(2*ang(j))) + z(12,:)*((4*rmin(i)^2-
3)*rmin(i)^2*sin(2*ang(j))) + ...
```

```
          z(13,:)*((10*rmin(i)^4-12*rmin(i)^2+3)*rmin(i)*cos(ang(j))) + z(14,:)*((10*rmin(i)^4-
12*rmin(i)^2+3)*rmin(i)*sin(ang(j))) + ...
          z(15,:)*(20*(rmin(i))^6-30*(rmin(i))^4+12*(rmin(i))^2-1)  + z(16,:)*(rmin(i)^4*cos(4*ang(j))) +
z(17,:)*(rmin(i)^4*sin(4*ang(j))) + ...
          z(18,:)*((5*rmin(i)^2-4)*rmin(i)^3*cos(3*ang(j))) + z(19,:)*((5*rmin(i)^2-
4)*rmin(i)^3*sin(3*ang(j))) + ...
          z(20,:)*((15*rmin(i)^4-20*rmin(i)^2+6)*rmin(i)^2*cos(2*ang(j))) + z(21,:)*((15*rmin(i)^4-
20*rmin(i)^2+6)*rmin(i)^2*sin(2*ang(j))) + ...
          z(22,:)*((35*rmin(i)^6-60*rmin(i)^4+30*rmin(i)^2-4)*rmin(i)*cos(ang(j))) +
z(23,:)*((35*rmin(i)^6-60*rmin(i)^4+30*rmin(i)^2-4)*rmin(i)*sin(ang(j))) + ...
          z(24,:)*((70*(rmin(i))^8-140*(rmin(i))^6+90*(rmin(i))^4-20*(rmin(i))^2+1)) +
z(25,:)*(rmin(i)^5*cos(5*ang(j))) + ...
          z(26,:)*(rmin(i)^5*sin(5*ang(j))) + z(27,:)*((6*rmin(i)^2-5)*rmin(i)^4*cos(4*ang(j))) + ...
          z(28,:)*((6*rmin(i)^2-5)*rmin(i)^4*sin(4*ang(j))) + z(29,:)*((21*rmin(i)^4-
30*rmin(i)^2+10)*rmin(i)^3*cos(3*ang(j))) + ...
          z(30,:)*((21*rmin(i)^4-30*rmin(i)^2+10)*rmin(i)^3*sin(3*ang(j))) + z(31,:)*((56*rmin(i)^6-
105*rmin(i)^4+60*rmin(i)^2-10)*rmin(i)^2*cos(2*ang(j))) + ...
          z(32,:)*((56*rmin(i)^6-105*rmin(i)^4+60*rmin(i)^2-10)*rmin(i)^2*sin(2*ang(j))) + ...
          z(33,:)*((126*rmin(i)^8-280*rmin(i)^6+210*rmin(i)^4-60*rmin(i)^2+5)*rmin(i)*cos(ang(j))) + ...
          z(34,:)*((126*rmin(i)^8-280*rmin(i)^6+210*rmin(i)^4-60*rmin(i)^2+5)*rmin(i)*sin(ang(j))) + ...
          z(35,:)*(252*rmin(i)^10-630*rmin(i)^8+560*rmin(i)^6-210*rmin(i)^4+30*rmin(i)^2-1);
   end
end
% 31 Non symmetric zernike numbers
for i = 1:size(rmin)
    for j = 1:size(ang)
       wexpnon(i,j) = z(1,:)*(rmin(i)*cos(ang(j))) + z(2,:)*(rmin(i)*sin(ang(j))) +
z(4,:)*(rmin(i)^2*2*cos(2*ang(j))) + ...
          z(5,:)*(rmin(i)^2*2*sin(2*ang(j))) + z(6,:)*((3*rmin(i)^2-2)*rmin(i)*cos(ang(j))) +
z(7,:)*((3*rmin(i)^2-2)*rmin(i)*sin(ang(j))) + ...
          z(9,:)*(rmin(i)^3*cos(3*ang(j))) + z(10,:)*(rmin(i)^3*sin(3*ang(j))) + ...
          z(11,:)*((4*rmin(i)^2-3)*rmin(i)^2*cos(2*ang(j))) + z(12,:)*((4*rmin(i)^2-
3)*rmin(i)^2*sin(2*ang(j))) + ...
          z(13,:)*((10*rmin(i)^4-12*rmin(i)^2+3)*rmin(i)*cos(ang(j))) + z(14,:)*((10*rmin(i)^4-
12*rmin(i)^2+3)*rmin (i)*sin(ang(j))) + ...
          z(16,:)*(rmin(i)^4*cos(4*ang(j))) + z(17,:)*(rmin(i)^4*sin(4*ang(j))) + ...
          z(18,:)*((5*rmin(i)^2-4)*rmin(i)^3*cos(3*ang(j))) + z(19,:)*((5*rmin(i)^2-
4)*rmin(i)^3*sin(3*ang(j))) + ...
          z(20,:)*((15*rmin(i)^4-20*rmin(i)^2+6)*rmin(i)^2*cos(2*ang(j))) + z(21,:)*((15*rmin(i)^4-
20*rmin(i)^2+6)*rmin(i)^2*sin(2*ang(j))) + ...
          z(22,:)*((35*rmin(i)^6-60*rmin(i)^4+30*rmin(i)^2-4)*rmin(i)*cos(ang(j))) +
z(23,:)*((35*rmin(i)^6-60*rmin(i)^4+30*rmin(i)^2-4)*rmin(i)*sin(ang(j))) + ...
          z(25,:)*(rmin(i)^5*cos(5*ang(j))) + z(26,:)*(rmin(i)^5*sin(5*ang(j))) + z(27,:)*((6*rmin(i)^2-
5)*rmin(i)^4*cos(4*ang(j))) + ...
          z(28,:)*((6*rmin(i)^2-5)*rmin(i)^4*sin(4*ang(j))) + z(29,:)*((21*rmin(i)^4-
30*rmin(i)^2+10)*rmin(i)^3*cos(3*ang(j))) + ...
          z(30,:)*((21*rmin(i)^4-30*rmin(i)^2+10)*rmin(i)^3*sin(3*ang(j))) + z(31,:)*((56*rmin(i)^6-
105*rmin(i)^4+60*rmin(i)^2-10)*rmin(i)^2*cos(2*ang(j))) + ...
          z(32,:)*((56*rmin(i)^6-105*rmin(i)^4+60*rmin(i)^2-10)*rmin(i)^2*sin(2*ang(j))) + ...
          z(33,:)*((126*rmin(i)^8-280*rmin(i)^6+210*rmin(i)^4-60*rmin(i)^2+5)*rmin(i)*cos(ang(j))) + ...
          z(34,:)*((126*rmin(i)^8-280*rmin(i)^6+210*rmin(i)^4-60*rmin(i)^2+5)*rmin(i)*sin(ang(j)));
   end
end
```

Appendix B: Code Operation

For most users of the finite element code, the function file above called Program was created that will ask simple questions about the system. The user answers these questions and the program runs for about 30 seconds while calculations are completed and various plots are produced. The program will currently produce the following plots:
Figure 1—4 plots of Original Experimental Data (Zernike and Raw data)
Figure 2—4 plots of Reduced Experimental Data
Figure 3—Experimental and FEM solution on same plot, Difference of two solutions
Figure 4—Experimental and FEM solution on different plot
Figure 5—All 35 Experimental Zernike numbers along different center lines (different angles)
Figure 6—Same as Figure 5 for just the non-axisymmetric Zernike numbers
Figure 7—The addition of the many centerlines for all angles around the membrane
This concludes the basic guide for the everyday user of the program.

For a more advanced user, it may be necessary to understand the code in more depth. The files included in Appendix A are the main files that a user may need to make changes to for specific conditions. All the necessary files (as well as other files created during the development of the original code) are included on a CD with this thesis.

Some of these files will be discussed now to supply the reader with more understanding and knowledge. Basic understanding of the input commands in MATLAB is assumed.
As stated before, most of the important code is included in Appendix A. The first file that will be discussed is ***testr2***. This file contains the material properties and has inputs related to the configuration and number of elements. The size of the radius is defined at the top. It is to be noted that the first number cannot be set to zero or there will be an overflow in the calculations. The layup defined is the polymer membrane followed by the piezo layer; therefore, the material properties are listed in this fashion. For example, there is one line that reads:

```
youngsperlayer=diag([100 261000]);
```

The first number in the brackets is the modulus for the membrane and the second is for the piezo layer. This is the same for all the material properties. Mostly, only the modulus, thickness and possibly the density (if running a dynamic solution) should be changed in this file. The input variables are listed in the top function line:

```
testr2(numel,p,t,v,order,verb,dyn,mode,alpha,beta,config);
```

They are in order:

Numel: number of elements along one radial line
P: Pressure term (usually this should be assigned zero)

T: Tension term
V: Voltage applied to the region
Order: Perturbation order desired (this should usually be set to 2)
Verb: Verbose command If set to anything but zero, the program has plots that it will output that were used in the dissertation.
Dyn: Set to 1 if a dynamic solution is desired
Mode: Used if a dynamic solution is being solved. Wasn't used during this study.
Alpha, Beta: Not used in static study.
Config: Allows the user to quickly pick a different configuration of the piezo activation zones. For example, configuration 5 is approximately a 1" center circle (for the plots since will only represent half of this on the plots due to the modeling of a radial line). As it is noticed near the bottom of this file, the configuration is defined by:

```
elseif config == 5
      volts=v*[ones(2,numel/3) zeros(2,numel/3) zeros(2,numel/3) zeros(2,numel/3) zeros(2,numel/3)];
```

Notice there are five zones over the membrane with a 3" radius. Therefore each zone is 3/5" in length. Most of the zones are zero except for the most left one which represents the center. If another one of these was changed to ***ones*** (let's say the third one), there would be a 6/5" circle in the center and a ring with an inner diameter of 6/5" and outer diameter of 9/5" that would be activated. With enough imagination and slight changes in the code can create all sorts of symmetric activation zones. It is advisable to keep the zones at a reasonable size, not allowing them to get too small, just to prevent losing information across each zone. Usually, an odd number of elements is best and depending on whether odd or even number are used will confine to which configuration can be used.

As with all the original finite element codes, it is best to run the function script ***Program*** rather than running one at a time. The other program that is needed is ***runzernsingle***. It will actually run the above file (***testr2***), so it requires inputs of the number of elements, verbose command (set to zero) and the desired configuration. There is nothing to be changed in this file.

The ***Program*** and ***Deflection*** files are the main front end files. The ***deflection*** script will probably never need too much modification. The ***program*** script runs the show and it can be setup to just run or have questions setup on the command line allowing the user to answer the questions. All the definitions of the properties are near the top of the file. This program can be run from the command line by typing *program* if the directory is set properly. Otherwise, there is a run button if the file is open in Matlab. There is not much to this file and modifications to the graphs can be completed at the bottom. The center area is running the other scripts defined above. Any basic operation of the program should be directed to Capt Brian Lutz.

Vita

Brian Lutz was born in Phoenixville, Pa. He graduated from Cypress Lake High School in Fort Myers, FL in 1995 and Case Western Reserve University in 1999. He proceeded to Officer Training School at Maxwell AFB in May 1999. He was commissioned a Second Lieutenant on 20 August 1999.

Second Lieutenant Brian Lutz was assigned to the Directed Energy Directorate of the Air Force Research Laboratory, Kirtland AFB, NM. While assigned there, he worked on the Membrane Mirror Project and helped further the advancement of this future space telescope technology.

He was selected to attend the Air Force Institute of Technology starting in fall 2002 to study Aeronautical Engineering and earn a Masters of Science Degree. He will proceed to Arnold Engineering Development Center for his next assignment.

REPORT DOCUMENTATION PAGE	*Form Approved* *OMB No. 074-0188*

The public reporting burden for this collection of information is estimated to aver age 1 hour per response, including the time for reviewing instructions, searching existing data sources, gathering and maintaining the data needed, and completing and reviewing the collection of information. Send comments regarding this burden estimate or any other aspect of the collection of information, including suggestions for reducing this burden to Department of Defense, Washington Headquarters Services, Directorate for Information Operations and Reports (0704-0188), 1215 Jefferson Davis Highway, Suite 1204, Arlington, VA 22202-4302. Respondents should be aware that notwithstanding any other provision of law, no person shall be subject to an penalty for failing to comply with a collection of information if it does not display a currently valid OMB control number.

PLEASE DO NOT RETURN YOUR FORM TO THE ABOVE ADDRESS.

1. REPORT DATE *(DD-MM-YYYY)* 23 Mar 04	**2. REPORT TYPE** **Master's Thesis**	**3. DATES COVERED** *(From – To)* 9 SEPT 02 – 23 MAR 04

4. TITLE AND SUBTITLE AXISYMMETRIC OPTICAL MEMBRANE MODELING BASED ON EXPERIMENTAL RESULTS	**5a. CONTRACT NUMBER**
	5b. GRANT NUMBER
	5c. PROGRAM ELEMENT NUMBER
6. AUTHOR(S) LUTZ, BRIAN J., Captain, USAF	**5d. PROJECT NUMBER**
	5e. TASK NUMBER
	5f. WORK UNIT NUMBER

7. PERFORMING ORGANIZATION NAMES(S) AND ADDRESS(S) Air Force Institute of Technology Graduate School of Engineering and Management (AFIT/EN) 2950 Hobson Way WPAFB OH 45433-7765	**8. PERFORMING ORGANIZATION REPORT NUMBER** AFIT/GAE/ENY/04-M11
9. SPONSORING/MONITORING AGENCY NAME(S) AND ADDRESS(ES) AFRL/DEBS Attn: Mr. Dan Marker 3550 Aberdeen Rd. SE Kirtland AFB NM 87117-5776 DSN: 246-2871	**10. SPONSOR/MONITOR'S ACRONYM(S)** **11. SPONSOR/MONITOR'S REPORT NUMBER(S)**

12. DISTRIBUTION/AVAILABILITY STATEMENT
APPROVED FOR PUBLIC RELEASE; DISTRIBUTION UNLIMITED.

13. SUPPLEMENTARY NOTES

14. ABSTRACT The United States Air Force, Department of Defense and commercial industry have recognized the great value of near-earth space development, specifically in satellites for use in communications, ground and space surveillance and more active roles. However, resolution, or the primary optic's diameter, has been a limitation, especially for ground surveillance. Deployable optics has been investigated to allow larger optics in space and membrane optics has received increasing attention recently. The membrane's flexible nature requires some passive and possibly active control to reduce optical distortion caused by manufacturing, deployment, or other effects during use. Piezoelectric surface controllers are one option to actively control the membrane on the order of optical measurements (micron displacement or less). Multiple configurations of transverse displacements are feasible depending on the piezo zone locations and activation.

The current thrust of industry is reducing the effort, time and cost of manufacturing and testing through use of computerized modeling and simulation; therefore, this was investigated for a membrane mirror and piezoelectric combination. Prior experiments using 6-inch diameter membranes have been conducted with an axisymmetric piezoelectric material layer on the non-optical surface. Various voltage differentials were applied to the piezo and the transverse displacement was measured. A finite element code, using perturbation techniques, was written in MATLAB and tested to check the feasibility of using computer models for the micro-displacements occurring with the membrane-piezo lay-up. The computer program considered was developed for axisymmetric conditions; however, in many cases, these conditions tended to dominate. Under these conditions, the finite element code produces results that represent the axisymmetrically reduced experimental data.

15. SUBJECT TERMS
Membrane Mirror, Finite Element Modeling, Perturbation Techniques, Wavefront Sensor, MATLAB

16. SECURITY CLASSIFICATION OF:			**17. LIMITATION OF ABSTRACT**	**18. NUMBER OF PAGES**	**19a. NAME OF RESPONSIBLE PERSON** ANTHONY N PALAZOTTO
REPORT U	**ABSTRACT** U	**c. THIS PAGE** U	UU	135	**19b. TELEPHONE NUMBER** *(Include area code)* (937) 255-6565, e-mail: ANTHONY.PALAZOTTO@afit.edu

Standard Form 298 (Rev: 8-98)
Prescribed by ANSI Std. Z39-18